Fall 2018

Enhancement of heat transfer coefficient using nanofluids for multi-stage flash desalination (MSF) plant

Nasser Zouli

Department: Chemical and Biochemical Engineering

ENHANCEMENT OF HEAT TRANSFER COEFFICIENT USING NANOFLUIDS FOR MULTI-STAGE FLASH DESALINATION (MSF) PLANT

by

NASSER ZOULI

A DISSERTATION

Presented to the Faculty of the Graduate School of the

MISSOURI UNIVERSITY OF SCIENCE AND TECHNOLOGY

In Partial Fulfillment of the Requirements for the Degree

DOCTOR OF PHILOSOPHY

in

CHEMICAL ENGINEERING

2018

Approved by

Dr. Muthanna Al-Dahhan, Advisor
Dr. Xinhua Liang
Dr. Fateme Rezaei
Dr. Dipak Barua
Dr. Fatih Dogan

PUBLICATION DISSERTATION OPTION

This dissertation consists of the following three articles, which have been submitted for publication as follows:

Paper I: Pages 11-66. Enhancement of thermal conductivity and local heat transfer coefficients using Fe_2O_3/water nanofluid for improved thermal desalination processes. It has been submitted to the Journal of Nanofluids.

Paper II: Pages 67-120. Impact of nanoparticles material on thermal conductivity and heat transfer coefficients of nanofluids. It has been submitted to the Journal of Experimental Nanoscience.

Paper III: Pages 121-158. Nanofluid effect on water evaporation/condensation rate and heat transfer coefficient. It has been submitted to Desalination Journal.

ABSTRACT

The enhancement of thermal conductivity and local heat transfer coefficient, under laminar and turbulent flow regimes, of water-based spherical Al_2O_3, CuO, and Fe_2O_3 nanofluids have been experimentally investigated for the improvement of the thermal desalination processes using a newly developed sophisticated noninvasive heat transfer coefficient probe that is flush mounted on the inner wall surface of the test section. The nanoparticles have been selected because of their superior thermal conductivity and low cost, as well as the magnetic characteristic of Fe_2O_3 nanoparticle since a magnet can collect it and reuse. Also, Fe_2O_3 nanoparticles with saline water representing seawater has been investigated for the first time for improvement of evaporation and heat transfer characteristics to enhance the performance of multi stage flash (MSF) units in thermal desalination process. The thermal conductivity and local heat transfer coefficient increased with the increase of the volume fraction and temperature of the nanofluids also with decreasing the nanoparticle size. Also, the results show that the material from which the particle is produced is a key factor in determining the nanofluids thermal conductivity and local heat transfer coefficient. Regarding the application of nanofluids with saline water as a base fluid, stable saline water nanofluid showed lower boiling temperatures and fast boiling. This would preheat the cooling seawater quickly and at low temperatures before reaching the brine heater in real MSF process. The improvement of local heat transfer obtained represents the first step to estimate the water production increase amount by using saline water nanofluid.

ACKNOWLEDGMENTS

First and foremost, thanks and praises to ALLAH for his kindness and blessing. Thanks for giving me faith to believe in guidance and myself to overcome my weakness. Thanks for granting me patience through the hard times and thankfulness through the good times. I would like to express my sincere gratitude to my advisor, Professor. Muthanna H. Al -Dahhan, for his encouragement, considerable efforts, support, and guidance throughout my study. I have experienced an excellent academic study under his supervision and his invaluable recommendations and support helped me to plan my further academic studies in the best way. I appreciatively would also like to thank my advisory committee members, Dr. Xinhua Liang, Dr. Fateme Rezaei, Dr. Dipak Barua, and Dr. Fatih Dogan for taking an interest in my work, examining my dissertation, and guidance that help to make it the best. In addition, I would like to thank the colleagues at Multiphase Reactors Engineering and Application Laboratory (mReal), Chemical and Biochemical Engineering Department at Missouri University of Science and Technology (Missouri S&T), Rolla, Missouri (USA), for providing help while conducting experiments. I appreciatively would like to thank Marlene Albrecht, Emily Kost, Dawn Schacht, Krista Welschmeyer, Emily Seals, and Dean Lenz, for providing all the assistance that the students need. Also I would like to thank my sponsor, the University of Jazan for its the financial support during my academic study. Special thanks are due to my parents, brother and sisters for their encouragement and support throughout the years. Finally, this thesis would not have been possible without the support of my lovely wife (Laila) and my children (Malaz, Hala, Nariz, and Amir). I am grateful to them for their never-ending love, encouragement and patience.

TABLE OF CONTENTS

LIST OF ILLUSTRATIONS

LIST OF TABLES

PAPER I

PAPER II

1. INTRODUCTION

Freshwater security is becoming one important challenge faced by many countries suffering from water scarcity. The climate change around the globe, high population, and industrial growth are making significant impacts on the freshwater availability for life. According to a recent modeling study from MIT, 52% of the world population will suffer from water stress by 2050 [1]. Water stress was calculated as a ratio of its mean annual total water requirements (TWR) to the mean annual runoff (RUN) generated within the sub-region plus inflow (INF) from any upstream that flows directly into the sub-region. Figure 1.1. shows the water stress in the world by 2040 according to the estimation of the World Resources Institute (WRI).

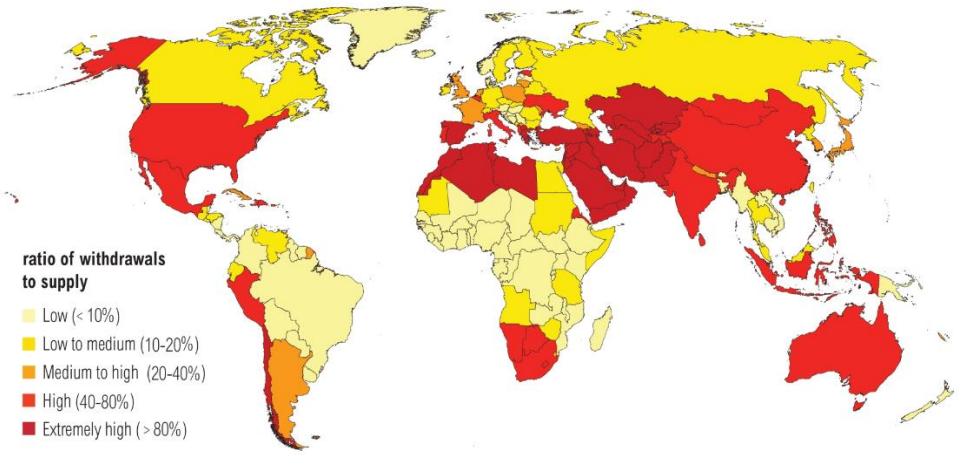

Figure 1.1: Water stress expectation by 2040 [2].

Due to its abundance on the earth, seawater represents the first solution to produce fresh water by desalination processes with are growing fast. To desalinate seawater, two

technologies were developed with different principles and performances. These are thermal based on distillation and reversis Osmosis (RO) based on membrane separation. While the competition between these processes is very high and recently in favor of the RO membrane desalination (Figure 1.2), the thermal desalination remains the oldest, most robust, and most reliable desalination technology. Contrary to this, RO desalination is well accepted to be site specific due to its high sensitivity to the seawater feed quality, requiring high pretreatment and energy costs.

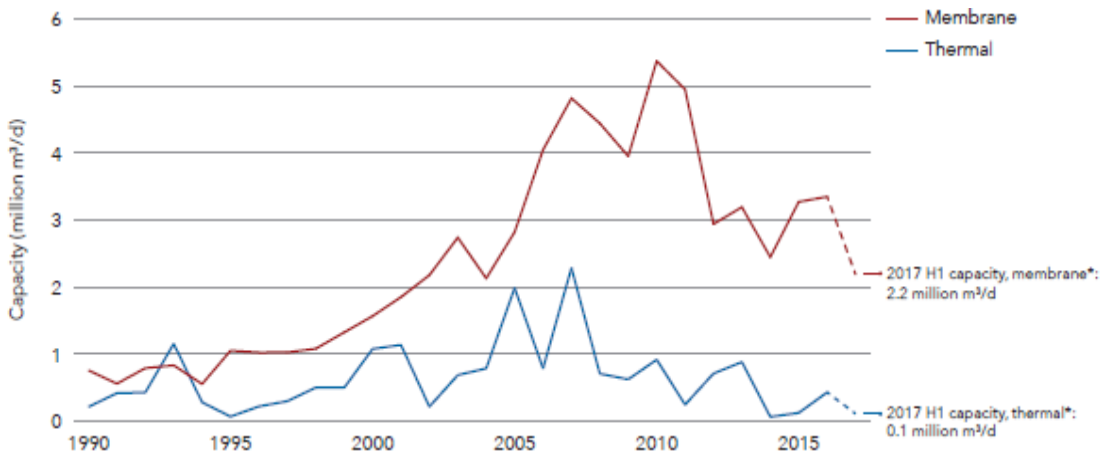

Figure 1.2: Worldwide installed desalination technologies [3].

Among thermal desalination processes, Multi-Stage-Flushing (MSF) is dominant in most arid countries such as in Gulf Council Countries (GCC). Due to the cheap fossil fuel used to produce steam necessary for MSF desalination, GCC countries adopted this technology with more than 40 years of record. The success factor of this technology is based on the sustainability of the heat transfer. Indeed, due to the concentrated brine and high temperature, inorganic scale develops a thermal resistance at the heat exchanger tube

surface, which requires the use of chemical and physical methods to disturb this scale. Within this context, the operation cost rises including energy (thermal and electrical), chemicals, etc.

MSF desalination implemented worldwide follows the Brine Recycle (BR) configuration with practical Top Brine Temperature (TBT) reaching 110 °C. This temperature is ensured through a low-pressure heating steam produced from large capacity fossil fuel fired boilers. It is well accepted that heating energy added to the pumping energy represents about 68% of the operation expenditure (OPEX) cost of MSF technology [3]. The breakdown of MSF OPEX for a plant producing 450,000 m^3/d with seawater salinity of 40,000 ppm is illustrated in Figure 1.3.

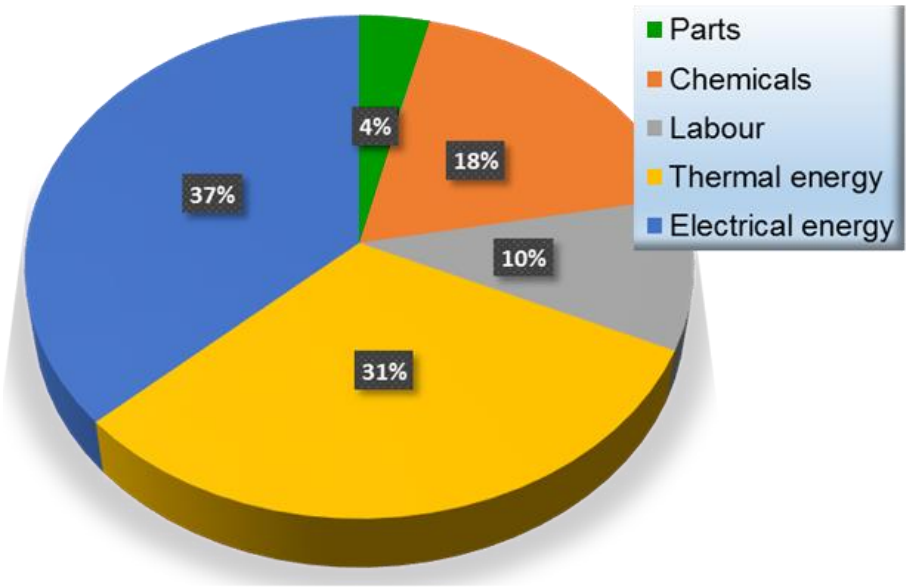

Figure 1.3: OPEX breakdown for an MSF plant with a production capacity of 450,000 m^3/d [2].

Therefore, the competitiveness of other desalination technologies starts from an energy perspective to reduce water production cost. That is why RO membrane desalination is gaining worldwide acceptance in addition to its low CO_2 emission [4].

The thermal energy increase in MSF desalination plant is dependent on the heat transfer performance, which is a function of condenser tubing material and scaling phenomenon. Most MSF desalination plants use cupronickel alloy as tubing material due to its high thermal conductivity. In some limited cases, titanium is recommended for long life reliability depending on the market opportunity. For scale control, the use of high-temperature antiscalant chemicals dominates over the acid operation method. Antiscalant chemicals are associated with a ball cleaning system to control fouling factor as per design values. However, after a certain number of running production must be stopped to conduct acid cleaning to restore the performance of the desalination MSF unit [5].

One of the some ideas to enhance the heat transfer is to increase the heat transfer area by corrugated condenser tubes were suggested without significant end-user acceptance [6]. Also, some authors tackled the modeling of the scaling phenomenon to anticipate the heat transfer decline offering smart operation practice [7]. Chemical antiscalants are undergoing continuous development, but their function is limited to the delay of the scaling.

Since the heat transfer is a function of the convection part (flowing condition), surface thermal resistance (scale), and the wall thermal conductivity (tube material). The focus of this work is to study the impact of nanofluids on the heat transfer coefficient of the flowing water to be heated and on the evaporation of the water to produce the quality water.

1.1. RESEARCH MOTIVATION

Of the many methods currently available to enhance thermal conductivity and heat transfer coefficient of heat transfer fluids, is the addition of inert additives such as nanoparticles to the conventional base fluid, such as water, ethylene glycol, or engine oil [8,9]. Nanofluids consist of a solution containing suspended nanoparticles (typically <100 nm) with different geometries and concentrations in different heat transfer base fluids. In the present work, which is related to the water industry, we focus on the water as the base fluid.

This mixture of nanoparticles/fluid has superior thermophysical properties such as thermal properties (thermal conductivity, specific heat, density, viscosity, and heat transfer coefficient-HTC) which improves thermal energy conversion from 20-40 % [10]. Most of the experimental research has been focused on enhancing the heat transfer coefficient using metal oxide nanoparticles (Such as: aluminum oxide, copper oxide, iron oxide, and silicon oxide) [11]. However, many studies obtained results indicating an increase of the critical heat flux (CHF) and absence of significant enhancement of nucleate boiling heat transfer coefficient [12,13].

Several reviews have been reported in the literature discussing nanoparticles effect on heat transfer characteristics over conventional heat transfer fluids along with mechanisms of forced convection heat transfer enhancement [14–17]. While the literature is divided on the nanofluids impact on HTC and CHF, in most of the studies, an enhancement of these two parameters is reported with the uses of nanofluids [16,18]. However, in some studies, a reduction of the HTC or CHF has been reported for Al_2O_3-water nanofluids. This atypical behavior is due to use of large nanoparticle size (~155nm)

[19]. It is exciting to note the high interest to alumina nanoparticles and water as a base in the formulation of nanofluid as reported by Suganthy *et al.*[20]

Starting from the last decade, there has been a growing interest in nanofluids heat transfer and in the boiling behavior with nanofluids for a pool of flow conditions due to its potential applications in MSF desalination, power generation, refrigeration, chemical processing, and electronics thermal management [21].

Based on the above-mentioned attributes of nanofluids, it is highly expected that the nanoparticles presence will affect the evaporation rate and saturated vapor pressure. Unfortunately, Tso *et al.*[22] reported the lack of research about the pool evaporation rate of nanofluids where authors focused only on the droplet evaporation of nanofluids and water.

Previous works showed that the improvement of the droplet evaporation rate is affected by the type of the incorporated nanoparticles and the presence of stabilizers [23,24]. Such a difference in the performance between nanofluids was attributed to several factors including surface tension and nanoparticles concentration [25,26].

Although there are many research efforts on the heat transfer improvement, it seems that the desalination industry did not take the complete benefits. Among the very promising technologies in heat transfer enhancement, are the use of the nanofluids, which represent an exciting opportunity with their super thermophysical properties that can be beneficial to the heat transfer in MSF desalination plants. Various studies are available in the literature where most of the authors used nanofluid as a superabsorbent of the solar energy to heat conventional MSF or humidification/dehumidification desalination or to enhance solar pond for remote area application [27–29].

Accordingly, the previous studies were limited to the combination of renewable energy with nanofluids to run small-scale MSF desalination process or to produce fresh water in a remote area by solar ponds. However, renewable energy still costly as an option for the near future of desalination when considering the water production capacity required to satisfy the growing population. This present a severe limitation to the implementation and the exploration of the different way by implementing nanofluid into MSF plant seems necessary. However, the use of nanofluid technology directly in the MSF plant represents a very low capital investment with high-expected improvement, in particular if magnetic iron based nanoparticles are used, which can be collected by magnets and recycled back. The question to be answered is whether the nanofluid will improve heat transfer coefficient and evaporation that will lead to enhancement of water production and BR-MSF desalination process performance by reducing the energy consumption.

1.2. RESEARCH OBJECTIVES

The current study aims to investigate experimentally the enhancement of thermal conductivity, and local heat transfer coefficient of water-based spherical Al_2O_3, CuO, and Fe_2O_3 nanofluids for the improvement of the thermal desalination processes using a newly developed sophisticated non-invasive heat transfer coefficient probe that is flush mounted on the inner wall surface of the test section; as well as to study the enhancement in the evaporation and boing temperature and time with Fe_2O_3 nanoparticles. In this work, sophisticated measurement techniques to measure local heat transfer coefficient in nanofluids has been implemented for the first time. Also, magnetic Fe_2O_3 nanoparticles with saline water representing seawater has been investigated for the first time for improvement of evaporation and heat transfer characteristics to enhance the performance

of multi stage flash (MSF) units in thermal desalination process. The general objectives of the current study can be outlined as follows:

1. Design and develop, a recirculation flow loop equipped with an advanced noninvasive heat transfer coefficient probe that is flus mounted on the inner surface of the test section wall, in conjunction with thermal conductivity meter to simultaneously measure the thermal conductivity and the local instantaneous and average heat transfer coefficient, by measuring the heat flux, surface temperature, and bulk temperature.
2. To investigate the thermal conductivity and local heat transfer coefficient to provide experimental high benchmarking data for verifying and validation of thermal efficiency for any correlation or model for thermal desalination plants.
3. To advance and address the gaps in the open literature the nanofluid to be incorporated in the Brine Recycle – Multi Stage Flash process for enhancement of water production and performance by reducing the boiling temperature.
4. Studying the effect of using different types of base fluids (Distilled and saline waters) and nanoparticles (size and concentration) on local heat transfer coefficient, thermal conductivity, evaporation, boiling temperature and time.

1.3. ORGANIZATION OF DISSERTATION

The dissertation is structured in the following papers:

- Section 1. Introduction and motivation which provide a brief literature review relevant to the work done in this dissertation, and the objectives of this study.
- Paper I. Enhancement of thermal conductivity and local heat transfer coefficients using Fe_2O_3/water nanofluid for improved thermal desalination processes.
    - In this paper, the enhancement of thermal conductivity and local convective heat transfer coefficient by nanofluid of Fe_2O_3/water has been studied experimentally for the improvement of the thermal desalination processes using a newly developed sophisticated noninvasive heat transfer coefficient probe that is flush mounted on the inner wall surface of the test section
- Paper II. Impact of nanoparticles material on thermal conductivity and heat transfer coefficients of nanofluids.
    - In this paper, the thermal conductivity, local heat transfer coefficients and thermal boundary layer of water-based spherical Al_2O_3, Fe_2O_3, and CuO nanofluids have been experimentally investigated
- Paper III. Nanofluid effect on water evaporation/condensation rate and heat transfer coefficient.
    - In this paper, a laboratory test was conducted to determine the different physical properties of saline water nanofluid including stability, thermal conductivity, evaporation quantity and rate,

boiling temperature and time, and local heat transfer coefficient in stagnant conditions.

- Section 2. Presents remarks, and suggestions for future works.
- Appendix: Experimental investigation of the thermal properties of saline water nanofluids
    - In this paper, the effect of saline water as base fluid over the thermal conductivity, heat transfer coefficient and boiling temperature is investigated, using Fe_2O_3 nanoparticles.

PAPER

I. ENHANCEMENT OF THERMAL CONDUCTIVITY AND LOCAL HEAT TRANSFER COEFFICIENTS USING Fe_2O_3/WATER NANOFLUID FOR IMPROVED THERMAL DESALINATION PROCESSES

ABSTRACT

The enhancement of thermal conductivity and local convective heat transfer coefficient by nanofluid of Fe_2O_3/water has been studied experimentally for the improvement of the thermal desalination processes using a newly developed sophisticated noninvasive heat transfer coefficient probe that is flush mounted on the inner wall surface of the test section. Fe_2O_3 nanoparticles have been selected due to their magnetic characteristic for improving the thermal efficiency of desalination since they can be collected by magnet and reused. The volume fraction of 0.01–0.09% using different nanoparticle sizes of 3 nm, 10 nm, and 20 nm has been used at varying experimental temperatures of 25, 45, and 65°C in laminar and turbulent flow regimes. The thermal conductivity and local heat transfer coefficient increased with the increase of the Fe_2O_3/water nanofluids volume fraction and temperature. Also, decreasing the nanoparticle size enhanced the thermal conductivity as well as the local heat transfer coefficient. For example, the enhancement in the thermal conductivity for 20 nm, 10 nm, and 3 nm was 23%, 28%, and 32%, respectively, while the enhancement of the local heat transfer coefficient was 55%, 62%, and 70% for 20 nm, 10 nm, and 3 nm, respectively, at 0.09 of volume fraction and 65°C. In the laminar flow regime, the change in the thermal boundary layer film thickness is small compared with that of the turbulent flow regime. Therefore,

the enhancement of the local heat transfer coefficient in the turbulent flow regime is larger than that of the laminar flow regime for all the experimental conditions. The maximum enhancement in the thermal conductivity was 32%, whereas the enhancement in the local heat transfer coefficient was 70% for 3 nm at 0.09 volume fraction and 65°C. The improvement in the local heat transfer coefficient, which is the ratio of the thermal conductivity to the film thickness, was larger than that in the thermal conductivity due to a decrease in the thermal boundary layer film thickness. The correlation of Xuan and Li (2003) which accounts for the nanoparticles, presence in terms of volume fraction, predicts our results well and their trends for the conditions studied at 65°C with the variation in nanoparticles volume fraction and size. It is worth mentioning that the improvement we obtained in the thermal conductivity and local heat transfer coefficient will enable thermal improvement of desalination processes.

Keywords: Heat transfer coefficient, Fe_2O_3 nanoparticles, Thermal conductivity, Thermal boundary layer film thickness, Nusselt number, thermal desalination processes

1. INTRODUCTION

Nanofluids are defined as the suspension of nanometer-sized particles (typically <100 nm) in base fluids such as water (W), ethylene glycol (EG), or engine oil. They possess superior thermo-physical properties than those of their base fluids [1-3]. Nanofluids have emerged as novel fluids during the last decade and have attracted much attention from researchers and scientists because of their unique chemical, physical, mechanical, and thermal properties. Nanofluids have the potential for several applications in a wide range of fields of science and engineering, such as cooling electronic circuits,

engine cooling, engine transmission oil, drilling, lubrication, solar refrigerator, solar water heating, thermal storage, mass transfer enhancement, and biomedical applications [4-6]. Because of the smaller sizes of nanoparticles (1-100 nm), they are considered as a candidate solution for minimizing erosion, sedimentation, and clogging that plagued the previously used or existing solid-liquid mixtures of larger particles [7]. Efforts have been made to employ nanofluids to enhance the heat transfer rate and energy efficiency of thermal conducting systems for various applications. For this, the most important feature observed in the literature using nanofluids has been the enhancement in liquid thermal conductivity [8-10]. Choi [11] carried out experiments on the energy-efficient heat transfer fluids using copper nanoparticles in water. He found that the nanoparticles enhance the thermal conductivity. It is worth mentioning that Choi used the hot-wire method (THW) for measuring the thermal conductivity of nanofluids. Furthermore, Choi and other researchers [12-15] reported that the thermal conductivity of the nanofluids depends on the thermal conductivity of the base fluid, volume fraction, shape and size of nanoparticles, flow regime, and operating temperature. Das et al. [16], Wen and Ding [17], and Li et al. [18] studied the effects of operating temperature on the thermal conductivity enhancement in great detail using a steady-state test facility in a vacuum chamber. The vacuum chamber had a pair of copper rods separated by an O-ring to form the test cell, which contained several thermocouples soldered into the copper bars to measure the heat flux and surface temperatures. Their results indicated that the thermal conductivity enhancement increases with increasing the operating temperature. Related to the effect of metallic nanoparticles on the thermal conductivity, the thermal conductivity of copper at room temperature is greater than that of water by a factor of about 700, and about a factor of 3000 greater than

that of engine oil. Even in liquid form, metals have much greater thermal conductivity than nonmetallic liquids. Subsequently, metal particles suspended in fluids are expected to show enhanced thermal conductivities relative to pure fluids [19]. The effect of the base fluid on the thermal conductivity enhancement was studied by Xie et al. [20], where the solid particles (Al_2O_3 nanoparticle) were de-agglomerating via an intensive ultra-sonication after mixing with deionized water, ethylene glycol, and engine oil which were used as base fluids, and then homogenizing the suspensions by magnetic force agitation. The results showed that the nanoparticle suspensions, containing a small amount of Al_2O_3, have substantially higher thermal conductivity than the base fluids. This enhancement in thermal conductivity is directly proportional to an increase in the volume fraction of Al_2O_3. Thermal conductivities of different nanofluids, such as TiO_2/water, TiO_2/ethylene glycol, Al_2O_3/water, and Al_2O_3/ethylene glycol, were compared with those of their corresponding base fluids, and in all cases, it was found that the nanofluids had a higher thermal conductivity than those of their respective base fluids [21]. Xie et al. [20] reported that the thermal conductivity of Al_2O_3/water nanofluid was found to increase proportionally with increasing nanoparticle concentration. This enhancement could be attributed to an increase in the active surface area due to existing suspending nanoparticles and the interaction and collision between particles. Lee et al. [22] measured the thermal conductivity for Al_2O_3/water nanofluid using the transient hot-wire method (THW). Their results indicated a 20% enhancement in thermal conductivity for nanofluids of Al_2O_3/water with a 4% volume fraction increase, which is much higher than that of non-nanofluid working fluids. Philip et al. [23] stated that the use of a ferrofluid such as Fe_3O_4 in kerosene with a volume fraction of 6.3% and an average size diameter of 6.7 nm enhances the thermal conductivity

of the fluid by 300%. Furthermore, Sundar et al. [24] studied Fe_3O_4-water nanofluid with a volume fraction of 2% and found that Fe_3O_4 causes nearly 50% enhancement of thermal conductivity at 60°C. According to Masuda et al. [25], TiO_2/water and γ-Al_2O_3/water nanofluids with the volume fraction of 4.3% were both found to have enhanced thermal conductivities, which were recorded to be 11% and 32%, respectively. Wang et al. [26] studied the effect of the particle volume fraction of CuO/ethylene glycol nanofluid over a range of 1–10% volume fraction of CuO powders by employing the one-dimensional steady-state parallel-plate technique and observed that with a volume fraction of just 15% CuO particles, the thermal conductivity increased significantly. Many studies have reported monotonic increases in the thermal conductivity with decreasing nanoparticle size [27-29]. Hong et al. [30] carried out a comprehensive experimental study of the thermal conductivity of the water-based iron oxide magnetite (Fe_3O_4) and hematite (Fe_2O_3) nanofluids at various volume fractions, temperatures, and the magnetic field strengths. The varies in the strength of the magnetic field cause the thermal conductivity ratio of the ferrofluid with respect to water without nanoparticles to increase from 15% to 38.5% and from 13% to 175% for magnetite and hematite nanofluids, respectively. A detailed summary of the thermal conductivity studies conducted in the last few years putting into consideration the factors that play a crucial role in enhancing the thermal conductivity of nanofluids is presented in Table 1.

One more important advantage of using nanofluid, as a result of the enhancement of thermal conductivity, is the improvement of the convective heat transfer coefficients. Considering this, most of the experimental research has been on metal oxide nanoparticles assisted heat transfer coefficient enhancement (For example: copper oxide, aluminum

oxide, titanium oxide, and silicon oxide) as summarized in Table 2. Farajollahi et al. [31] were able to show the increase in the overall heat transfer coefficient and Nusselt number for the nanofluids with increasing volume fraction (φ=1–3%) and Reynolds number when they investigated the convective heat transfer coefficient of γAl_2O_3/water and TiO_2/water nanofluids in a turbulent flow regime. It is worth mentioning that Farajollahi et al. (2010) have estimated the convective heat transfer coefficient by implementing energy balance around the test section with using the measured heat flux, mass flow rate, and inlet and outlet temperatures of nanofluids. Their results in terms of the Nusselt number were compared to that predicted by the correlation of Xuan and Li [32] below:

$$Nu_{nf} = 0.0059(1 + 7.6286\varphi^{0.6886} {pe_d}^{0.001}) {Re_{nf}}^{0.9238} {pr_{nf}}^{0.4} \quad (1)$$

where φ is volume fraction, *Nu* ($\frac{h.d}{k}$) is a Nusselt number, *Re* ($\frac{pvd}{\mu}$) is Reynolds number, *Pe* ($\frac{Lv}{D}$) is a Peclet number, and *Pr* ($\frac{C_p\,\mu}{K}$) is the Prandtl number of nanofluid. The results of Farajollahi et al. (2010) revealed that at 0.5 volume fraction of γ Al_2O_3 nanoparticles and 0.3 volume fraction of TiO_2 nanoparticles, good qualitative and quantitative agreement exist between the predicted values by Xuan and Li [32] and their experimental results. Wen and Ding [17] assessed the convective heat transfer coefficients of a segment of the length of γ-Al_2O_3/water nanofluids using a set of small thermocouples for the inner wall temperature measurements in the test section of a copper tube with 970 mm length and 4.5 mm inner diameter in the laminar flow regime under thermal boundary conditions of isoflux. They measured the nanofluid temperatures by using two thermocouples (T-type), which were inserted at the inlet and outlet of the test section. Five more thermocouples (T-type) were mounted on the test section at various axial positions in mm of 118 (T1), 285

(T2), 524 (T3), 662 (T4), and 782 (T5) from the inlet of the test section to measure the inner wall temperatures along the length of the test section. Wen and Ding [17] have measured the convective heat transfer coefficients of the segment of length of γ-Al_2O_3/water nanofluids with implementing the same approach of Farajollahi et al. [31]. The study demonstrated that such segment of length heat transfer coefficient in the entrance region was found to be 41% higher than that of the base fluid at the same flow rate. It was observed that the enhancement is particularly significant in the entrance region and decreases with axial distance. Particle migration was one of the reasons for the enhancement of the convective heat transfer coefficients. Also, there are more studies in the literature (summarized in Table 2) regarding the investigation of heat transfer coefficients for nanofluids.

It is worth mentioning that all the current experimental studies in the literature have estimated the overall and segment of length convective heat transfer coefficients by implementing the basis of energy balance across the test section with measuring the supplied heat flux, nanofluid temperatures (at the inlet and outlet of the test section), wall surface temperatures and physical properties of the nanofluid (density, viscosity, heat capacity, and thermal conductivity) with primitive techniques (thermocouples and DC power supply with digital reader). Unfortunately, this way of measuring the convective heat transfer coefficients neglect the effect of axial heating conduction along the solid wall of the test section as well as heat losses that could cause an error in the estimation of the heat transfer coefficients. Hence, Multiphase Reactors and Engineering and Applications Laboratory (mReal) at Missouri University of Science and Technology has designed and developed, for the first time, a noninvasive heat transfer coefficient probe [33-35] that is

flush wall mounted to simultaneously measure the local instantaneous heat flux through the heated foil sensor (flush mounted on the inner surface of test section) and its surface temperature by a thermocouple at the foil surface. The bulk temperature is measured by a thermocouple adjacent to the sensor. This method of measuring the heat transfer coefficients overcomes all the mentioned limitations in literature. Furthermore, by measuring the thermal conductivity (k) besides the local convective heat transfer coefficient (h) variations in the presence of nanoparticles, the thermal boundary layer film thickness can be obtained as follows:

$$\delta = \frac{k}{h} \tag{2}$$

where h is the local heat transfer coefficient, k is the thermal conductivity, δ is the thermal boundary layer thickness. This could help explain the change in h in terms of both k and δ. Such enhancement in forced convective heat transfer coefficients benefits many thermal processes, including the desalination thermal process. With an increasing need for fresh water around the world, the necessity for desalination of seawater and brackish water is becoming a primary environmental focus. One of the most common processes for desalination is the multi-stage flash (MSF) thermal desalination process. This process consists of three sections (brine heater, heat recovery, and heat rejection). The seawater is pumped through these three sections. After which, the heated seawater experienced flashing to generate distillate water. The focus of this work is then how to enhance the efficiency of heating the seawater using nanofluid during these three sections by enhancing its thermal conductivity, thermal film thickness, and hence enhancing heat transfer coefficients to the seawater while it is heated. To investigate the enhancement of the thermal performance of a new nanofluid that could lead to enhancement of the MSF, Fe_2O_3

nanoparticles have been selected. Fe_2O_3 nanoparticles were selected due to magnetic properties and superior thermal conductivity [36-38]. Due to their magnetic features, Fe_2O_3 nanoparticles will be easily separated and collected from the sections of MSF by using magnet arrangements. At this stage, deionized water has been used as a base for comparison since nanoparticles and water were used in the literature and related correlations were developed. This also will be used as a base for comparison when saline water will be used for future study in our laboratory. Hence, in the current study, Fe_2O_3 nanoparticles with deionized water are used. The research team at mReal has designed and developed, for the first time, a recirculation flow loop equipped with an advanced noninvasive heat transfer coefficient probe in conjunction with thermal conductivity meter to simultaneously measure the thermal conductivity and the local instantaneous heat flux, surface temperature, bulk temperature, and hence heat transfer coefficient. Three different sizes of Fe_2O_3 nanoparticles (3, 10, and 20 nm) have been used with a range of volume fractions for the current work under turbulent and laminar flow regimes (Reynold's number ranging from 1000 to 12000). This method of measuring the heat transfer coefficients overcomes all the mentioned limitations in literature and will be discussed in the section 2 for more details. By measuring the convective heat transfer coefficient and thermal conductivity, we explored the enhanced thermal performance of Fe_2O_3/water nanofluid that could lead to enhancing desalination thermal processes.

2. EXPERIMENTAL WORK

The experimental work consists of nanofluid preparation, measurement techniques, and experimental setup as discussed below.

2.1 NANOFLUID PREPARATION

In general, preparation of the nanofluids with suspension characteristics during the utilization is essential for successful use of nanofluids. Fe_2O_3 nanoparticles with three different diameters (3, 10, and 20 nm) (manufactured by Alfa Aesar, USA) were suspended with deionized water to prepare the nanofluids. Different volume fractions (ranging from 0.01 to 0.09 with an increment of 0.01) of Fe_2O_3 nanoparticles were mixed with the deionized water using IKA ULTRA-TURRAXR T-25 Digital Homogenizer at 5000 rpm for 45 min to ensure complete dispersion of the nanoparticles in the base fluid. Then, an ultrasonic bath (manufactured by Fisher Scientific, USA) was used to break down the finer nanoparticle aggregates for 60 min. The settling did not occur after one day of sample preparation. To validate this, a stability test was conducted by taking a sample of nanofluids after one day of nanofluid preparation at 25^{o}C and analyzing it by a Zetasizer instrument (manufactured by Malvern Instruments) to determine the zeta potential, which indicates the stability of Fe_2O_3/water nanofluids. The results showed that zeta potential values of Fe_2O_3/water nanofluids were 40, 38, and 35 mV for 3, 10, and 20 nm, respectively, for one hour of ultrasonication. The stability of Fe_2O_3/water nanofluids is physically stable without any observable sedimentation for one month, as shown in Figure 1. This finding matches with the literature [22].

2.2 MEASUREMENT TECHNIQUES

2.2.1 Thermal Conductivity Meter. For thermal conductivity measurement, a Transient Line Source (TLS-100) probe for analyzing thermal properties (Thermtest Inc., Canada) was used with an operating range of (0.1–5 W/m.k). The TLS-100 instrument

consists of a digital handset controller and needle sensor, which is inserted vertically into the nanofluid sample medium. TLS-100 has a single-needle sensor, which is 100 mm in length and 2.0 mm in diameter and is connected to a digital handset microprocessor for measuring the thermal conductivity of the nanofluids. The accuracy and reproducibility of the TLS-100 probe was found better than 5% and 2%, respectively (supplied by the manufacturer). The measurements were recorded for various samples at different temperatures (25–65 ^{o}C) by inserting the sensor probe into the sample container. The measurements were carried out for different nanoparticle volume fractions (0.01–0.09 %). The meter was calibrated before the measurements using standard solutions of known thermal conductivity such as ASTM-D5334 standard (recommended and supplied by the manufacturer). To obtain measurements with higher reliability, the experiment was repeated five times for each sample, and each temperature and the average values were taken for analysis.

2.2.2 The Noninvasive Flush-Mounted Heat Transfer Coefficient Probe. An advanced noninvasive heat transfer coefficient probe has been designed and developed in our laboratory to measure simultaneously the local heat transfer coefficient and wall surface temperature of the sensor. The heat transfer coefficient probe consists of a micro-foil sensor (6.35 mm x 17.78 mm x 0.08 mm) that **is** flush mounted on the inner wall surface of the test section (175 mm in an axial distance from the entrance of the test section) using high-temperature glue. The micro-foil sensor has a fast response time of about 0.02 sec and thermal resistance of 0.173 cm °C/W, and has two components: thermocouple and a heat flux foil sensor, as shown in Figure 2. Therefore, this micro-foil sensor has been used in the current work to measure both the surface temperature of the sensor and the local heat

flux between the sensor and adjacent fluid. In addition to that, a probe containing two (T-type) thermocouple sensors (1.6 mm in diameter) were mounted at the front of the heat transfer foil sensor, as shown in Figure 2. The axial position of the two thermocouple sensors were mounted at x1 = 150 mm (Tb1) and x2 = 200 mm (Tb2), and the average value of the temperatures along the test section obtained by these thermocouples was taken as the characteristic bulk temperature which was measured with and without Fe2O3 nanoparticles in the test section. A small cartridge heater, as a source of heat for the heat flux foil sensor, was installed at the outer surface of the test section behind the flushed-mounted foil sensor (Figure 2). The DC power was supplied to the cartridge heater through a variac to regulate the supplied power in the range of 0–50 V. The local heat transfer coefficient can be obtained by measuring simultaneously the surface temperature of the sensor, the flowing characteristic bulk temperature, and the local instantaneous heat flux between the surface of the sensor and the adjacent fluid.

The local instantaneous heat transfer coefficient (h_i) and the local time-averaged heat transfer coefficients (h_{avg}) can be estimated by the following relations:

$$h_i = \frac{q_i}{T_{s,i} - T_{b,i}} \tag{3}$$

$$h_{avg} = \frac{1}{n}\sum_{i=1}^{n}\frac{q_i}{T_{s,i} - T_{b,i}} = \frac{1}{n}\sum_{i=1}^{n} h_i \tag{4}$$

where h_i: local instantaneous heat transfer coefficient (kW/m^2.k), q_i: instantaneous heat flux measured by the sensor (kW/m^2), T_{si}: instantaneous surface temperature of the probe (K), T_{bi}: instantaneous bulk temperature of the media (K), h_{avg}: local time-averaged heat transfer coefficients (kW/m^2.k), and n: is the number of the collected data points (2000

data points). It is worth mentioning that the current experimental studies in the literature have estimated only the overall and the segment of length convective heat transfer coefficients by implementing the basis of the energy balance across the test section with implementing thermocouples and DC power supply. This way of measuring the heat transfer coefficients neglects the effect of axial heating conduction along the solid wall of the test section, as well as heat losses. Hence, the developed heat transfer coefficient probe at mReal, in this study, overcomes all the limitations in the literature and provides more reliable measurements.

2.2.3 Data Acquisition (DAQ) System. The data acquisition (DAQ) system (NI SCXI-1303, USA) of a combination of chassis with the controller and chassis power card, one amplifier, and a computer were used for the data collection and analysis. The DAQ system uses LabVIEW software. The measured signals of the heat flux were in the range of microvolts, and hence, an amplifier was used to amplify the measured signals before being processed by the DAQ system. The measured signals from the heat flux sensor as well as thermocouples were sampled at 50 Hz for about 40 seconds simultaneously. To obtain results that are more reliable and to quantify the experimental error, the experiment was repeated three times.

2.3 EXPERIMENTAL SETUP

The picture and schematic diagram of the current experimental setup for measuring the local heat transfer coefficient are exhibited in Figures 3 and 4, respectively. The experimental setup consists of a closed flow loop made from a straight copper tube with 950 mm length, 25.4 ± 0.02 mm inner diameter, and 31 ± 0.05 mm outer diameter

connected to a reservoir tank and circulating pump. The loop has a test section of a length 400 mm and 25.4 mm inner diameter where the measurements are performed throughout this test section. In addition, the test section mainly contains two thermocouples (T-type) and a heat flux foil sensor attached to a heater. The test section surface is heated using a small cartridge heater (120V AC, 6.35 mm diameter, 38 mm length, and 150 W) to provide the heat through the sensor. The DC power supply (HY5003), which was manufactured by RSR Electronics, USA, was used to provide the required power to the cartridge heater through a variac to regulate the supplied power. Also, the test section is surrounded by a ceramic fiber blanket to minimize the heat losses to the environment. Two T-thermocouples (Model TQSS-18G-6- Omega Engineering Inc. USA) are inserted into the flow section at the inlet and outlet of the horizontal test section to measure the bulk temperature. The micro-foil sensor from RdF Corporation (model no 27036-1) was flushed mounted on the inner wall surface of the test section at a distance x = 125 mm from the entrance of the test section. Therefore, this micro-foil sensor can measure both the local heat flux (magnitude and direction) and the surface temperature. A magnetic drive pump (Procon, USA) was used to circulate the nanofluid through the test section. The flow rate was measured by a turbine flowmeter (TM050, GPI, USA) in a range from 1 to 6 L/min. Two adjusting valves, one at the main flow loop and the other at the bypass line, control the flow rate. All readings during the experimental runs in terms of the heat flux, surface temperature, and bulk temperature were collected by a DAQ system and were processed in a computer.

3. RESULTS AND DISCUSSION

3.1 EFFECTS OF PARTICLE VOLUME FRACTION, NANOPARTICLE SIZE, AND TEMPERATURE ON THE THERMAL CONDUCTIVITY

The measured thermal conductivity of the nanofluid is normalized with respect to the thermal conductivity of the base fluid. This has been used here to present the results. Figures 5–7 show the relationship between the thermal conductivity ratio of the nanofluid to the base fluid (k_{nf}/ K_{bf}) and the volume fraction of Fe_2O_3/water nanofluid at various experimental temperatures of 25°C, 45°C, 55°C, and 65°C for different nanoparticle sizes (3, 10, 20 nm). It is clear from Figures 5–7 that the thermal conductivity ratio (k_{nf}/ K_{bf}) increases with increasing particles volume fraction. It is also apparent that even at the lowest volume fraction, the thermal conductivity of Fe_2O_3 nanofluid was higher than that of the base fluid (i.e., water) and as these volume fractions were increased, enhancements of the thermal conductivity were observed. This observation is consistent with Wu et al. [39], who studied the effect of volume fraction of Fe_3O_4/water nanofluid on the thermal conductivities. The thermal conductivity of the water without the addition of Fe_2O_3 nanoparticles at 25°C was measured to be 0.595 W/m.K; however, after the addition of the Fe_2O_3 nanoparticles (0.09 vol.%) to water, the thermal conductivity was increased to be 0.679, 0.708, and 0.735 W/m.K at 25°C for 20, 10, and 3 nm, respectively. This enhancement in thermal conductivities of Fe_2O_3 nanofluid was attributed to an increase in the active surface area of the nanoparticles as well as the interaction and collision between particles [32]. Furthermore, Figures 6–8 show the dependence of thermal conductivity on the temperature for various volume fractions and nanoparticle sizes. It was found that the thermal conductivity of Fe_2O_3/water nanofluid, in terms of thermal conductivity ratio (k_{nf}/

K_{bf}), increases with increasing the temperature. This enhancement in the thermal conductivity could be attributed to the Brownian motion [40]. This motion gives the particles the ability to move randomly in solution and interact with all possible neighboring particles and subsequently increase the thermal conductivity. This observation is also consistent with previous studies in the literature, even for different nanofluids (i.e., Al_2O_3 or CuO nanofluids) [13, 17, 41]. On the other hand, one can remark that the thermal conductivity of the Fe_2O_3/water nanofluid increases with decreasing the size of the nanoparticles, as shown in Figures 5–7. The results showed that 3 nm Fe_2O_3 in water has achieved the highest thermal conductivity enhancement among the other nanoparticle sizes (10 nm and 20 nm) for all experimental conditions. The thermal conductivity is enhanced by 23%, 28%, and 32% for 20, 10, and 3 nm, respectively, at 0.09 vol% for 65 ^{o}C. This increase in the thermal conductivity with decreasing the nanoparticle size could be attributed to micro-convection around nanoparticles as a result of Brownian motion [40, 42, 43]. It is worth mentioning that the relative enhancement in thermal conductivity was significant at a high experimental temperature (65 ^{o}C).

3.2 COMPARISON OF THERMAL CONDUCTIVITY MODELS WITH EXPERIMENTAL DATA

In this study, the experimental thermal conductivity data are combined to provide a meaningful comparison with theoretical models (Maxwell model [44] and Lu and Lin model [45]) that were reported in the literature. These two models are applicable for low volume-fraction mixtures of liquid-solid suspensions of monodisperse spherical particles, which match with the current conditions [24]. The Maxwell model is as follows:

$$\frac{k_{nf}}{k_{bf}} = \frac{k_p + 2k_{bf} + 2(k_p - k_{bf})\emptyset}{k_p + 2k_{bf} - (k_p - k_{bf})\emptyset} \quad (5)$$

where the particle volume fraction and the thermal conductivity of the basefluid (i.e., subscript *(b_f)*) and the particle (i.e., subscript (*p*)) were represented by $\emptyset$, k_{bf} , and k_p, respectively. This model assumes a spherical shape for the discontinuous phase and that the thermal conductivity of nanofluids depends on the base fluid type, particle volume fraction, and the thermal conductivity of spherical particles. The Lu and Lin model is expressed as follows:

$$\frac{k_{nf}}{k_{bf}} = 1 + a\,\emptyset + b\,\emptyset^2 \quad (6)$$

Where a = 2.25 and b = 2.27. It is obvious that the Maxwell and Lu and Lin models are nonlinear. However, with a narrow range of low volume fraction of nanoparticles (ranging from 0.01 to 0.09 with an increment of 0.01), these models show an approximation to a straight line trend. Results are presented for all experimental conditions. Figures 8–10 show the comparison of the current experimental results of the thermal conductivity ratio for Fe_2O_3/water nanofluid with theoretical models as a function of particle volume fraction and nanoparticle size at 25°C, 45°C, and 65°C. The deviation between the current experimental and predicted results from the models is presented in terms of the average absolute relative error (AARE). The results showed a qualitative and quantitative similarity between the current experimental data and predicted values from the theoretical models for all experimental conditions, as shown in Figures 8–10 and Table 3. It is clear from the results that the current experimental data deviate from the predictive models with increasing the operating temperature. This deviation could be attributed to the assumptions

of these models, which are based on the room temperature. Under the current experimental conditions, the maximum deviation in terms of AARE observed was 12.6% for 65ºC at 3 nm.

3.3 LOCAL CONVECTIVE HEAT TRANSFER COEFFICIENTS OF Fe_2O_3/WATER NANOFLUIDS

3.3.1 Effect of Nanoparticle Volume Fraction and Flow Regime. The local heat transfer coefficients of Fe_2O_3 nanofluid under isoflux thermal conditions has been investigated at 25ºC and 65ºC for two different flow regimes (laminar and turbulent) at different nanoparticle sizes (3, 10, and 20 nm) and volume fraction (0.02, 0.04, 0.06, and 0.09). Figures 11–19 show the variations of the local heat transfer coefficients with Reynolds-number $R_e = \frac{p_{nf} v d}{\mu_{nf}}$, $p_{nf} = (1 - \emptyset)\, p_{bf} + \emptyset\, p_p$, and $\mu_{nf} = (1 + 2.5\emptyset)\mu_{bf}$ at different experimental conditions for Reynolds number ranging from 1000 to 12000. It is found that the local heat transfer coefficients increase with increasing the volume fraction and temperature, but also increase with decreasing the nanoparticle size for all experimental conditions. The highest volume fraction employed in this study was 0.09 vol. % Fe_2O_3 nanoparticles, which led to 70% enhancement in the local heat transfer coefficient for 3 nm. It is generally understood that the enhancement of the heat transfer coefficient depends on the thermal conductivity of fluid and thermal boundary layer film thickness. The heat transfer coefficient has been defined as $h = \frac{k}{\delta}$. The increase in thermal conductivity and/or the decrease in the film thickness enhances the local convective heat transfer coefficient of the Fe_2O_3/water nanofluids. However, the increase in the viscosity increases the thermal boundary layer film thickness and hence reduces the *h* if *k* remains unchanged or slightly varies. Our results show that with using nanofluid, the heat transfer

coefficient increases due to an increase in the thermal conductivity and a reduction in the thermal boundary layer thickness, as shown in Table 4. In the laminar flow regime, the change in the thermal boundary layer film thickness is small compared with that of the turbulent flow regime. Therefore, the enhancement of the local heat transfer coefficient in the turbulent flow regime is higher than that of the laminar flow regime for all experimental conditions, as shown in Table 4. The heat transfer coefficient enhancement values were obtained from Equation (6) below:

$$\text{Heat transfer coefficient enhancement} = \left(\frac{h_{nf} - h_{bf}}{h_{bf}}\right) x\ 100. \quad (7)$$

Tables 4-12 show an enhancement of the thermal conductivity and local heat transfer coefficient for Fe_2O_3/water nanofluids of 20 nm, 10 nm, and 3 nm (at 25°C and 65°C for laminar and turbulent flow regimes). The results clearly state that the enhancement of the local convective heat transfer coefficients of Fe_2O_3/water nanofluids was due to the increased thermal conductivity. Thermal conductivity was more dominant of an effect than thermal boundary layer film thickness of the nanofluids. It is clear that the thickness of the film is larger than the sizes of the nanoparticles used. This allows the nanoparticles to penetrate the film and into the wall, which creates within the film micro eddies and local mixing. Thus, this also contributes to the enhancement of the local heat transfer coefficient. Other possible contributing factors to the local heat transfer coefficient enhancement of nanofluids as suggested by some research groups are that in turbulent flow, nanoparticles migrate toward the tube wall (into the boundary layer) due to the Brownian motion and thermophoresis [46, 47]. On the other hand, the results showed a significant increase in local heat transfer coefficient of nanofluids with Reynolds number. In addition,

at a constant Reynolds number, the local heat transfer coefficient was found to increase with increasing the nanoparticle volume fraction. As shown from Figures 11–19, a remarkable increase in heat transfer coefficient was observed by the addition of nanoparticles to the water base fluid. It is well known that the flow characteristics of the fluid affect the convective heat transfer to a greater extent. Increasing the flow rate induces eddies in the flow, which ultimately help in increasing the heat transfer coefficient. Also, the results showed that the 3 nm Fe_2O_3 in water at 65°C under turbulent flow regime achieved the highest local heat transfer coefficient among the other nanoparticle sizes (10 nm and 20 nm) for all experimental conditions. The local heat transfer coefficient is enhanced by 55%, 62%, and 70% for 20, 10, and 3 nm, respectively, at 0.09 vol.% for 65°C.

3.3.2 Effects of Nanoparticle Size. Figures 20–22 and Table 13 show the effect of nanoparticle size on the local heat transfer coefficient (h). Three different nanoparticle sizes of iron oxide (3, 10, and 20 nm) have been used at 25°C and 65°C under laminar and turbulent flow regimes. In the laminar and turbulent flow regimes of 0.09% volume fraction nanoparticles at 25°C, Figures 20 and 21 show that there is no effect of nanoparticle sizes on the heat transfer coefficients (Table 13). However, in the turbulent flow regime at 65°C using 0.09% volume fraction nanoparticles, the 3 nm nanoparticle size has larger heat transfer coefficients with respect to 20 nm with 8.5% difference as shown in Figure 22 and Table 13. The percentage differences between heat transfer coefficients are lower for nanofluids between 3 nm and 10 nm, and between 10 nm and 20 nm are lower (4.2% and 4.3%, respectively). Hence, it is expected that the percentage difference should be small between 20 nm and larger sizes such as 30 nm, which has usually been used in the literature

and recommended for practice due to the cost and their practical implementation. This indicates that when the nanoparticle sizes become very small, the effect of such small size on the heat transfer coefficients would be relatively larger than the larger size nanoparticles. However, larger nanoparticle sizes (~10 nm – 60 nm) have been used in the literature investigation since they are more practical to be implemented in practice as compared to the smaller size nanoparticles where the cost of their preparation increases significantly with reduction in sizes.

3.3.3 Comparison Between the Experimental Convective Heat Transfer Coefficients and the Predicted Values from Literature Correlations. There are many empirical correlations reported in the literature to predict the convective heat transfer data using nanofluids under forced convection (Table 2). The following correlations have been selected in this study since they were developed based on investigating the effects of nanofluids on convective heat transfer coefficient under operating conditions similar or close to this study:

$Nu = 0.4328(1 + 11.285\ \emptyset^{0.754} Pe^{0.218}) Re^{0.333} Pr^{0.4}$ Xuan and Li correlation for laminar[32] (8-a)

$Nu = 0.0059(1 + 7.6286\ \emptyset^{0.6886} Pe^{0.001}) Re^{0.9238} Pr^{0.4}$ Xuan and Li correlation for turbulent (8-b)

$Nu = 0.012\ (Re^{0.87} - 280)\ Pr^{0.3}$ Gnielinski correlation [31] (9)

$Nu = 0.023\ Re^{0.8} Pr^{0.3}$ Dittus-Boelter correlation [48] (10)

where $\emptyset$ is the percentage of the volume fraction, $Nu\ (\frac{h.d}{k})$ is a Nusselt number, $Re\ (\frac{pvd}{\mu})$ is Reynolds number, $Pe\ (\frac{Lv}{D})$ is a Peclet number, and $Pr\ (\frac{C_p\ \mu}{K})$ is the Prandtl number of nanofluid. The relationships between Nusselt number and Reynolds number for Fe_2O_3/water nanofluid are shown in Figures 23–28 for the selected conditions of 25^{o}C and 65^{o}C and at 3 nm, 10 nm, and 20 nm for Reynolds number ranging from 1000 to 12000.

Correlation of Xuan and Li [32] (Equations 8-a and 8-b) gives better predictions of our results compared to the correlations above (Equations 9 and 10). This is because the correlation of Xuan and Li [32] accounts for the presence of nanoparticles in terms of the percentage of the volume fraction ($\emptyset$). In this case, to predict our results well by the Xuan and Li [32] correlation, $\emptyset$ in Equations 8-a and 8-b needs to be a substitute as a percentage of volume fraction. This means that for $\emptyset = 0.09\%$, the value of 0.09 needs to be substituted in the above mentioned correlations. Thus, Xuan and Li [32] correlation (Equation 8-b) predicts our results well at 65^{o}C at turbulent flow regime for 3, 10, and 20 nm nanoparticles with the average absolute relative differences (AARD) of 8.1%, 8.6%, and 10.5%, respectively as shown in Figures 23, 24, and 25. However, at 25^{o}C, the AARD of Xuan and Li [32] correlations for laminar and turbulent flow regimes (Equation 8-a and 8-b) are 15.6%, 21.5%, and 29.2% for 3 nm, 10 nm, and 20 nm, respectively which are larger than those at 65^{o}C with proper trend as shown in Figures 26, 27, and 28. This is due to the change in physical properties for which the correlations favored the modified properties at high temperature. For lower temperature and/or for a wide range of temperatures, the correlation needs further adjustment to the constant or modification. It is worth mentioning that the correlation of Jung et al. [60] (Equation 11) for laminar flow regime only includes the volume fraction of the nanoparticles:

$$Nu = 0.014\emptyset^{0.095}Re^{0.4}pr^{0.6}. \quad (11)$$

Hence, it is worth assessing its predictions against our experimental values for laminar flow regime. It has been found that the average absolute relative difference (AARD), between the predictions of Jung et al. [60] (Equation 11) and our experimental data is about 38%, which is larger than that of Xuan and Li [32] correlation (Equation 8-

a). This could be due to the use of larger nanoparticle size of 170 nm in a rectangular microchannel of 50µm x 50µm.

4. REMARKS

An advanced non-invasive heat transfer coefficient probe that is flush mounted on the inner wall surface of the test section was developed and employed, for the first time, to measure simultaneously the local heat transfer coefficient and wall surface temperature in conjunction with the thermal conductivity measurements. Due to a magnetic characteristic of Fe_2O_3 nanoparticles, these have been selected for improving the thermal efficiency of desalination since they can be collected by magnet and reuse. Hence, the effects of Fe_2O_3/water nanofluid on thermal conductivity and local heat transfer coefficients have been studied using 0.01–0.09 vol.% of different sizes (3, 10, and 20 nm) nanoparticle at different temperatures (25, 45, and 65°C) in laminar and turbulent flow regimes. The findings demonstrate the potential of improving the thermal efficiency and hence the performance of the desalination thermal processes which will be further studied in subsequent manuscripts from our research group. The deduced remarks of the current work are as follows:

- The thermal conductivity and local heat transfer coefficient increased with the increase of the Fe_2O_3/water nanofluids volume fraction and temperature.
- Decreasing the nanoparticle size enhances the thermal conductivity as well as the local heat transfer coefficient. For example, the enhancement in the thermal conductivity for 20nm, 10 nm, and 3 nm are 23%, 28%, and 32 %, respectively.

While the enhancement in the local heat transfer coefficient was 55%, 62%, and 70 % for 20 nm, 10 nm, and 3 nm, respectively at 0.09 vol.% and 65°C.

- The local heat transfer coefficients of Fe_2O_3/water nanofluid improved with Reynolds number compared with that of a base fluid at the same Reynolds number. For instance, by increasing the Reynolds number from 2000 to 12000, the local heat transfer coefficients increase by 24% and 70%, respectively for 3 nm at the highest volume fraction (0.09 vol. %) of Fe_2O_3/water nanofluid.
- In the laminar flow regime, the change in thermal boundary layer film thickness is small compared with the turbulent flow regime. Hence, the enhancement of the local heat transfer coefficient in the turbulent flow regime is larger than that of the laminar flow regime for all experimental conditions. Such as, with 20 nm nanoparticles, the thermal boundary layer film thickness for laminar and turbulent flow regimes decreased by 3% and 21%, respectively. However, the local heat transfer coefficient increases from 17% to 45% of 0.09 vol.% at 25°C.
- In the turbulent flow regime at 65^{o}C using 0.09 vol.%, the 3nm nanoparticle size has larger heat transfer coefficients with respect to 20 nm with 8.5% difference. The percentage differences between heat transfer coefficients of nanofluids 3 nm and 10 nm, and between 10 nm and 20 nm are lower (4.2% and 4.3%, respectively).
- The results indicate that when the nanoparticle sizes become very small, the effect of such small size on the heat transfer coefficients would be relatively larger than the larger size nanoparticles. However, larger nanoparticle sizes (~10 nm – 60 nm) have been used in the literature investigation since they are more practical to be

implemented in practice as compared to the smaller sizes nanoparticles where the cost of their preparation increases significantly with reduction in sizes.

- The experimental results in terms of the Nusselt number at 65°C were found to be in good agreement with the predicted values by Xuan and Li correlation (Equations 8-b) for turbulent flow regime**.** It was found average absolute relative differences (AARD) of 8.1%, 8.6%, and 10.5%, for 3, 10, and 20 nm nanoparticles, respectively, this could be attributed to the accounting for the presence of the nanoparticle in terms of volume fraction percentage that is not accounted for in the other correlations (Gnielinski and Dittus-Boelter) (Equations 9 and 10).
- Xuan and Li [28] predictions at 25^{o}C have larger AARD of 15.6%, 21.5%, and 29.2 % for laminar and turbulent flow regimes compared to those at 65^{o}C. This could be due to the effect of the physical properties and hence, these correlations need to be adjusted for their constants or modified.
- The maximum enhancement in the thermal conductivity is 32%, whereas the enhancement in the local heat transfer coefficient was 70% for 3 nm nanoparticles of 0.09 vol.% at 65°C. The enhancement of the local heat transfer coefficient was larger than that in the thermal conductivity due to also the decrease in the thermal boundary layer film thickness by 25%.
- The results indicate that the improvement we obtained in the thermal conductivity and local heat transfer coefficient will enable thermal improvement of desalination processes.

ACKNOWLEDGMENT

The author (Zouli) would like to thank the colleagues at Multiphase Reactors Engineering and Application Laboratory (mReal), Chemical and Biochemical Engineering Department at Missouri University of Science and Technology (Missouri S&T), Rolla, Missouri (USA), for providing help while conducting experiments. The author (Zouli) also would like to thank the University of Jazan for giving him the financial support.

NOMENCLATURE

D	tube diameter [m]	*Greek symbols*	
C_p	fluid heat capacity [J/kg K]	α	fluid thermal diffusivity [m^2/s]
h	heat transfer coefficient [W/m^2 k]	δ	thermal boundary layer thickness [m]
K	thermal conductivity [W/m K]	μ	fluid dynamic viscosity [$N.s/m^2$]
AARE	average absolute relative error	ρ	fluid density [kg/m^3]
Nu	Nusselt number [-]	∅	Volume fraction [-]
Re	Reynolds number [-]		
Pe	Peclet number [-]	*Subscript*	
Pr	Prandtl number [-]	bf	base fluid
q_i	heat flux [W/m^2]	nf	Nanofluids
n	Empirical shape factor [-]	p	Particle
T	Temperature [K]	s	surface
v	fluid velocity [m/s]	b	bulk

Table 1: Summary of the experimental studies of the thermal conductivity enhancement using nanofluids

Reference	Particle Type	Base Fluid *	Particle Size (nm)	Particle Volume Fraction (%)	Method	Maximum Enhancement (k) (%)	Temperature range
Masuda et al.[25]	Al_2O_3 TiO_2 SiO_2	Water	13 27 12	1.3 – 4.3 3.1 – 4.3 1.1 – 2.4	Transient hot wire	32.4 10.8 1.1	31 – 87 ºC
Wang et al. [26]	Al_2O_3 Al_2O_3 CuO	Water / EG EO / PO Water / EG	28 28 23	3.00 –5.5 / 5 -8 2.25 –7.4 /5-7.1 4.5–9.7/6.2-14.8	Transient hot wire	16/41 32/20 34/54	Room temperature
Lee et al. [49]	Al_2O_3 CuO	Water / EG	38.4 23.6	1–4.30 / 1–5 1–3.41 / 1–4	Transient hot wire	10/18 12/23	Room temperature
Eastman et al. [12]	Cu	EG	<10	0.01–0.56	Transient hot wire	41	Room temperature
Das et al. [13]	CuO Al_2O_3	Water	28.6 38.4	1.0 – 4.0 1.0 – 4.0	Temperature oscillation	36 24	21 – 51 ºC
Li and Peterson. [18]	CuO Al_2O_3	Water	29 36	2.0 – 6.0 2.0 -10.0	Transient hot wire	51 29	28.9 – 33.4 ºC 27.5 – 34.7 ºC
Ding et al. [50]	MWCNT	Water	40	0.05-0.49	Device KD2 Thermal analyzer	79	20 – 30 ºC
Hong et al. [30]	Fe	EG	10	0.10–0.55	Transient hot wire	18	Effect of clustering was investigated.
Turgut et al. [15]	TiO_2	Water	21	0.2 – 3.0	3ω hot-wire	7.4	13 – 55 ºC
Mintsa et al. [14]	CuO Al_2O_3	Water	29 36/47	0 – 16 0 – 18	Device KD2 Thermal analyzer	24 31/31	20 – 48 ºC
Beck et al. [51]	Al_2O_3 Al_2O_3	Water EG	8-282 12-282	1.86–4.0 2.0–3.01	Transient hot wire	20 19	Effect of particle size was examined.
Kwek et al. [52]	Al_2O_3	Water	25	1 – 5	Transient hot wire	6 / 20	25 ºC
Suresh et al. [53]	CuO	Water	15	0.1 – 0.3	KD2 thermal property meter	20	27 ºC
Fedele et al.(2012) [54]	TiO_2	Water	76	0.2 – 11	TPS 2500 S (Hot Disk)	38	20 - 80 ºC
Sundar et al. [55]	Fe_3O_4	Water	13	0 -2	Transient hot wire	48	20 - 60 ºC
Manikandan and Rajan. [56]	MgO	propylene glycol	30-40	0 - 2	KD2 thermal property meter	20	30 ºC
Mahbubul et al.[57]	Al_2O_3	Water	13	0.5	KD2 thermal property meter	32	10 - 50 ºC

Table 1: Summary of the experimental studies of the thermal conductivity enhancement using nanofluids (cont.)

Reference	Particle Type	Base Fluid *	Particle Size (nm)	Particle Volume Fraction (%)	Method	Maximum Enhancement (k) (%)	Temperature range
Solangi et al.[58]	Graphene	Water		0.025 – 0.1	KD2 thermal property meter	20 / 32	25 - 50 ºC
Agarwal et al. [59]	Al_2O_3	Water / EG	53	0 – 2	KD2 thermal property meter	30 / 31	10 - 70 ºC
Nikkama and Toprakb [60]	Ag	EG Water / EG Water	25	1 - 2	Transient hot wire	10 12.4 7	20 ºC

Table 2: Summary of the experimental studies of the convective heat transfer coefficient using nanofluids

Reference	Nanoparticles	Base fluid	Particle size	Volume fraction (vol %)	Dimension	Flow regime	Correlations	Remarks
Pak and Cho.[61]	γAl_2O_3/ TiO_2	Water	13/27nm	1–3	ID: 1.066cm Length: 480 cm S.S. tube	Turbulent	$Nu = 0.21Re^{0.8}pr^{0.5}$	Nu increases with increase in φ and Re
Xuan and Li.[32]	Cu	Water	<100nm	0.3, 0.5, 0.8,1, 1.2, 1.5, 2	ID: 10mm Length: 800mm Brass tube	Turbulent	$Nu = 0.0059(1 + 7.6286Ø^{0.6886}pe^{0.0}$ $Re^{0.9238}pr^{0.4}$	Conv. HTC increases with increase in φ and flow velocity
Xuan and Li.[32]	Cu	Water	26nm	0.5, 1, 1.5, 2	ID: 10mm Length: 800mm Brass tube	Laminar	$Nu = 0.4328(1 + 11.285Ø^{0.754}pe^{0.21}$ $Re^{0.333}pr^{0.4}$	Nu ratio varies from 1.06 to 1.39 when w increases from 0.5 to 2%
Wen and Ding.[17]	γAl_2O_3	Water	26-56nm	0.6, 1, 1.6	ID: 4.5mm Length: 970mm Copper tube	Laminar	No correlation	For φ= 1.6%, the HTC is 41% higher than the base fluid
Yang et al. [62]	Graphite	Oil	20-40nm	0.7–1.0	ID: 4.57mm Smooth tube	Laminar	$Nu = cRe^m pr^{\frac{1}{3}}(\frac{D}{L})^{\frac{1}{3}}(\frac{\mu_b}{\mu_\infty}$	HTC is 22% higher at 50 ºC and is 15% higher at 70 ºC for 2.5 wt%. c and m are nanofluid and temperature dependent empirical parameters.
Ding et al. [50]	MWCNT	Water	100 nm	0.1–1.0	ID: 4.5mm Length: 970mm Copper tube	Laminar	No correlation	350% enhancement
\Williams et al. [65]	$A1_2O_3$ ZrO_2	Water	46nm 60nm	0.9–3.6 0.2–0.9	OD: 1.27cm Thick.=1.65mmS.S. tube	Turbulent	No correlation	Considerable heat transfer enhancement is observed
Jung et al. [66]	$A1_2O_3$	Water	170nm	0.5–1.8	Rectangular microchannel(50μmx 50μm)	Laminar	$Nu = 0.014Ø^{0.095}Re^{0.4}$	Conv. HTC increases by 32

Table 2: Summary of the experimental studies of the convective heat transfer coefficient using nanofluids (cont.)

Lai et al. [67]	$A1_2O_3$	Water	20nm	0–1	ID: 1mm S.S. tube	Laminar	No correlation	Nu enhancement is of 8% for φ= 1%. $A1_2O_3$ nanofluid at Re = 270
Farajollahi et al. [12, 31]	γAl_2O_3/ TiO_2	Water	25/10nm	0.3-2 0.15-0.75	ID: 55.6 mm Length: 815mm S.S. tube	Turbulent	No correlation	Overall heat transfer coefficient of nanofluids increases significantly with Peclet number.
Nasiri et al. [68]	TiO_2/ γAl_2O_3	Water	10/25nm	0.1-1.5	ID: 10 mm Length: 2100mm S.S. tube	Turbulent	No correlation	Nusselt number of nanofluids is higher than that of the base fluid
Anoop et al. [69]	Sio_2	Water	20nm	0.2-1	Microchannel	Laminar	No correlation	The heat transfer increases with flow rate for both water and nanofluid samples
Wu et al. [70]	γAl_2O_3	Water	40nm	0.78-7.04	Copper tube	Laminar-Turbulent	No correlation	The heat transfer enhancement of the nanofluids is from 0.37% to 3.43% compared to water
Vermahmoudi et al. [71]	Fe_2O_3	Water	40nm	0.15,0.4, 0.65	Length: 385 mm aluminum	Laminar	No correlation	The heat transfer coefficient increases with the increasing volume concentration of nanoparticles
Sun et al. [72]	Fe_2O_3	Water	50nm	0.1 – 0.4	ID: 8.66 mm Length: 1400 mm Copper tube	Laminar	No correlation	The heat transfer coefficient increases with the increase Re
Solangi et al.[58]	Graphene	Water		0.025 – 0.1	ID: 4 mm Length: 1500 mm Copper tube	Turbulent	No correlation	Nusselt number and friction factor of the nanofluid increases with increase particle volume concentration and Reynolds number
Sha, Ju et al. [36]	Fe_3O_4	Water	20nm	0.5 - 3	ID: 3 mm Length: 600 mm Copper tube	Turbulent	No correlation	The heat transfer coefficient increases with the increase the temperature and volume concentration
Masoudeh and Willing [73]	CuO	Water	40nm	0.25 - 1	ID: 4.8 mm Length: 1095 mm Copper tube	Laminar/ Turbulent	No correlation	The heat transfer enhancement

Table 3: AARE between the experimental data and theoretical models for thermal conductivity measurements. ($\boldsymbol{AARE} = \frac{1}{N}\sum_{i=1}^{i=N} \frac{\mathbf{Nu}_{\text{predicted},i} - \mathbf{Nu}_{\text{experimental},i}}{\mathbf{Nu}_{\text{experimental},i}}$)

Experimental condition for Fe_2O_3/water nanofluid	**AARE% between experimental data and Maxwell model**	**AARE% between experimental data and Lu and Lin model**
3 nm at 25ºC	3.1	4.4
10 nm at 25ºC	2.8	1.7
20 nm at 25ºC	6.6	4.2
3 nm at 45ºC	9.3	11.2
10 nm at 45ºC	3.9	6.1
20 nm at 45ºC	1.8	1.4
3 nm at 65ºC	10.7	12.6
10 nm at 65ºC	6.9	8.8
20 nm at 65ºC	3.1	5.2

Table 4: Enhancement of the heat transfer coefficient for Fe_2O_3/water nanofluids of 20 nm (25°C) for laminar flow regime.

Concentration of Fe_2O_3 nanoparticle (vol.%)	**Thermal conductivity of Fe_2O_3/water nanofluids (W/m.k)**	**Heat transfer coefficient ($W/m^2.k$)**	**Thermal boundary layer thickness (mm)**	**Enhancement (k) (%)**	**Enhancement (h) (%)**	**Decrease (δ) % $= \left\lvert \frac{\delta_{bf} - \delta_{nf}}{\delta_{bf}} \right\rvert$ x 100**
0	0.595	515	1.15	0	0	0
0.01	0.601	528	1.14	1	2.5	0.9
0.02	0.609	540	1.13	2	5	2
0.04	0.628	558	1.13	5.5	8	2
0.06	0.648	578	1.12	9	12	3
0.09	0.679	605	1.12	14	17	3

Table 5: Enhancement of the heat transfer coefficient for Fe_2O_3/water nanofluids of 20 nm (25°C) for turbulent flow regime.

Concentration of Fe_2O_3 nanoparticle (vol.%)	Thermal conductivity of Fe_2O_3/water nanofluids (W/m.k)	Heat transfer coefficient ($W/m^2.k$)	Thermal boundary layer thickness (mm)	Enhancement (k) (%)	Enhancement (h) (%)	Decrease (δ) (%)
0	0.595	1060	0.56	0	0	0
0.01	0.601	1094	0.55	1	3	2
0.02	0.609	1182	0.51	2	12	9
0.04	0.628	1268	0.5	5.5	20	11
0.06	0.648	1340	0.48	9	26	14
0.09	0.679	1542	0.44	14	45	21

Table 6: Enhancement of the heat transfer coefficient for Fe_2O_3/water nanofluids of 20 nm (65°C) for turbulent flow regime.

Concentration of Fe_2O_3 nanoparticle (vol.%)	Thermal conductivity of Fe_2O_3/water nanofluids (W/m.k)	Heat transfer coefficient ($W/m^2.k$)	Thermal boundary layer thickness (mm)	Enhancement (k) (%)	Enhancement (h) (%)	Decrease (δ) (%)
0	0.645	2307	0.28	0	0	0
0.01	0.652	2614	0.25	1	13	10
0.02	0.661	2801	0.24	2	21	15
0.04	0.693	2991	0.23	7	30	18
0.06	0.733	3215	0.23	14	39	18
0.09	0.798	3585	0.22	23	55	21.4

Table 7: Enhancement of the heat transfer coefficient for Fe_2O_3/water nanofluids of 10 nm (25°C) for laminar flow regime.

Concentration of Fe_2O_3 nanoparticle (vol.%)	Thermal conductivity of Fe_2O_3/water nanofluids (W/m.k)	Heat transfer coefficient ($W/m^2.k$)	Thermal boundary layer thickness (mm)	Enhancement (k) (%)	Enhancement (h) (%)	Decrease (δ) (%)
0	0.595	515	1.15	0	0	0
0.01	0.629	542	1.16	5	6	0.8
0.02	0.64	557	1.14	7	8	0.9
0.04	0.66	574	1.14	10	12	0.9
0.06	0.681	592	1.151	14	15	0.1
0.09	0.708	614	1.153	18	20	0.2

Table 8: Enhancement of the heat transfer coefficient for Fe_2O_3/water nanofluids of 10 nm (25°C) for turbulent flow regime.

Concentration of Fe_2O_3 nanoparticle (vol.%)	Thermal conductivity of Fe_2O_3/water nanofluids (W/m.k)	Heat transfer coefficient ($W/m^2.k$)	Thermal boundary layer thickness (mm)	Enhancement (k) (%)	Enhancement (h) (%)	Decrease (δ) (%)
0	0.595	1060	0.56	0	0	0
0.01	0.629	1121	0.55	5	6	2
0.02	0.64	1183	0.54	7	12	4
0.04	0.66	1276	0.52	10	20	7.8
0.06	0.681	1348	0.50	14	27	11
0.09	0.708	1582	0.45	18	49	19.6

Table 9: Enhancement of the heat transfer coefficient for Fe_2O_3/water nanofluids of 10 nm (65°C) for turbulent flow regime.

Concentration of Fe_2O_3 nanoparticle (vol.%)	Thermal conductivity of Fe_2O_3/water nanofluids (W/m.k)	Heat transfer coefficient ($W/m^2.k$)	Thermal boundary layer thickness (mm)	Enhancement (k) (%)	Enhancement (h) (%)	Decrease (δ) (%)
0	0.645	2307	0.28	0	0	0
0.01	0.656	2753	0.24	2	19	15
0.02	0.678	2986	0.23	5	29	18
0.04	0.711	3102	0.23	10	34	18
0.06	0.761	3374	0.23	18	46	18
0.09	0.827	3753	0.22	28	62	21.4

Table 10: Enhancement of the heat transfer coefficient for Fe_2O_3/water nanofluids of 3 nm (25°C) for laminar flow regime

Concentration of Fe_2O_3 nanoparticle (vol.%)	Thermal conductivity of Fe_2O_3/water nanofluids (W/m.k)	Heat transfer coefficient ($W/m^2.k$)	Thermal boundary layer thickness (mm)	Enhancement (k) (%)	Enhancement (h) (%)	Decrease (δ) (%)
0	0.595	515	1.15	0	0	0
0.01	0.652	557	1.17	9	9	1.6
0.02	0.665	565	1.17	11	12	1.6
0.04	0.686	587	1.16	15	15	0.8
0.06	0.709	602	1.16	19	19	0.8
0.09	0.735	642	1.14	23	24	0.9

Table 11: Enhancement of the heat transfer coefficient for Fe_2O_3/water nanofluids of 3 nm (25°C) for turbulent flow regime.

Concentration of Fe_2O_3 nanoparticle (vol.%)	Thermal conductivity of Fe_2O_3/water nanofluids (W/m.k)	Heat transfer coefficient ($W/m^2.k$)	Thermal boundary layer thickness (mm)	Enhancement (k) (%)	Enhancement (h) (%)	Decrease (δ) (%)
0	0.595	1060	0.56	0	0	0
0.01	0.652	1165	0.55	9	10	2
0.02	0.665	1226	0.54	11	16	4
0.04	0.686	1341	0.51	15	27	9
0.06	0.709	1454	0.48	19	37	14
0.09	0.735	1619	0.45	23	52	19.6

Table 12: Enhancement of the heat transfer coefficient for Fe_2O_3/water nanofluids of 3 nm (65°C) for turbulent flow regime.

Concentration of Fe_2O_3 nanoparticle (vol.%)	Thermal conductivity of Fe_2O_3/water nanofluids (W/m.k)	Heat transfer coefficient ($W/m^2.k$)	Thermal boundary layer thickness (mm)	Enhancement (k) (%)	Enhancement (h) (%)	Decrease (δ) (%)
0	0.645	2307	0.28	0	0	0
0.01	0.685	2895	0.24	6	25	15
0.02	0.711	3143	0.23	10	36	18
0.04	0.746	3343	0.22	16	45	21.4
0.06	0.791	3587	0.22	23	55	21.4
0.09	0.854	3918	0.21	32	70	25

Table 13: Average Absolute Relative Difference (AARD) of the local heat transfer coefficients with different diameter of the nanoparticles at 0.09 of volume fraction.

Size (nm)	Local heat transfer coefficients, (h) [$W/m^2 \cdot {}^oC$]			Size	AARD		
	Laminar flow at Re=2100 and 25 ^oC	Turbulent flow at Re=4800 and 25 ^oC	Turbulent flow at Re=12000 and 65 ^oC		%	%	%
20	605	1542	3585	(3-20 nm)	5.7	4.7	8.5
10	614	1582	3753	(3-10 nm)	4.3	2.2	4.2
3	642	1619	3918	(10-20 nm)	1.4	2.4	4.3

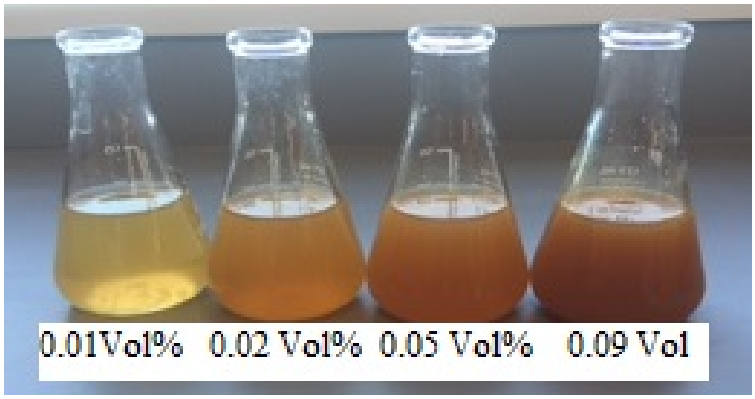

Figure 1: Stable Fe_2O_3 nanofluids with concentrations for selected volume fractions (0.01, 0.02, 0.05 and 0.09 vol. %) after 30 days

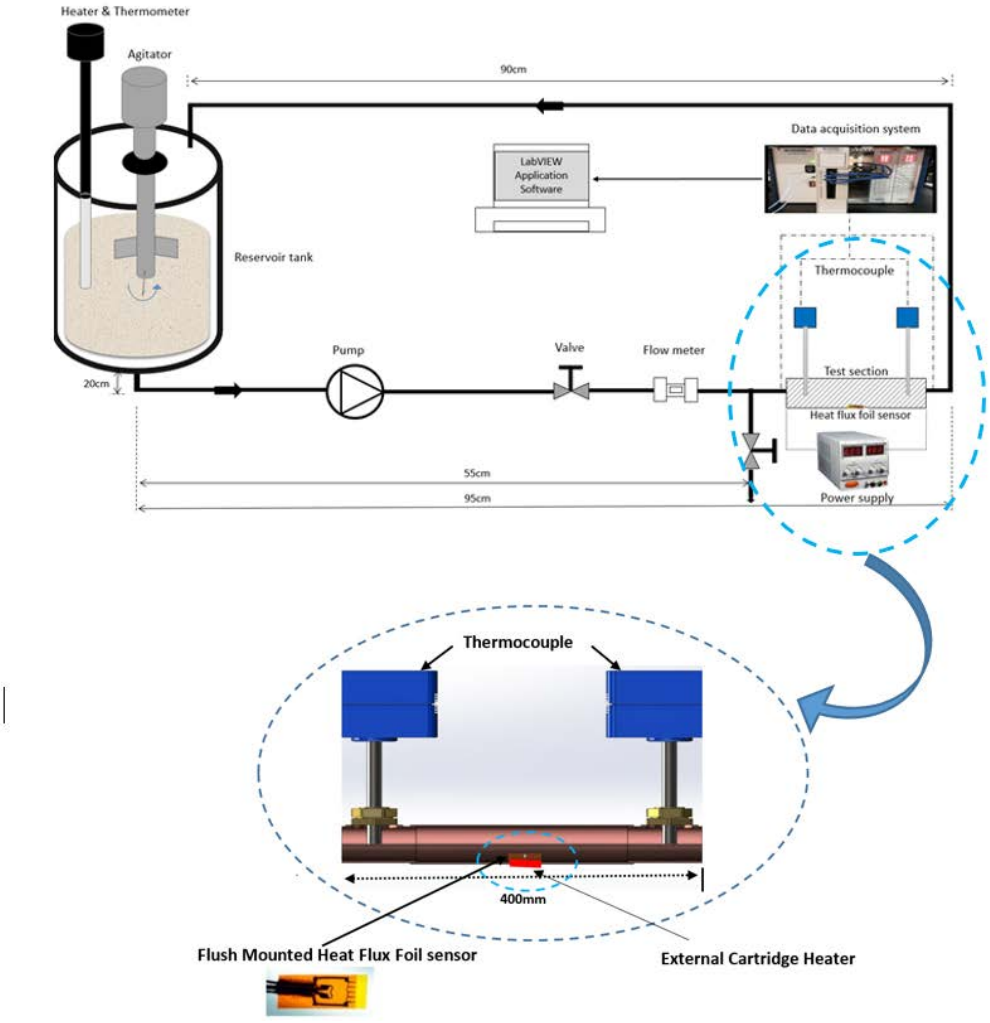

Figure 2: Schematic diagram of the non-invasive heat transfer coefficient probe (flushed mounted on the inner wall surface in conjunction with an external cartridge heater)

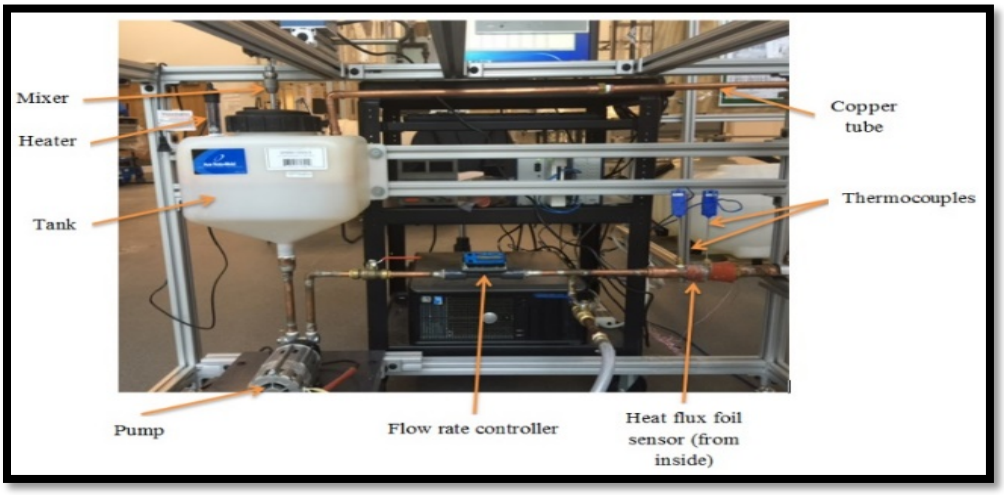

Figure 3: Photographic view of experimental setup

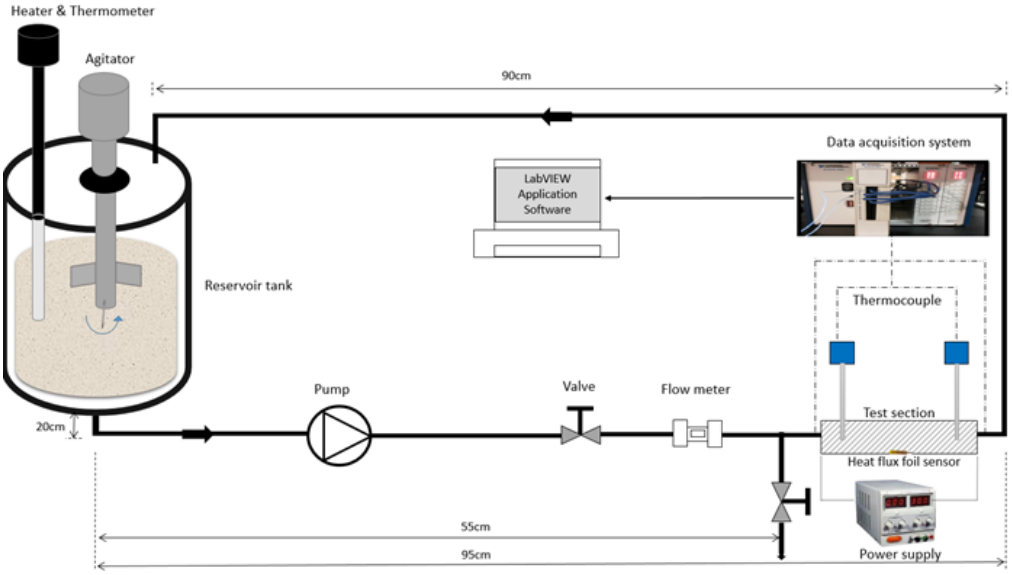

Figure 4: Schematic diagram of experimental setup

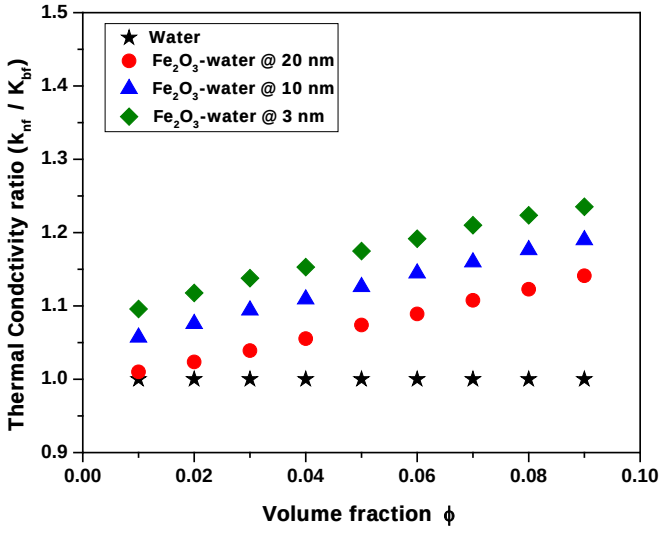

Figure 5: Effects of particle volume fraction on the thermal conductivity of Nanofluids at 25°C.

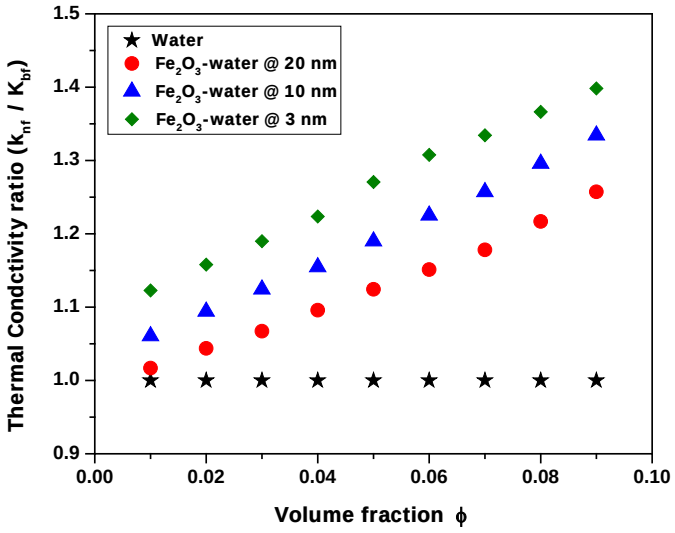

Figure 6: Effects of particle volume fraction on the thermal conductivity of Nanofluids at 45°C.

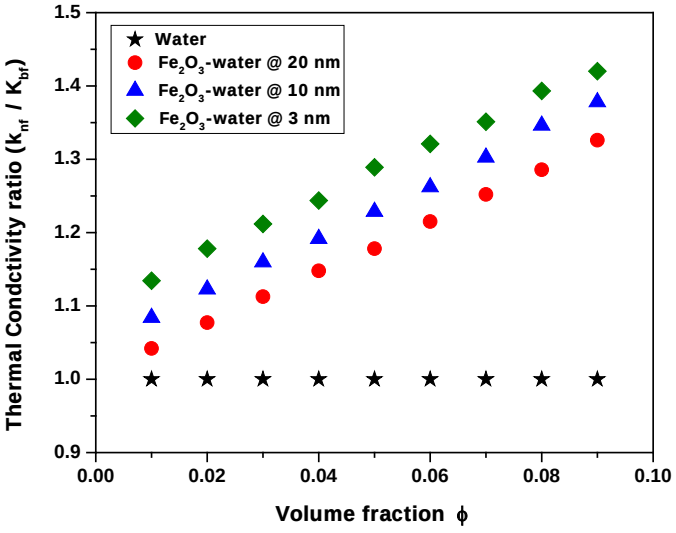

Figure 7: Effects of particle volume fraction on the thermal conductivity of Nanofluids at 65°C.

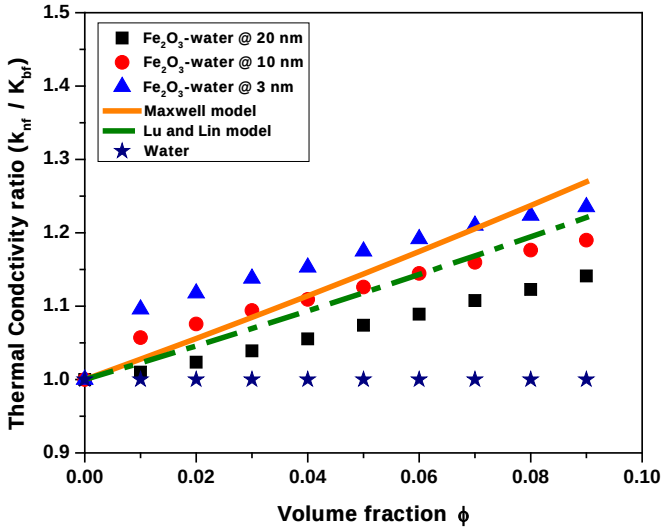

Figure 8: Comparison of the experimental results of the thermal conductivity ratio for Fe_2O_3/water nanofluid with theoretical models as a function of particle volume fraction at 25°C.

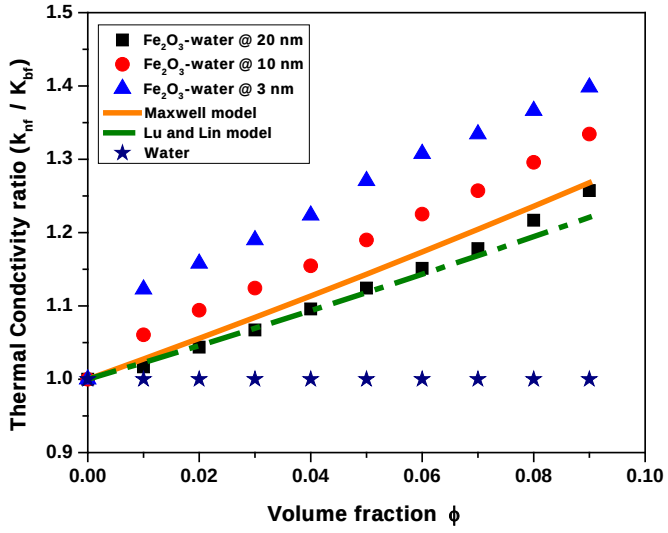

Figure 9: Comparison of the experimental results of the thermal conductivity ratio for Fe_2O_3/water nanofluid with theoretical models as a function of particle volume fraction at 45°C

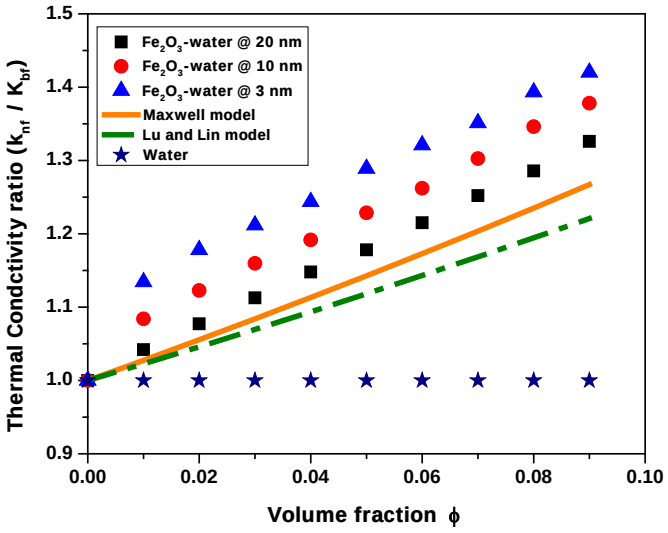

Figure 10: Comparison of the experimental results of the thermal conductivity ratio for Fe_2O_3/water nanofluid with theoretical models as a function of particle volume fraction at 65°C

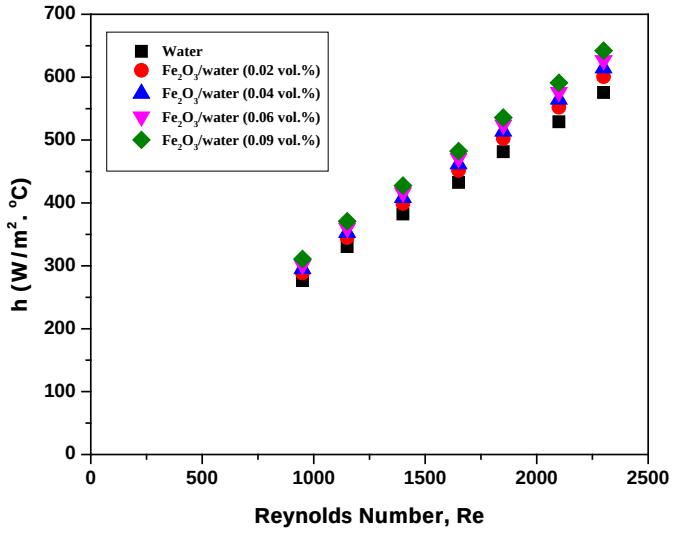

Figure 11: Local convective heat transfer coefficient of Fe_2O_3/water nanofluid as a function of Reynolds number at different volume fraction in the laminar flow region at 25°C for 3 nm

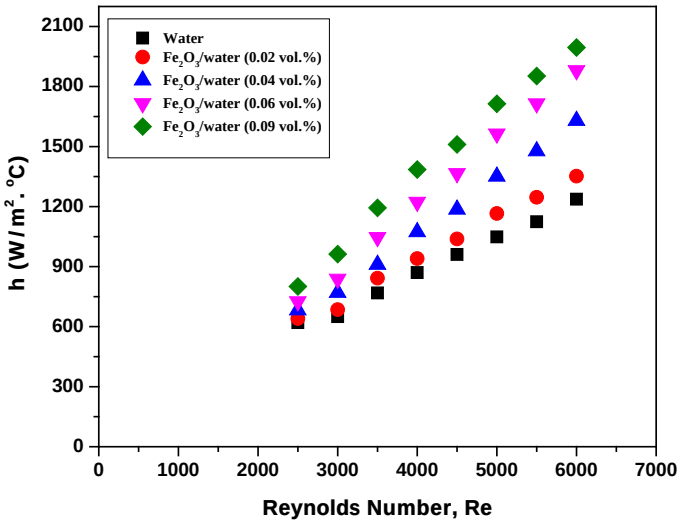

Figure 12: Local convective heat transfer coefficient of Fe_2O_3/water nanofluid as a function of Reynolds number at different volume fraction in the turbulent flow region at 25°C for 3 nm

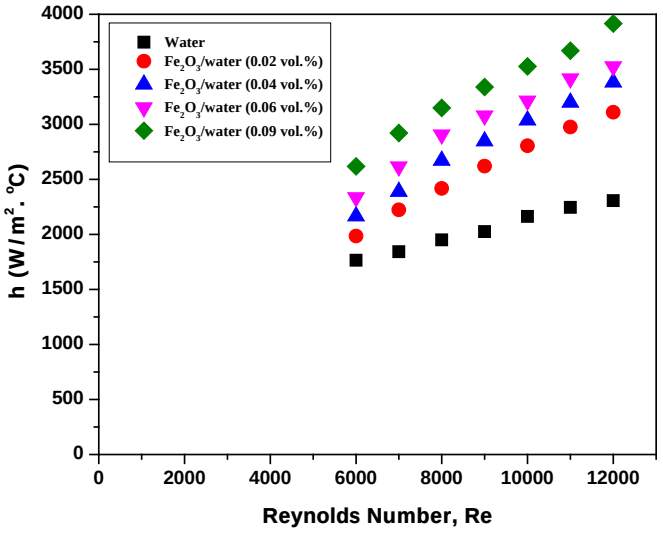

Figure 13: Local convective heat transfer coefficient of Fe_2O_3/water nanofluid as a function of Reynolds number at different volume fraction in the turbulent flow region at 65°C for 3 nm

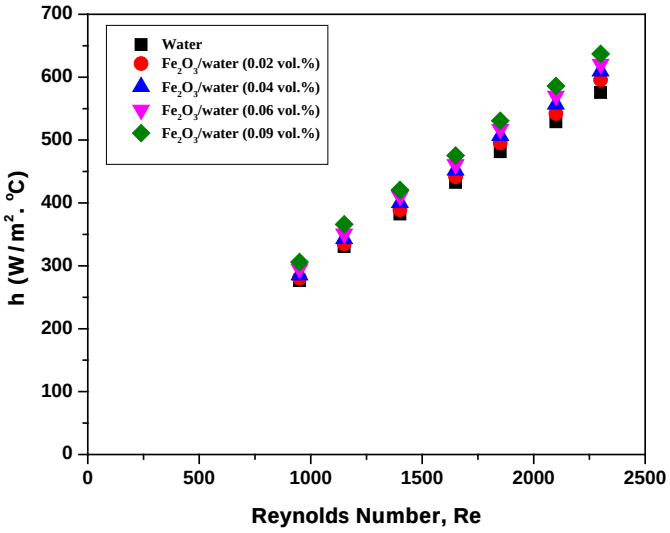

Figure 14: Local convective heat transfer coefficient of Fe_2O_3/water nanofluid as a function of Reynolds number at different volume fraction in the laminar flow region at 25°C for 10 nm

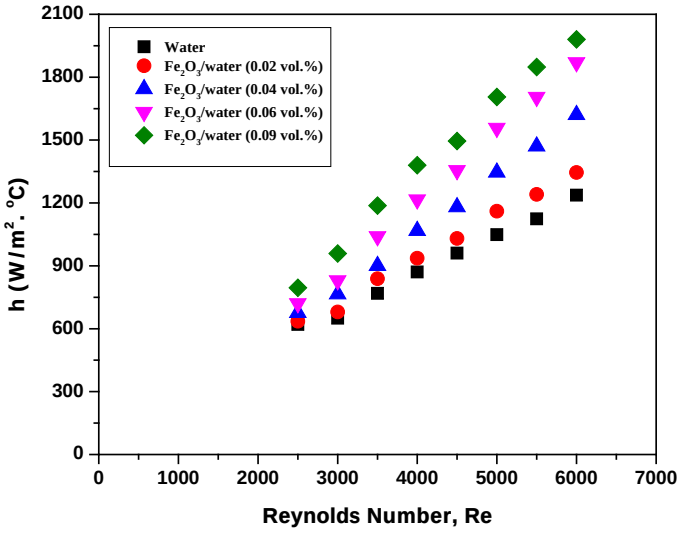

Figure 15: Local convective heat transfer coefficient of Fe_2O_3/water nanofluid as a function of Reynolds number at different volume fraction in the turbulent flow region at 25°C for 10 nm

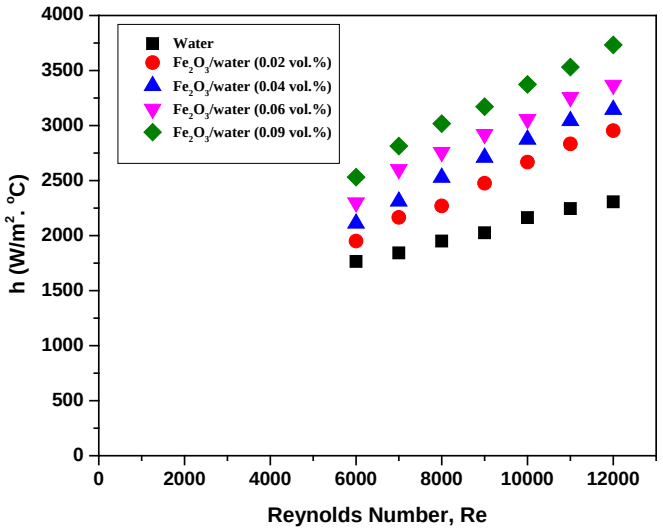

Figure 16: Local convective heat transfer coefficient of Fe_2O_3/water nanofluid as a function of Reynolds number at different volume fraction in the turbulent flow region at 65°C for 10 nm

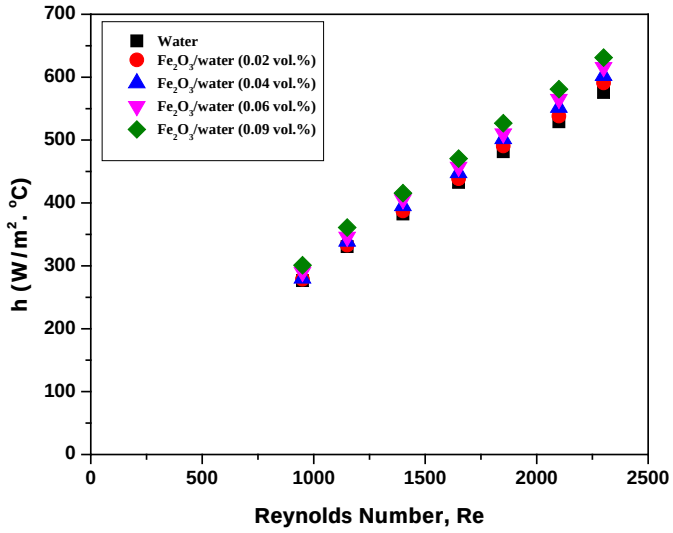

Figure 17: Local convective heat transfer coefficient of Fe_2O_3/water nanofluid as a function of Reynolds number at different volume fraction in the laminar flow region at 25°C for 20 nm

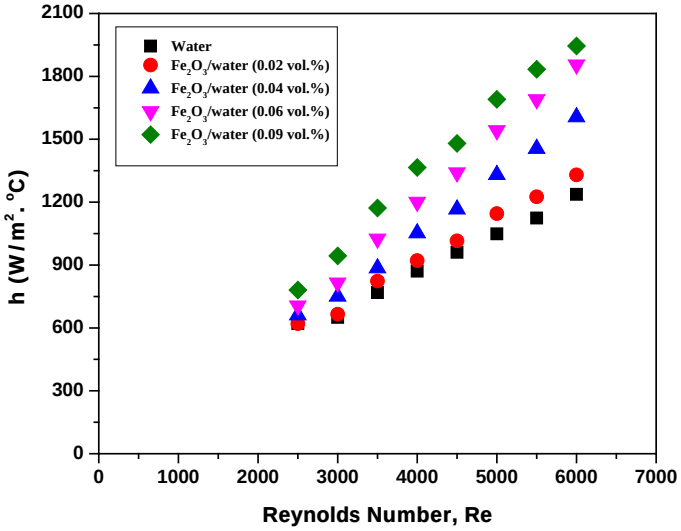

Figure 18: Local convective heat transfer coefficient of Fe_2O_3/water nanofluid as a function of Reynolds number at different volume fraction in the turbulent flow region at 25°C for 20 nm

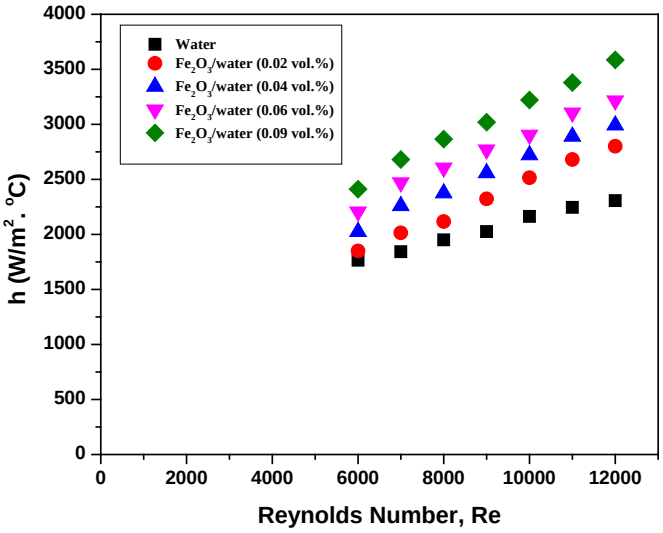

Figure 19: Local convective heat transfer coefficient of Fe_2O_3/water nanofluid as a function of Reynolds number at different volume fraction in the turbulent flow region at 65°C for 20 nm

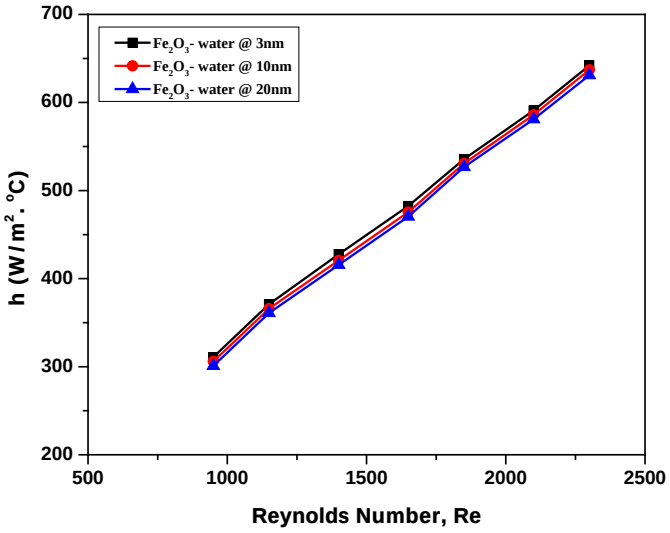

Figure 20: Local convective heat transfer coefficient of Fe_2O_3/water nanofluid as a function of Reynolds number in the laminar flow region of 0.09% volume fraction at 25°C

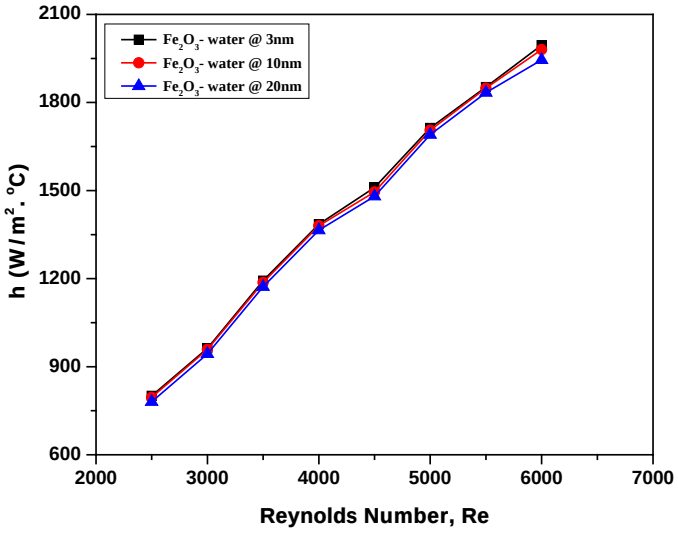

Figure 21: Local convective heat transfer coefficient of Fe_2O_3/water nanofluid as a function of Reynolds number in the turbulent flow region of 0.09% volume fraction at 25°C

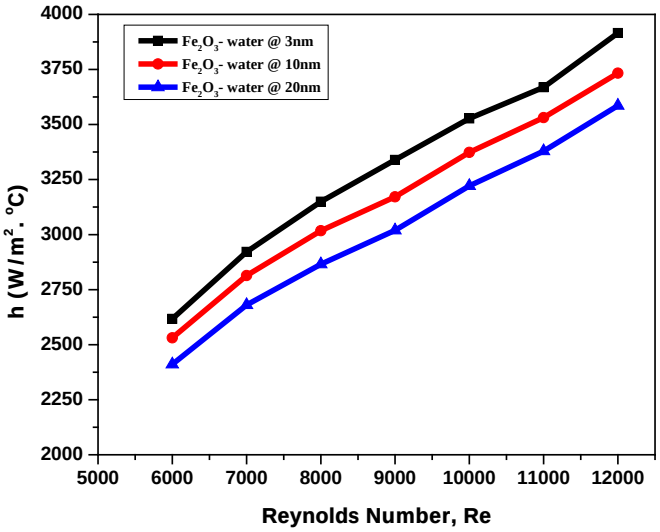

Figure 22: Local convective heat transfer coefficient of Fe_2O_3/water nanofluid as a function of Reynolds number in the turbulent flow region of 0.09% volume fraction at 65°C

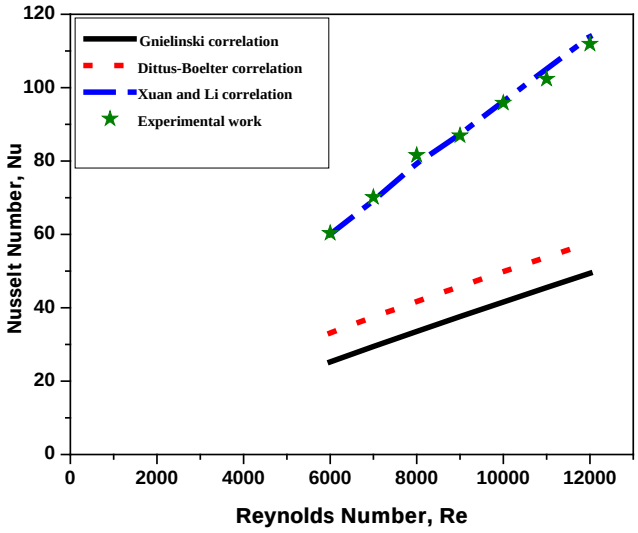

Figure 23: Comparison of the experimental Nusselt numbers with the predicted ones by existing convective heat transfer correlations at 65°C for 3 nm

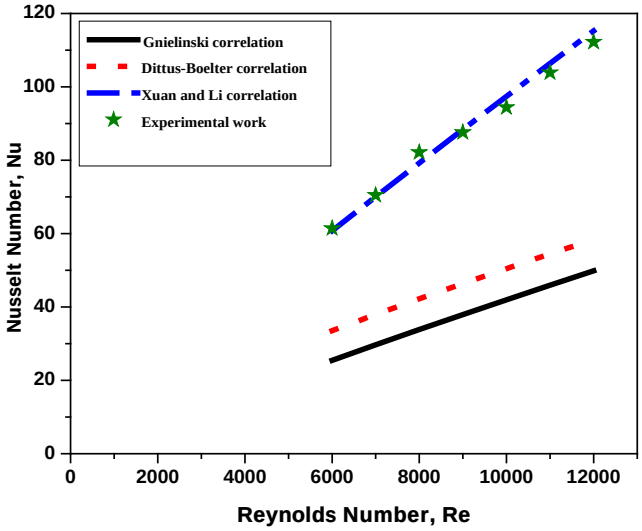

Figure 24: Comparison of the experimental Nusselt numbers with the predicted ones by existing convective heat transfer correlations at 65°C for 10 nm

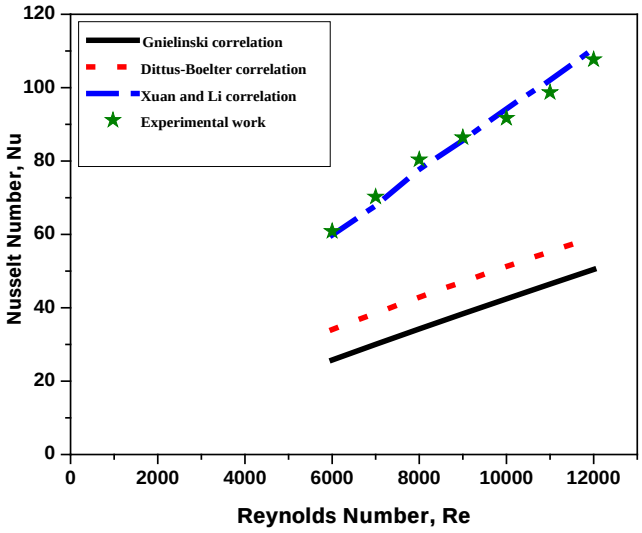

Figure 25: Comparison of the experimental Nusselt numbers with the predicted ones by existing convective heat transfer correlations at 65°C for 20 nm

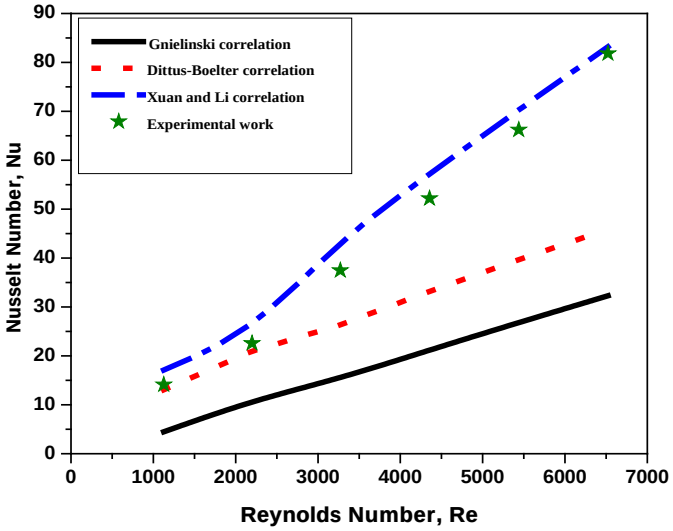

Figure 26: Comparison of the experimental Nusselt numbers with the predicted ones by existing convective heat transfer correlations at 25°C for 3 nm

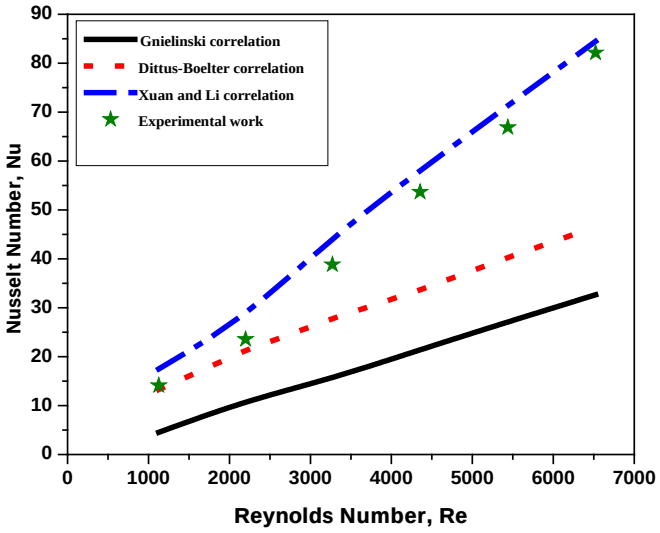

Figure 27: Comparison of the experimental Nusselt numbers with the predicted ones by existing convective heat transfer correlations at 25°C for 10 nm

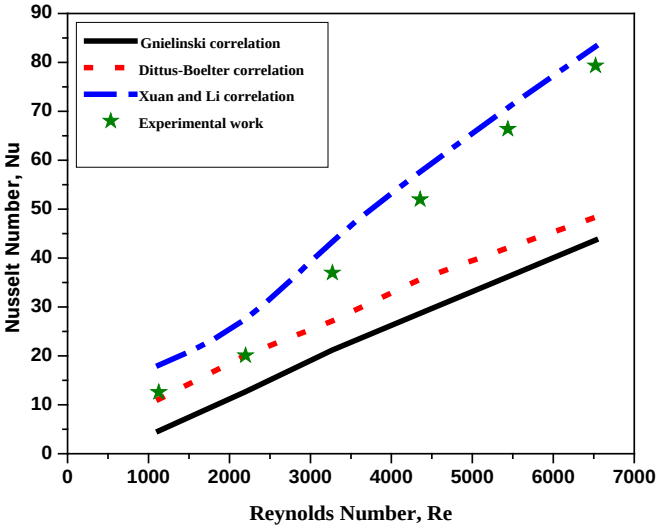

Figure 28: Comparison of the experimental Nusselt numbers with the predicted ones by existing convective heat transfer correlations at 25°C for 20 nm

REFERENCES

[1] Amiri, A., et al., *Toward improved engine performance with crumpled nitrogen-doped graphene based water–ethylene glycol coolant.* Chemical Engineering Journal, 2016. **289**: p. 583-595.

[2] Naik, B.A.K. and A.V. Vinod, *Heat transfer enhancement using non-Newtonian nanofluids in a shell and helical coil heat exchanger.* Experimental Thermal and Fluid Science, 2018. **90**: p. 132-142.

[3] Sahota, L., Shyam, and G.N. Tiwari, *Energy matrices, enviroeconomic and exergoeconomic analysis of passive double slope solar still with water based nanofluids.* Desalination, 2017. **409**: p. 66-79.

[4] Kabeel, A.E. and E.M.S. El-Said, *Applicability of flashing desalination technique for small scale needs using a novel integrated system coupled with nanofluid-based solar collector.* Desalination, 2014. **333**: p. 10-22.

[5] Wu, D., et al., *Critical issues in nanofluids preparation, characterization and thermal conductivity.* Current Nanoscience, 2009. **5**(1): p. 103-112.

[6] Chen, W., et al., *Application of recoverable carbon nanotube nanofluids in solar desalination system: An experimental investigation.* Desalination, 2017.

[7] Buongiorno, J.,Venerus,D.C.,Prabhat,N.,McKrell,T.,Townsend,J.,Christianson,R., Tolmachev,Y.V.,Keblinski,P.,Hu,L.W.,Alvarado,J.L.,Bang,I.C.,Bishnoi,S.W., Bonetti, M.,Botz,F.,Cecere,A.,Chang,Y.,Chen,G.,Chen,H.,Chung,S.J.,Chyu,M. K., Das,S.K.,DiPaola,R.,Ding,Y.,Dubois,F.,Dzido,G.,Eapen,J.,Escher,W., Funfschilling, D.,Galand,Q.,Gao,J.,Gharagozloo,P.E.,Goodson,K.E.,Gutierrez, J.G., Hong,H.,Horton,M.,Hwang,K.S.,Iorio,C.S.,Jang,S.P.,Jarzebski,A.B.,Jiang, Y.,Jin,L.,Kabelac,S.,Kamath,A.,Kedzierski,M.A.,Kieng,L.G.,Kim,C.,Kim,J.H., Kim, S.,Lee,S.H.,Leong,K.C.,Manna,I.,Michel,B.,Ni,R.,Patel,H.E.,Philip,J., Poulikakos, D.,Reynaud,C.,Savino,R.,Singh,P.K.,Song,P.,Sundararajan,T., Timofeeva,E.,Tritcak,T.,Turanov,A.N.,Vaerenbergh,S.V.,Wen,D.,Witharana, S., Yang,C.,Yeh,W.H.,Zhao,X.Z.,Zhou,S.Q.,, *A benchmark study on the thermal conductivity of nanofluids.* J. Appl. Phys., 2009. **109**.

[8] Keblinski, P., et al., *Mechanisms of Heat Flow in Suspensions of Nano-Sized Particles (Nano Fluids).* Vol. 45. 2002. 855-863.

[9] Xuan, Y. and Q. Li, *Heat transfer enhancement of nanofluids.* International Journal of Heat and Fluid Flow, 2000. **21**(1): p. 58-64.

[10] Gupta, N.K., A.K. Tiwari, and S.K. Ghosh, *Heat transfer mechanisms in heat pipes using nanofluids – A review.* Experimental Thermal and Fluid Science, 2018. **90**: p. 84-100.

[11] Choi, S.U.S., *Enhancing thermal conductivity of fluids with nanoparticles. in American Society of Mechanical Engineers.* Fluids Engineering Division, 1995.

[12] Eastman, J.A., et al., *Anomalously increased effective thermal conductivities of ethylene glycol-based nanofluids containing copper nanoparticles.* Applied Physics Letters, 2001. **78**(6): p. 718-720.

[13] Das, S.K., et al., *Temperature Dependence of Thermal Conductivity Enhancement for Nanofluids.* Journal of Heat Transfer, 2003. **125**(4): p. 567.

[14] Mintsa, H.A., et al., *New temperature dependent thermal conductivity data for water-based nanofluids.* International Journal of Thermal Sciences, 2009. **48**(2): p. 363-371.

[15] Turgut, A., et al., *Thermal Conductivity and Viscosity Measurements of Water-Based TiO2 Nanofluids.* International Journal of Thermophysics, 2009. **30**(4): p. 1213-1226.

[16] Das, S.K., et al., *Temperature dependence of thermal conductivity enhancement for nanofluids.* Journal of Heat Transfer, 2003. **125**(4): p. 567-574.

[17] Wen, D. and Y. Ding, *Experimental investigation into convective heat transfer of nanofluids at the entrance region under laminar flow conditions.* International Journal of Heat and Mass Transfer, 2004. **47**(24): p. 5181-5188.

[18] Li, C.H. and G.P. Peterson, *Experimental investigation of temperature and volume fraction variations on the effective thermal conductivity of nanoparticle suspensions (nanofluids).* Journal of Applied Physics, 2006. **99**(8).

[19] Choi, S.U.S., *Nanofluid technology: current status and future research.* Technical Conference on Strategic Technologies, Vienna, VA,US, 1998.

[20] Xie, H., et al., *Thermal conductivity enhancement of suspensions containing nanosized alumina particles.* Journal of Applied Physics, 2002. **91**(7): p. 4568-4572.

[21] Murshed, S.M.S., K.C. Leong, and C. Yang, *Investigations of thermal conductivity and viscosity of nanofluids.* International Journal of Thermal Sciences, 2008. **47**(5): p. 560-568.

[22] Lee, J.-H., et al., *Effective viscosities and thermal conductivities of aqueous nanofluids containing low volume concentrations of Al2O3 nanoparticles.* International Journal of Heat and Mass Transfer, 2008. **51**(11-12): p. 2651-2656.

[23] J. Philip, P.D. Shima, and B. Raj, *Enhancement of thermal conductivity in magnetite based nanofluid due to chainlike structures.* Applied Physics Letters, 2007. **91**(20).

[24] Syam Sundar, L., M.K. Singh, and A.C.M. Sousa, *Investigation of thermal conductivity and viscosity of Fe3O4 nanofluid for heat transfer applications.* International Communications in Heat and Mass Transfer, 2013. **44**: p. 7-14.

[25] Masuda, H., et al., *Alteration of Thermal Conductivity and Viscosity of Liquid by Dispersing Ultra-Fine Particles Dispersion of Al2O3, SiO2 and TiO2 Ultra-Fine Particles.* Netsu Bussei, 1993. **7**(4): p. 227-233.

[26] Wang, X., X. Xu, and S.U.S. Choi, *Thermal conductivity of nanoparticle-fluid mixture.* Journal of thermophysics and heat transfer, 1999. **13**(4): p. 474-480.

[27] Koo, J. and C. Kleinstreuer, *A new thermal conductivity model for nanofluids.* Journal of Nanoparticle Research, 2004. **6**(6): p. 577-588.

[28] Bhattacharya, P., et al., *Brownian dynamics simulation to determine the effective thermal conductivity of nanofluids.* Journal of Applied Physics, 2004. **95**(11 I): p. 6492-6494.

[29] Jang, S.P. and S.U.S. Choi, *Role of Brownian motion in the enhanced thermal conductivity of nanofluids.* Applied Physics Letters, 2004. **84**(21): p. 4316-4318.

[30] Hong, K.S., T.K. Hong, and H.S. Yang, *Thermal conductivity of Fe nanofluids depending on the cluster size of nanoparticles.* Applied Physics Letters, 2006. **88**(3): p. 1-3.

[31] Farajollahi, B., S.G. Etemad, and M. Hojjat, *Heat transfer of nanofluids in a shell and tube heat exchanger.* International Journal of Heat and Mass Transfer, 2010. **53**(1): p. 12-17.

[32] Y.M. Xuan and Q. Li, *Investigation on convective heat transfer and flow features of nanofluids.* ASME J. Heat Transfer 2003. **125**: p. 151–155.

[33] Abdulmohsin, R.S. and M.H. Al-Dahhan, *Characteristics of convective heat transport in a packed pebble-bed reactor.* Nuclear Engineering and Design, 2015. **284**: p. 143-152.

[34] Said, I.A., et al., *Investigation of natural convection heat transfer in a unique scaled-down dual-channel facility.* AIChE Journal, 2017. **63**(1): p. 387-396.

[35] Said, I.A., et al., *Experimental investigation of the helium natural circulation heat transfer in two channels facility using varying riser channel heat fluxes.* Experimental Thermal and Fluid Science, 2018. **93**: p. 195-209.

[36] Sha, L., Y. Ju, and H. Zhang, *The influence of the magnetic field on the convective heat transfer characteristics of Fe 3 O 4 /water nanofluids.* Applied Thermal Engineering, 2017. **126**: p. 108-116.

[37] Mohammed, S., N. Zouli, and M. Al-Dahhan, *Removal of benzoic acid from wastewater by pickering emulsion liquid membrane stabilized by magnetic Fe2O3 nanoparticles*. Vol. 68. 2017. 114-121.

[38] Sun, B., et al., *Investigation on the flow and convective heat transfer characteristics of nanofluids in the plate heat exchanger.* Experimental Thermal and Fluid Science, 2016. **76**: p. 75-86.

[39] D. Wu, et al., *Critical issues in nanofluids preparation, characterization and thermal conductivity.* Curr. Nanosci, 2009. **5**: p. 103–112.

[40] zerinc, S.O., et al., *Enhanced thermal conductivity of nanofluids: a state-of-the-art review.* Microfluid Nanofluid, 2010. **8**: p. 145–170.

[41] Zhang, X., H. Gu, and M. Fujii, *Effective thermal conductivity and thermal diffusivity of nanofluids containing spherical and cylindrical nanoparticles.* Experimental Thermal and Fluid Science, 2007. **31**(6): p. 593-599.

[42] Raja, M., et al., *Review on nanofluids characterization, heat transfer characteristics and applications.* Renewable and Sustainable Energy Reviews, 2016. **64**: p. 163-173.

[43] RL, H. and CrosserOK, *Thermal condi=uctivity of heterogenous two componennt systems.* I and EC Fundam, 1962. **1**: p. 187-191.

[44] Maxwell, J., *A treatise on electricity and magnetism*. 1873, Oxford: Clarendon Press.

[45] Lu, S.-Y. and H.C. Lin, *Effective conductivity of composites containing aligned spheroidal inclusions of finite conductivity*. Vol. 79. 1996. 6761-6769.

[46] Aghabozorg, M.H., A. Rashidi, and S. Mohammadi, *Experimental investigation of heat transfer enhancement of Fe2O3-CNT/water magnetic nanofluids under laminar, transient and turbulent flow inside a horizontal shell and tube heat exchanger*. Experimental Thermal and Fluid Science, 2016. **72**: p. 182-189.

[47] Peyghambarzadeh, S.M., et al., *Improving the cooling performance of automobile radiator with Al2O3/water nanofluid.* Applied Thermal Engineering, 2011. **31**(10): p. 1833-1838.

[48] Manay, E., et al., *Use of nanofluids in microchannels.* Engineer and Machine, 2012. **627**(53): p. 28-42.

[49] Lee, S., S. Li, and J.A. Eastman, *Measuring thermal conductivity of fluids containing oxide nanoparticles.* Journal of Heat Transfer, 1999. **121**(2): p. 280-289.

[50] Ding, Y., et al., *Heat transfer of aqueous suspensions of carbon nanotubes (CNT nanofluids).* International Journal of Heat and Mass Transfer, 2006. **49**(1-2): p. 240-250.

[51] Beck, M.P., et al., *The effect of particle size on the thermal conductivity of alumina nanofluids.* Journal of Nanoparticle Research, 2009. **11**(5): p. 1129-1136.

[52] Kwek, D., A. Crivoi, and F. Duan, *Effects of Temperature and Particle Size on the Thermal Property Measurements of Al2O3−Water Nanofluids*. Vol. 55. 2010.

[53] Chandrasekar, M., S. Suresh, and A. Chandra Bose, *Experimental studies on heat transfer and friction factor characteristics of Al2O3/water nanofluid in a circular pipe under laminar flow with wire coil inserts.* Experimental Thermal and Fluid Science, 2010. **34**(2): p. 122-130.

[54] Fedele, L., L. Colla, and S. Bobbo, *Viscosity and thermal conductivity measurements of water-based nanofluids containing titanium oxide nanoparticles.* International Journal of Refrigeration, 2012. **35**(5): p. 1359-1366.

[55] L.S. Sundar, M.K. Singh, and A.C.M. Sousa, *Thermal conductivity of ethylene glycol and water mixture based Fe3O4 nanofluid.* International Communications in Heat and Mass Transfer,, 2013. **17-24**.

[56] Manikandan, S. and K.S. Rajan, *Rapid synthesis of MgO nanoparticles & their utilization for formulation of a propylene glycol based nanofluid with superior transport properties.* RSC Adv., 2014. **4**(93): p. 51830-51837.

[57] Mahbubul, I.M., et al., *Experimental investigation on effect of ultrasonication duration on colloidal dispersion and thermophysical properties of alumina–water nanofluid.* International Journal of Heat and Mass Transfer, 2015. **88**: p. 73-81.

[58] Solangi, K.H., et al., *Experimental investigation of the propylene glycol-treated graphene nanoplatelets for the enhancement of closed conduit turbulent convective heat transfer.* International Communications in Heat and Mass Transfer, 2016. **73**: p. 43-53.

[59] Agarwal, R., et al., *Sensitivity of thermal conductivity for Al 2 O 3 nanofluids.* Experimental Thermal and Fluid Science, 2017. **80**: p. 19-26.

[60] Nikkam, N. and M.S. Toprak, *Fabrication and thermo-physical characterization of silver nanofluids: An experimental investigation on the effect of base liquid.* International Communications in Heat and Mass Transfer, 2018. **91**: p. 196-200.

[61] B.C. Pak and Y.I. Cho, *Hydrodynamic and heat transfer study of dispersed fluids with submicron metallic oxide particles.* Exp. Heat Transfer 1999. **11**: p. 151–170.

[62] Yang, Y., et al., *Heat transfer properties of nanoparticle-in-fluid dispersions (nanofluids) in laminar flow.* International Journal of Heat and Mass Transfer, 2005. **48**(6): p. 1107-1116.

[63] S.Z., H., S.G. Etemad, and M.N. Esfahany, *Experimental investigation of oxide nanofluids laminar flow convective heat transfer.* International Communications in Heat and Mass Transfer, 2006. **33**(4): p. 529-535.

[64] Zeinali Heris, S., M. Nasr Esfahany, and S.G. Etemad, *Experimental investigation of convective heat transfer of Al2O3/water nanofluid in circular tube.* International Journal of Heat and Fluid Flow, 2007. **28**(2): p. 203-210.

[65] Williams, W., J. Buongiorno, and L.-W. Hu, *Experimental Investigation of Turbulent Convective Heat Transfer and Pressure Loss of Alumina/Water and Zirconia/Water Nanoparticle Colloids (Nanofluids) in Horizontal Tubes.* Journal of Heat Transfer, 2008. **130**(4): p. 042412.

[66] Jung, J.-Y., H.-S. Oh, and H.-Y. Kwak, *Forced convective heat transfer of nanofluids in microchannels.* International Journal of Heat and Mass Transfer, 2009. **52**(1-2): p. 466-472.

[67] Lai, W.Y., et al., *Convective Heat Transfer for Water-Based Alumina Nanofluids in a Single 1.02-mm Tube.* Journal of Heat Transfer, 2009. **131**(11): p. 112401.

[68] Nasiri, M., S.G. Etemad, and R. Bagheri, *Experimental heat transfer of nanofluid through an annular duct.* International Communications in Heat and Mass Transfer, 2011. **38**(7): p. 958-963.

[69] Anoop, K., et al., *Experimental study of forced convective heat transfer of nanofluids in a microchannel.* International Communications in Heat and Mass Transfer, 2012. **39**(9): p. 1325-1330.

[70] Wu, Z., L. Wang, and B. Sundén, *Pressure drop and convective heat transfer of water and nanofluids in a double-pipe helical heat exchanger.* Applied Thermal Engineering, 2013. **60**(1-2): p. 266-274.

[71] Vermahmoudi, Y., et al., *Experimental investigation on heat transfer performance of /water nanofluid in an air-finned heat exchanger*. European Journal of Mechanics - B/Fluids, 2014. **44**: p. 32-41.

[72] Sun, B., W. Lei, and D. Yang, *Flow and convective heat transfer characteristics of Fe_2O_3–water nanofluids inside copper tubes.* International Communications in Heat and Mass Transfer, 2015. **64**: p. 21-28.

[73] Ahmadi, M. and G. Willing, *Heat transfer measurment in water based nanofluids.* International Journal of Heat and Mass Transfer, 2018. **118**: p. 40-47.

II. IMPACT OF NANOPARTICLES MATERIAL ON THERMAL CONDUCTIVITY AND HEAT TRANSFER COEFFICIENTS OF NANOFLUIDS

ABSTRACT

The thermal conductivity and local heat transfer coefficients of water-based spherical Al_2O_3, Fe_2O_3, and CuO nanofluids have been experimentally investigated using a newly developed sophisticated noninvasive heat transfer coefficient probe that is flush mounted on the inner wall surface of the test section. The Al_2O_3, CuO, and, Fe_2O_3 nanoparticles have been selected because of their superior thermal conductivity and low cost, as well as the magnetic characteristic of Fe_2O_3 nanoparticle since a magnet can collect it and reuse. The six-volume concentrations (0, 0.01, 0.02, 0.03, 0,04 and 0.05 vol.%) have been used at varying experimental temperatures of 25, 35, 45, and 55°C under laminar and turbulent flow regimes (Reynold numbers 1,000 to 10,000). The results showed an enhancement of thermal conductivity and local heat transfer coefficient. The thermal conductivity and local heat transfer coefficient increased with the increased volume concentration (φ) and temperature of the Al_2O_3/water, Fe_2O_3/water, and CuO/water nanofluids. The greatest enhancements in thermal conductivity were found to be 19%, 21%, and 25% for Al_2O_3/water, Fe_2O_3/water, and CuO/water nanofluids, respectively at $\varphi = 0.05\%$ and 55°C. The maximum enhancements in the local heat transfer coefficients were 44%, 50%, and 53%, respectively, at the same conditions. The results also showed that the CuO/water nanofluid at 0.05 vol.% and 55 ^{o}C under turbulent flow regime achieved the highest local heat transfer coefficient for all three nanofluids for all experimental conditions due to increase in thermal conductivity by 25% and a reduction in the thermal

boundary layer film thickness by 19%. It is clear that the thickness of the film is greater than the size of the nanoparticles used in this work (30 nm). The greater thickness allows the nanoparticles to penetrate the film toward the wall and generate local micro eddies and local mixing within the film. This contributed to the enhancement of the local heat transfer coefficient. The experimental results regarding the Nusselt numbers were found to be in good agreement with the values predicted by the Xuan-Li correlation for the conditions studied at 55°C with the variation in nanoparticle volume concentration and material. This good agreement could be attributed to the accounting for the presence of nanoparticles in terms of the percentage of the volume concentration (φ) where the range is close in this work to that used in the work of Xuan-Li correlation, which was not the case with the other correlations.

Keywords: Thermal conductivity, Local heat transfer coefficient, nanoparticles, Thermal boundary layer film thickness, Nusselt number

1. INTRODUCTION

Of the many methods currently available to enhance thermal conductivity and heat transfer coefficient of heat transfer fluids, is the addition of inert additives such as nanoparticles to the conventional base fluid, such as water, ethylene glycol, or engine oil [1, 2]. Addition of nanoparticles (typically <100 nm) to such base fluids forms a stable suspension called a nanofluid. Nanofluids have emerged as new fluids during the last decade and have attracted much attention from researchers and scientists because of their unique physical, chemical, and thermal properties. Nanofluids have the potential for several applications in a wide range of fields of science and engineering, such as engine

cooling, cooling electronic circuits, engine transmission oil, biomedical applications, solar water heating, thermal storage, and mass transfer enhancement [3, 4]. Various efforts have been taken to increase the heat transfer rate and energy efficiency of thermal conducting systems for various applications. For this, the most significant feature observed in the literature using nanofluid has been the enhanced thermal conductivity of the fluid and heat transfer coefficients [5-7]. The thermal conductivity of the solid material from which the particle is manufactured, metallic such as Cu, Al, and Ag or nonmetallic such as CuO, Al_2O_3, and SiO_2 are typically an order-of-magnitude higher than the base fluids and should result in a significant increase in the heat transfer coefficient even at low nanoparticle concentrations (Table 1)[8]. Many researchers have confirmed the enhancement of convective heat transfer using nanofluids with anomalously high thermal conductivity even at very low nanoparticle concentrations [7, 9].

The material from which the particle is produced is a key factor in determining the nanofluids thermal conductivity. Initially one might think that the high thermal conductivity of the particles might be the reason for the increase in thermal conductivity of the nanofluids. However, the addition of CuO nanoparticles causes a more significant increase in thermal conductivity than the addition of Al_2O_3 nanoparticles [10].

Several researchers have addressed the influence of adding different types of nanoparticle materials to enhance thermal conductivity and heat transfer coefficient. Among these researchers, Wen and Ding [11], Das et al. [12], and Li et al. [13] have experimentally investigated the effect of fluid temperature on thermal conductivity enhancement using the hot-wire method for the nanofluids CuO/water and Al_2O_3/water.

Their results revealed that the enhancement of thermal conductivity was increased with increasing fluid temperature.

Lee et al. [10], Das et al. [9], Wang et al. [14], and Xie et al. [15, 16] studied the effect of the material of the nanoparticles on thermal conductivity enhancement by keeping all other parameters approximately constant (e.g., base fluid, temperature, and particle size). It was found that thermal conductivity increased with the presence of the nanoparticles, but a given degree of enhancement occurred at a lower concentration when the particle material was of a higher thermal conductivity (i.e., metal particles produce the same enhancement as oxide particles but at a much lower volume concentration).

Kumar and Sonawane [17] studied the effect of fluid temperature of CuO/water and TiO_2/water nanofluids on the thermal conductivity under different volume fractions (i.e., 0.02%, 0.04%, and 0.06%) using a KD2 Prob Thermal Properties analyzer. Their results indicated that the thermal conductivity increased with both increasing operating temperature and volume fractions.

Hwang et al. [18] investigated the effect of using different types of nanofluids such as multiwalled carbon nanotube (MWCNT/water), CuO/water, SiO_2/water, and CuO/ethylene glycol on the thermal conductivity using the hot-wire method. They found that the thermal conductivity enhancement depends on the thermal conductivities of both nanoparticles and the base fluid.

Zhang et al. [19] studied the effective thermal conductivity and thermal diffusivity of Au/toluene, CuO/water, TiO_2/water, Al_2O_3/water, and carbon nanotube CNT/water nanofluids at different temperatures and volume fractions. Their results showed that the

effective thermal conductivity and thermal diffusivity increased with increase of the volume fraction.

Mintsa et al. [20] investigated the effects of particles size, particles volume fraction, and temperature on thermal conductivity of CuO/water and Al_2O_3/water nanofluids. The results showed that the effective thermal conductivity increased with decrease in particle size and increase in particle volume fraction. The relative increase in thermal conductivity was significantly more at high fluid temperatures.

An additional and important result of enhanced thermal conductivity is an increase in convective heat transfer coefficient. Most of the experimental research has been focused on enhancing the heat transfer coefficient using metal oxide nanoparticles (Such as: aluminum oxide, copper oxide, iron oxide, and silicon oxide) [21]. They estimated the overall convective heat transfer coefficient by implementing energy balance around the test section using the measured mass flow rate, heat flux, and inlet and outlet temperatures of nanofluid.

Mikkola et al. [22] studied how nanoparticle size and thermal conductivity affected convective heat transfer of nanofluids using different kinds of nanoparticles such as Al_2O_3, SiO_2, micelles, and polystyrene. In their experimental work, they used the nanoparticle sizes varied from 8 and 58 nm and concentrations of the nanofluids varied between 0.1–1.8 vol%. Their results indicated that the convective heat transfer behavior of nanofluids can be explained through altered thermal properties alone. However, the addition of any type of nanoparticles was observed to change some fluid properties unfavorably: enhanced thermal conductivity was obtained, but the viscosity increased significantly.

Pak and Cho [23] investigated the influence of using two different nanofluids (i.e., γ-Al_2O_3/water and TiO_2/water) on the convective heat transfer under turbulent flow regime. Pak and Cho (1998) have estimated the convective heat transfer coefficient based on using the fundamenetal energy balance across the test section with using the measured heat flux, mass flow rate, and inlet and outlet temperatures of nanofluids.Their experimental results revealed that the heat transfer coefficients of the nanofluids were increased with increasing volume concentration of nanoparticles and flow rate. Additionally, their heat transfer coefficient data showed that the Nusselt numbers were 30% higher than predicted for water.

Heris et al. [24, 25] presented experimental results for the convective heat transfer coefficient of Al_2O_3/water and CuO/water nanofluids inside a circular tube with constant wall temperature. Heris et al. [24, 25] measured the overall convective heat transfer coefficients of the segment of length of Al_2O_3/water and CuO/water nanofluids with implementing the same approach of Pak and Cho [23]. Their results indicated that the increase in heat transfer was obtained because the suspension of nanoparticles was much greater than that predicted using correlations based on single-phase heat transfer with the effective properties of the nanofluids. However, the Al_2O_3/water nanofluid showed more enhancement than the CuO/water nanofluid.

Kim et al. [26] performed an experimental study to investigate the effect of nanofluids on convective heat transfer for nanofluid flow through a straight circular tube with constant heat flux and different flow regimes (i.e., laminar and turbulent). In this study, two nanofluids were used: Al_2O_3/water and amorphous carbonic/water. It was found that for the Al_2O_3/water nanofluid, the enhancement of the convective heat transfer

coefficient was 15% and 20% for laminar and turbulent flows, respectively. In the case of the amorphous carbonic nanofluids, the enhancement of convective heat transfer coefficient was only 8% for the laminar flow, while no increase in convective heat transfer was obtained for turbulent flow. Similar investigations have been carried out using TiO_2/water and CuO/water nanofluids; the results showed that the Nusselt number increased noticeably with flow rate, but only slightly with nanofluid volume fraction and temperature [27].

Farajollahi et al. [28] investigated the convective heat transfer of TiO_2/water and γ-Al_2O_3/water nanofluids in a turbulent flow regime. It is worth mentioning that Farajollahi et al. [28] estimated the convective heat transfer coefficient using an energy balance around the test section using the measured heat flux, mass flow rate, and inlet and outlet temperatures of the nanofluids. They showed an increase in overall heat transfer coefficient and Nusselt number with increasing Reynolds number and volume fraction (φ=1–3%).

In their experiments, Kim et al. [26] used a stainless steel tube of length 2000 mm with inner diameter 4.57 mm to measure the convective heat transfer coefficients of segments along the length of the tube for Al_2O_3/water and amorphous carbonic/water nanofluids. Kim et al. [26] used the same approach as Farajollahi et al. [28]. A series of small thermocouples measured the inner wall temperatures for both laminar and turbulent flow regimes under isoflux thermal boundary condition. They measured the inlet and outlet temperatures of the nanofluid using T-type thermocouples at the inlet and outlet of the steel tube. Eleven T-type thermocouples used to measure the inner wall temperatures were mounted along the tube at various distances from the inlet. The study demonstrated that the enhanced convective heat transfer coefficient in the turbulent region was 20% higher,

which was a greater enhancement than the 15% obtained in the laminar region for Al_2O_3 nanofluids with φ= 3 vol%. However, for amorphous carbonic nanofluid, the increase was only 8% for laminar flow with 3.5 vol%. It was observed that the enhancement was particularly significant in the entrance region, and decreased with axial distance along the tube. Particle migration was given as one of the reasons for the improvement of the convective heat transfer coefficients.

Many other experimental investigations have followed the same methods as those presented above for determining convective heat transfer coefficients [21, 29-32]. It is evident that the method of measuring the overall and segment of length convective heat transfer coefficients was based on using the fundamental energy balance across the test section employing the measured wall surface and fluid temperatures, the supplied heat flux, and physical properties of the nanofluid with relatively primitive measurement techniques (DC power supply and thermocouples). Unfortunately, this method of measuring the convective heat transfer coefficients neglects the effect of axial heat conduction along the solid wall of any test section as well as heat losses. Therefore, the Multiphase Flow and Reactors Engineering and Applications Laboratory (mFReal) at Missouri S&T designed and developed a noninvasive heat transfer coefficient probe [33-35] to simultaneously measure the local instantaneous heat flux through the heated foil sensor (flush mounted on the inner surface of the test section), and its surface temperature by a thermocouple at the foil surface. This method of measuring the heat transfer coefficients overcomes the limitations mentioned above. Zouli et al. [7] implemented such technique as a newly developed sophisticated noninvasive heat transfer coefficient probe to measured the local heat transfer coefficients whithin the segment of length using Fe_2O_3/water nanofluids at

the laminar and turbulent flow regimes under thermal boundary conditions of isoflux. They used a copper tube with a 950 mm length, 25.4 mm inner diameter, and 31 mm outer diameter. In their work, nanofluid temperatures were measured using two thermocouples (T-type), which were inserted at the inlet and outlet of the test section. The micro-foil sensor was flush mounted on the inner wall surface of the test section to measure simultaneously the inner wall surface temperatures and the local instantaneous heat flux along the length of the sensor.

Accordingly, in the current study, a recirculation flow closed loop equipped with a thermal conductivity meter in conjunction with the mFReal sophisticated noninvasive heat transfer coefficient probe has been used to stady the impact of nanoparticles material on simultaneously measured the thermal conductivity and local heat transfer coefficient. The local instantaneous heat flux, and inner wall surface temperature have been as well measured. Three different types of nanoparticles, each of 30 nm diameter (Al_2O_3, Fe_2O_3, and CuO) within deionized water, have been used as test nanofluids for the investigation of enhanced thermal conductivity and local heat transfer coefficient. The 30 nm nanoparticle size were used in this work, as it is more practical to be implemented in practice as compared to the smaller sizes nanoparticles where the cost of their preparation increases significantly with reduction in sizes, and for the same reason, bigger size nanoparticles (~30 nm) were widely used in the literature [36, 37]. The Al_2O_3, CuO and Fe_2O_3 nanoparticles were selected because of their superior thermal conductivity and low cost, as well as the magnetic characteristic of Fe_2O_3 nanoparticle is beneficial to consider since a magnet can collect it and reuse [38, 39]. The current work was carried out for different operating conditions: four experimental temperatures (25, 35, 45, and 55 ^oC) and

six-volume concentrations (0, 0.01, 0.02, 0.03, 0. 04 and 0.05 vol.%) under turbulent and laminar flow regimes (Reynold numbers 1,000 to 10,000). Moreover, by measuring the local convective heat transfer coefficient (h), as well as the thermal conductivity (k), variations in the thermal boundary layer film thickness due to the presence of nanoparticles can be obtained, using Equation (1):

$$\delta = \frac{k}{h} \tag{1}$$

where δ is the thermal boundary layer thickness (m), k is the thermal conductivity (W/m.K), and h is the local heat transfer coefficient (W/m^2.K). This could help explain how h changes due to changes in k and δ.

The experimental data obtained in this work can serve as base data for validation any correlation or model for thermal conductivity and heat transfer coefficient. Furthermore, the results could lead to enhance various industrial thermal processes including the thermal efficiency for thermal desalination plants.

2. EXPERIMENTAL WORK

2.1 PREPARATION OF NANOFLUID

In the present study, three different spherically-shaped nanoparticles: Al_2O_3, CuO, and Fe_2O_3 each with diameter of 30 nm (manufactured by Alfa Aesar, USA), were suspended in deionized water to prepare the nanofluids. It is worth mentioning that in our previous work smaller nanoparticles were used (3, 10, 20 nm), however, in this study 30 nm nanoparticles were selected since this size is widely used in literature [36,37], and it has been observed that reducing the nanoparticle size does not have a great effect over the

thermal propertuies of the nanofluid. Furthermore, the cost of the 30 nm nanoparticles is lower compared with nanoparticles of smaller size. Six volume concentrations ranging from φ =0.01% to 0.05% for each of the Al_2O_3, CuO, and Fe_2O_3 nanoparticles were intimately mixed with the deionized water using digital homogenizer IKA ULTRA-TURRAXR T-25 (at 5000 rpm for 60 minutes) to ensure complete dispersion of the nanoparticles in the water. The volume concentrations of the nanofluids were determined using Equation (2).

$$\varphi = \frac{\frac{m_p}{\rho_p}}{\frac{m_p}{\rho_p} + \frac{m_{bf}}{\rho_{bf}}} x\ 100\ \% \qquad (2)$$

Where φ is the percentage of the volume concentration (vol %), m_p is the mass of the nanoparticles (kg), m_{bf} is the mass of the base fluid (kg), ρ_p is the density of nanoparticles (kg/m^3), and ρ_{bf} is of the density of the base fluid (kg/m^3).

An ultrasonic bath (manufactured by Fisher Scientific, USA) was used for 1–4 hours duration to further break down the finer nanoparticle aggregates. No sedimentation was observed at any volume concentration after four hours. To validate this, a stability test was conducted by taking samples of the nanofluids one day after preparation at 25^{o}C and analyzed using in a Zetasizer (manufactured by Malvern Instruments) to determine the zeta potential which indicates the stability of the nanofluid. As shown in Figure 1 the zeta potential values were found to increase with ultrasonic time, and the highest zeta potential values of Al_2O_3/water, CuO/water, and Fe_2O_3/water nanofluids preparation were measured as 57mV, 55mV and 52 mV, respectively after 3 hours of ultrasonication. Similar values have been observed by other researcher [40, 41] who measured a maximum absolute zeta

potential value of about 50 mV after three hours of ultrasonication for Al_2O_3/water nanofluid. The nanofluids were very stable without any observable sedimentation four weeks after preparation.

2.2 THERMAL CONDUCTIVITY MEASUREMENT

In this investigation, a Transient Line Source (TLS-100) Probe thermal properties analyzer (Thermtest Inc, Canada) was used to measure the thermal conductivity of the nanofluids (Al_2O_3/water, CuO/water, and Fe_2O_3/water) under wide range of (i.e., 0.1-5.0 W/m.K) with the different volume concentrations at 25, 35, 45 and 55°C. The TLS-100 probe analyzer consists of a digital handset microprocessor controller and 2.0 mm diameter, 100 mm long, single needle sensor which is inserted vertically into the nanofluid sample to measure the thermal conductivity of the nanofluid. The meter was calibrated before the measurements using standard solutions of known thermal conductivity such as the ASTM- D5334 standard, as recommended and supplied by the manufacturer. The accuracy of the Probe device was found to be 5% (by the manufacturer). The measurements were recorded for different samples at different temperatures (25-55^{o}C). The measurements were carried out for different nanoparticle volume concentrations in the range 0.01-0.05 vol. %. The measurements of the thermal conductivity were repeated six times for each sample, and at each temperature and the average values were taken for analysis.

2.3 EXPERIMENTAL SETUP

Figure 2 shows a schematic diagram of the experimental setup used for measuring the local heat transfer coefficient. This consisted of a closed flow loop containing a 950 mm

length of straight copper tube with 25.4 mm inner diameter, 31 mm outer diameter, and connected to a circulating pump and reservoir tank of 9.5 liters with agitator and heater (manufactured by Den Hartog Industries, Inc., USA) and used to monitor the dispersion and stability of the nanofluids. A magnetic drive pump (Procon, USA) was used to circulate the nanofluid through the test section. The flow rate was measured by a turbine flowmeter (TM050, GPI, USA) in the range from 1 to 6 l/min. The flow rate was controlled by two adjustable valves, one in the main flow loop and the other in the by-pass line. The loop has a test section with an inner diameter of 25.4 mm and the length of 400 mm. This section contains of two T-type thermocouples and the heat flux sensor was flush mounted on the inner wall surface of the test section. The test section surface is heated using a small cartridge heater (38 mm length, 6.35 mm diameter, and see Figure 2) to provide heat flow through the sensor. The DC variable power supply (HY5003, RSR Electronics, USA) was used to supply the required power to the cartridge heater to regulate the supplied power. The test section is insulated by ceramic fiber blanket (thickness 50 mm, and thermal conductivity 0.07 W/m K) to reduce the heat loss from the heater to the surrounding environment. Two T-type thermocouples (model TQSS-18G-6 Omega Engineering Inc. USA) were implanted into the flow at the inlet and outlet of the horizontal test section to measure the bulk nanofluid temperature. The micro-foil sensor from RdF Corporation (model no. 27036-1) was flush mounted on the inner wall surface of the test section with its center at a distance x=125 mm from the entrance to the test section. This micro-foil sensor can simultaneously measure the surface temperature and local instantaneous heat flux with a maximum operating temperature of 260^{o}C, with time response 0.02 sec, maximum sensor resistance of 100 Ω, and uncertainty < 2.5%. All readings of surface

temperature, bulk temperature, and the heat flux taken during the experimental runs were collected by a data acquisition system and processed in a computer (see below).

2.4 THE NONINVASIVE HEAT TRANSFER COEFFICIENT PROBE TECHNIQUE

This study used the noninvasive sophisticated fast-response heat transfer coefficient probe designed and developed at Missouri S&T (mFReal), to simultaneously measure surface wall temperature and local heat flux of the sensor. The heat transfer probe consists of a micro-foil sensor (6.35 mm wide x 17.78 mm long x 0.08 mm thick), that was flush mounted on the inner wall surface of the test section (axially 175 mm from the entrance of the test section) using high-temperature glue, see Figure 3. The micro-foil sensor has a fast response time of about 0.02 sec and is comprised of two components: a heat flux foil sensor and thermocouples. This micro-foil sensor was used to measure both the surface temperature of the sensor and the local instantaneous heat flux between the surface of the sensor and adjacent fluid [33]. Two T-type thermocouples (1.6 mm in diameter) was mounted above and in front of the heat flux foil sensor as shown in Figure 4. The axial positions of the two thermocouples were at x_1=150 mm (T_{b1}) and x_2=200 mm (T_{b2}), and the averaged values of the characteristic bulk temperatures of the fluids along the test section were measured with and without nanoparticles by these thermocouples. A small cartridge heater, as a source of heat for the heat flux foil sensor, was installed on the outer surface of the test section behind the flush mounted foil sensor (Figure 4). The DC power, regulated by variac (0 - 50 V) was supplied to the cartridge heater. The local heat transfer coefficient can be obtained by measuring simultaneously the characteristic bulk

temperature of the fluid flow, the surface temperature of the sensor, and the local instantaneous heat flux between the surface of the sensor and the adjacent fluid.

The local instantaneous heat transfer coefficient (h_i) and the local time-averaged heat transfer coefficients (h_{avg}) can be estimated using Equations (3) and (4):

$$h_i = \frac{q_i}{T_{s,i} - T_{b,i}} \; ; \; \Delta T_i = T_{s,i} - T_{b,i} \tag{3}$$

$$h_{avg} = \frac{1}{n} \sum_{i=1}^{n} \frac{q_i}{T_{s,i} - T_{b,i}} = \frac{1}{n} \sum_{i=1}^{n} h_i \tag{4}$$

Where, h_i is the local instantaneous heat transfer coefficient (W/m^2.K), q_i is instantaneous heat flux measured by the sensor (W/m^2), T_{si} is the instantaneous surface temperature of the probe (K), T_{bi} is the instantaneous bulk temperature of the fluid medium (K), h_{avg} is local time-averaged heat transfer coefficient (W/m^2.K), and n is the number of the collected data points (2000 data points).

2.5 DATA ACQUISITION (DAQ) SYSTEM

The data acquisition (DAQ) system was a NI SCXI-1303 National Instrument terminal block, a combination of chassis with controller, and chassis power card in conjunction with one amplifier (model JH4300-AC, JH Technology) and speed computer were used for the data collection and analysis. The DAQ system uses LabVIEW software. The measured signals from the heat flux foil sensors were in the range of microvolts, and hence, an amplifier was used to amplify them before they were processed by the DAQ system, see Figure 5. The measured signals from the heat flux foil sensors as well as thermocouples were simultaneously sampled at 50 Hz for about 40 seconds. Note that the

heat flux foil sensors are capable of detecting the direction of heat transfer between the wall surface and adjacent fluid. Negative signals from the heat flux foil sensors mean that heat transfer was from the adjacent fluid to the inner wall of the test section. Positive signals from the heat flux foil sensors imply that the heat transfer was from the inner wall of the test section to the adjacent fluid. The sampling rate was selected based on previous tests using different sampling rates that showed no difference in the time-averaged heat transfer coefficient.

3. RESULTS AND DISCUSSION

3.1 EFFECT OF FLUID TEMPERATURES AND NANOPARTICLE VOLUME CONCENTRATION ON THE THERMAL CONDUCTIVITY

The relationships between the thermal conductivities of the three nanofluids (Al_2O_3/water, CuO/water, and Fe_2O_3/water) with nanofluid temperature and volume concentration of nanoparticles are shown in Figures 6-8. The results show that the thermal conductivity of all three nanofluids and deionized water increased with increasing temperature, although the increase in the case of the nanofluids was much more pronounced. It is clear from Figures 6-8 that the thermal conductivity of Al_2O_3/water, CuO/water, and Fe_2O_3/water nanofluids increased with increasing particle volume concentration. It is also apparent that even at the lowest concentration, (0.01%) the thermal conductivity of the nanofluids was higher than that of the deionized water and as these volume concentrations were increased, further enhancement of the thermal conductivity were observed.

It was observed that the thermal conductivity was a function of both bulk fluid temperature, volume concentration and the nanoparticles used, this can be seen in Figures 6, 7 and 8. For example at 55ºC, the Al_2O_3/water nanofluid with 0.05 vol %, experienced an increase in thermal conductivity of 19% compared to water at the same temperature (Figure 6). For Fe_2O_3/water and CuO/water nanofluids, at the same volume concentration and temperature, the maximum enhancements in thermal conductivity were 21% and 25%, respectively (Figures 7, 8) compared to water at the same temperature. Figures 9 (a and b) compare the thermal conductivity measurements of the three nanofluids with different volume concentrations at 25°C and 55°C. It was found that the CuO/water nanofluid had highest thermal conductivity and this is due to CuO having a higher thermal conductivity than either Fe_2O_3 or Al_2O_3 (see Table 2). It is worth mentioning that the relative increase in thermal conductivity was significantly greater at the highest experimental temperature (55 ºC).

It is important to note that the thermal conductivity of Al_2O_3 is higher than Fe_2O_3. With respect to Figure 9 this shows that the thermal conductivity of the nanofluid is not simply related to the thermal conductivity of the nanoparticle material. It is suggested that Brownian motion of the nanoparticles or the properties of the liquid/solid interface may take ownership [42]. An increase in temperature increases the Brownian motion of the nanoparticles. This gives the particles greater ability to move randomly in the solution, interacting with neighboring particles, transferring energy and thus increasing thermal conductivity. Other researcher [43], have claimed to have shown that the thermal conductivity of nanofluids increases as a result of increasing the nanoparticles' Brownian motion due to higher temperature conditions.

Figures 10 (a-c) present the measured results obtained by other researchers [18, 44, 45] for thermal conductivity ratio (i.e., thermal conductivity of the nanofluid to that of base fluid) as a function of volume concentration of the three nanofluids: Al_2O_3/water, Fe_2O_3/water, and CuO/water nanofluids. From Figures 10(a-c), it can be seen that the thermal conductivity of Al_2O_3/water, Fe_2O_3/water, and CuO/water nanofluids significantly increases with increasing volume concentration in all cases, this shows good qualitative agreement with this work. This is taken to mean that both the thermal conductivity measurements and sample preparation have been successful.

3.2. COMPARISON OF THERMAL CONDUCTIVITY MODELS WITH EXPERIMENTAL DATA

The experimental thermal conductivity data from the present study have been compared with the result obtained from the Maxwell model [19] and the Yu-Choi model [46, 47]. These models are appropriate for spherically shaped particles which matches the current conditions and can be expressed as follows:

$$\frac{k_{nf}}{k_{bf}} = \frac{k_p + 2k_{bf} + 2(k_p - k_{bf})\varphi}{k_p + 2k_{bf} - (k_p - k_{bf})\varphi} \quad \text{(Maxwell model)} \quad (5)$$

$$\frac{k_{nf}}{k_{bf}} = \frac{k_p + 2k_{bf} + 2(k_p - k_{bf})(1+\beta)^3\varphi}{k_p + 2k_{bf} - (k_p - k_{bf})(1+\beta)^3\varphi} \quad \text{(Yu-Choi model)} \quad (6)$$

Where φ is the volume concentration (vol %) of the nanoparticles, k_{bf} is the thermal conductivity of the basefluid (W/m.K), k_p is the thermal conductivity of the nanoparticles (W/m.K), k_{nf} is the thermal conductivity of the nanofluid (W/m.K), and β is the ratio of the nanolayer thickness to the original particle radius; it usually is assumed to be 0.1.

It is evident that the Maxwell and Yu-Chio models are nonlinear. Nevertheless, for a small range of low volume concentrations of nanoparticles (from 0.01 to 0.05 vol% with

an increment of 0.01) these models give a straight line trend. Figures 11-13 show the comparison of both models with current experimental results for the thermal conductivity ratio for Al_2O_3/water, CuO/water, and Fe_2O_3/water nanofluids as a function of particle volume concentration at 25°C and 55°C. From Figures 11-13 the results showed qualitative and quantitative similarities between the predicted values (from Equations 5 and 6) and current experimental data for all experimental conditions tested [48]. The average absolute relative difference (AARD) between the current experimental results and the values predicted by the Maxwell model (Equations 5) are 7.8%, 9.0%, and 8.4% for Al_2O_3/water, CuO/water, and Fe_2O_3/water nanofluids, respectively at 25°C; and 15.7%, 21.2%, and 18.9% respectively at 55°C. It is clear from the results that at a fluid temperature of 55°C the deviation of the experimental data from the model predictions increased (Equations 5 and 6), which could be attributed to the theoretical models assuming room temperature conditions [19]. These models would need modification to account for the effect of temperature.

3.3. LOCAL CONVECTIVE HEAT TRANSFER COEFFICIENTS OF NANOFLUIDS

3.3.1 Time Series of Heat Transfer Coefficients. Figure 14 shows the time series of heat transfer coefficients at laminar and turbulent flow conditions for different nanoparticles. From the figure it can be seen that at laminar flow conditions mean and the fluctuations of the local heat transfer coefficients are lower; at laminar flow conditions the results exhibited a mean between 1.506 – 1.567 and variance between 0.00042 – 0.0046, while at turbulent conditions, the mean was found between 3.310 – 3.439 and the variance between 0.020 – 0.022. This phenomena is expected as at the turbulent flow conditions,

due to the eddies, all the transport properties (heat, mass and momentum) were affected. However, local eddies facilitate the high heat transfer coefficient due to high mixing compared with the laminar flow conditions. At laminar conditions, high heat transfer coefficient was observed for CuO nanoparticles, while with Fe_2O_3 nanoparticles it is lower than CuO but higher than Al_2O_3. Similar trend has been observed at the turbulent conditions, however with higher magnitude of heat transfer coefficients.

3.3.2 Effect of Nanoparticle Volume Concentration and Fluid Temperatures on Heat Transfer Coefficient with the use of Nanofluids. The local heat transfer coefficients for three nanofluiuds Al_2O_3/water, Fe_2O_3/water, and CuO/water, under isoflux thermal conditions, has been investigated at three different volume concentrations (φ =0.01%, 0.03%, and 0.05%) and temperatures 25 and 55^{o}C for laminar and turbulent flow regimes with Reynolds number over the range 1000 - 10000.

Figures 15-17 show the variations of the local heat transfer coefficient with Reynolds number in the range 1000 to 3500 for the three nanofluids for the three volume concentrations at 25^{o}C. It is found that the local heat transfer coefficients increased with increased volume concentration and higher Re. As shown in Figure 15, the local heat transfer coefficients in the nanofluids are close to the one for the water due to the low volume concentration (0.01 vol%) of the nanoparticle, leading to differences of around 5.43% - 12.14%. However, at higher volume concentrations (0.05 vol%) the difference between the nanofluids and the water is increased (difference = 18.93% - 33.21%). At 25^{o}C, the maximum increase in local heat transfer coefficient of the Al_2O_3/water nanofluid with respect to water was 29% at a volume concentration (φ = 0.05%). Under the same conditions the maximum enhancements of local heat transfer coefficient for Fe_2O_3/water

and CuO/water nanofluids, were 34% and 37 %, respectively. These results show that the enhancement of local heat transfer coefficient with the CuO/water nanofluid can be attributed to its higher thermal conductivity, density, and lower specific heat compared to the other nanofluids, see Table 2.

Figures 18-20 show the variations of the local heat transfer coefficient with Reynolds number in the range 4000 to 10000 for the three nanofluids for the three volume concentrations at 55^{o}C. The results show a substantial increase in local heat transfer coefficient for all three nanofluids with Reynolds number. At the highest flow rate with the Al_2O_3/water nanofluid at a volume concentration ($\varphi = 0.05\%$), the local heat transfer coefficient increased by 44% compared to water under the same conditions. For the Fe_2O_3/water and CuO/water nanofluids the maximum enhancements of local heat transfer coefficient were 50% and 53%, respectively, are shown in the Figures 19 and 20. The enhancement of the local heat transfer coefficient depends on the thermal conductivity of the nanofluid and thermal boundary layer film thickness.

The forced convective heat transfer coefficient has been defined as $h=k/\delta$, where k is the thermal conductivity of the nanofluid and δ is the film thickness of the thermal boundary layer [38]. The increase in thermal conductivity or/and the decrease in the film thickness enhanced the local convective heat transfer coefficient of the nanofluids. The thermal conductivity of the nanofluid increased with increase in nanoparticle concentration, while decreasing the film thickness of the thermal boundary layer can be due to the migration of nanoparticles, mobility of the nanoparticles near the wall, and the reduction of viscosity in the near-wall region [49]. In comparison with Al_2O_3/water nanofluid, the viscosities of the Fe_2O_3/water and CuO/water nanofluids are lower. The

viscosity of nanofluids increases with increasing the volume concentration, and this more significant for the Al_2O_3/water nanofluid [50]. When the viscosity of nanofluids increases, the viscous forces are strong enough to overcome the Brownian motion of the nanoparticles. The thermal boundary layer film thickness under these conditions increases, therefore, the heat transfer coefficient decreases if thermal conductivity remains unchanged or varies only slightly. The thermophysical properties of the CuO/water nanofluid relative to other two nanofluids mean its local convective heat transfer coefficient is highest for all three volume concentrations, as shown in Figures 15-20.

3.3.3 Effect of Flow Regime on Thermal Conductivity and Heat Transfer Coefficient with the use of Nanofluids. It can be seen from Figures 15-20 that the local heat transfer coefficients increase with the increase of Reynolds number for all three nanofluids for all three volume concentrations and at both test temperatures. Tables 3-11 show the increase in thermal conductivity and local heat transfer coefficient for Al_2O_3/water, CuO/water, and Fe_2O_3/water nanofluids with volume concentration of $\varphi = 0.01 - 0.05\%$ for laminar and turbulent flow regimes at 25°C and 55°C. Our results show that using nanofluids the heat transfer coefficient increases due to increase in the thermal conductivity and reduction in the thermal boundary layer film thickness. In the laminar flow regime (Re=1000 to 3000) the change in the thermal boundary layer film thickness is small compared with that of the turbulent flow regime (Re=4000 to 10000). Hence, the enhancement of the local heat transfer coefficient in the turbulent flow regime is greater than that for the laminar flow regime for all experimental conditions, see Tables 3-11.

Another possible contributing factor to the enhancement of the local heat transfer coefficient for nanofluids, is when the thickness of the film is greater than the diameter of

the nanoparticle used (30 nm). This allows the nanoparticles to penetrating the film toward the wall and generate local micro eddies and local mixing within the film which will contribute to the enhancement of the local heat transfer coefficients [29, 51]. Also, at constant Reynolds number (Re=1000, 2800 and 10000), the local heat transfer coefficient was found to increase with increasing the nanoparticle volume concentrations (i. e. , $\varphi =$ 0.01, 0.03, and 0.05%) as shown in Figures 15-20. The results also showed that the CuO/water nanofluid at 0.05 vol.% and 55 ^{o}C under turbulent flow regime achieved the highest local heat transfer coefficient for all three nanofluids for all experimental conditions due to increase in thermal conductivity by 25% and a reduction in the thermal boundary layer film thickness by 19%.

3.3.4 Comparison Between the Experimental Convective Heat Transfer Coefficients and the Predicted Values from Literature Correlations. In our previous work, Xuan –Li [53] correlation were found to be better predict the experimental results of heat transfer coefficient when using Fe_2O_3 nanoparticle [7]. However, for other nanoparticles used in this work, this remains to be tested. The above correlation and the other correlations developed at similar operating conditions were used to predict the heat transfer coefficient in this study. The correlations used in this study are as follows:

Dittus-Boelter correlation [52]

$$Nu = 0.023\, Re^{0.87}\, Pr^{0.3} \quad (7)$$

Gnielinski correlation [28]

$$Nu = 0.012\, (Re^{0.87} - 280) Pr^{0.3} \quad (8)$$

Xuan-Li correlation [53] for laminar conditions

$$Nu = 0.4328(1 + 11.285\ \varphi^{0.754} Pe^{0.218}) Re^{0.333} Pr^{0.4} \quad (9)$$

Xuan-Li correlation [53] for Turbulent conditions

$$Nu = 0.0059(1 + 7.6286\ \varphi^{0.6886} Pe^{0.001}) Re^{0.9238} Pr^{0.4} \quad (10)$$

Where $Nu\ (\frac{h.d}{k})$ is a Nusselt number, $Re\ (\frac{pvd}{\mu})$ is Reynolds number, $Pr\ (\frac{C_p\,\mu}{K})$ is the Prandtl number, $Pe\ (\frac{Lv}{D})$ is a Peclet number and φ is the percentage of the volume concentration (vol %).

Figures 21-26 show the relationships between Reynolds number (Re) and Nusselt number (Nu) for Al_2O_3/water, Fe_2O_3/water and CuO/water nanofluids at 25 ^oC and 55 ^oC under laminar and turbulent flow regimes from 1000 to 10000. The predicted values obtained using the Dittus-Boelter correlation [52], the Gnielinski correlation [28], and the Xuan-Li correlation [53] were compared with our results for the measured Nusselt number.

Xuan-Li correlation [53] (Equations 9 and 10) compared to the correlations for Dittus-Boelter [49] and Gnielinski [28] (Equations 7 and 8) gives better predictions of our results. This good agreement could be attributed to the percentage of the volume concentration (φ) parameters being close to those used when deriving the Xuan-Li correlation [53] (Equations 9 and 10), which was not the case with the other correlations (Equations 7 and 8).

The results show good qualitative and quantitative similarity between the current experimental data and values predicted by the Xuan-Li correlation [53] (Equation 10) at 55^{o}C with the average absolute relative differences (AARD) of 11%, 10%, and 9% for Al_2O_3/water, Fe_2O_3/water, and CuO/water nanofluids, respectively at turbulent flow regime as shown in Figures 20, 21 and 22. While, at 25^{o}C the maximum observed deviation

in terms of AARE of Xuan-Li correlation [53] (Equation 9 and 10) for laminar and turbulent flow regimes are 18%, 17%, and 16% for Al_2O_3/water, Fe_2O_3/water, and CuO/water nanofluids, respectively which are more significant than those at 55^{o}C with proper trend as shown in Figures 24, 25 and 26. The changes of the thermophysical properties of nanofluids (i.e., density, specific heat capacity, thermal conductivity, and viscosity) caused the correlation to favor the modified properties at high temperature [54]. For lower temperature and/or for a wide range of temperatures, further adjustment to the modification or constant is needed for correlation.

4. REMARKS

In this work, the thermal conductivity and local heat transfer coefficient of Al_2O_3/water, Fe_2O_3/water, and CuO/water nanofluids have been experimentally investigated over the range 0.01% to 0.05% volume concentration, at bulk nanofluid temperatures 25-55°C in laminar and turbulent flow regimes. A new sophisticated noninvasive heat transfer coefficient probe that is flush mounted on the inner wall surface of the test section has been developed and employed, to measure simultaneously the wall surface temperature and local heat transfer coefficient. The following results were obtained:

- The use Al_2O_3, Fe_2O_3, and CuO nanoparticles as dispersed phase in water can significantly enhance the thermal conductivity and local heat transfer coefficient under the conditions of this work.

- The thermal conductivity and local heat transfer coefficient increased with increased volume concentration and temperature of the Al_2O_3/water, Fe_2O_3/water, and CuO/water nanofluids.
- The greatest enhancements in thermal conductivity were 19%, 21%, and 25% for Al_2O_3/water, Fe_2O_3/water, and CuO/water nanofluids, respectively when compared to water at $\varphi = 0.05\%$ and 55 °C.
- The Maxwell model and the Yu-Choi model for the thermal conductivity of the nanofluid led to good prediction at 25 ^oC, while at 55 ^oC high deviations in the predictions were found. Thus, these models would need modification to account for the effect of temperature.
- The mean and variance is lower for the laminar conditions whereas it increase for turbulent conditions. At laminar flow conditions the results exhibited a mean between 1.506 – 1.567 and variance between 0.00042 – 0.0046, while at turbulent conditions, the mean was found between 3.310 – 3.439 and the variance between 0.020 – 0.022
- The maximum enhancement in the local heat transfer coefficient are 44%, 50% and 53 %, respectively at $\varphi = 0.05\%$ and 55 °C.
- The results showed that the CuO/water nanofluid at 0.05 vol.% and 55 ^oC under a turbulent flow regime achieved the largest increase in local heat transfer coefficient of 53% compared to the other nanofluids due to an increase in thermal conductivity of 25% and a reduction in the thermal boundary layer film thickness of 19%.
- It is clear that the boundary layer film thickness is larger than the diameter of the nanoparticles used in this work (30 nm). This allows the nanoparticles to

penetrating the film toward the wall and generate local micro eddies and local mixing within the film. This contributes to the enhancement of the local heat transfer coefficient.

- Xuan and Li correlation (Equation 10) for turbulent flow regime predicts well our results at 65 ^{o}C for Al_2O_3/water, Fe_2O_3/water, and CuO/water nanofluids with the average absolute relative differences (AARD) of 11, 10, and 9 %, respectively. This good agreement could be attributed to the percentage of the volume concentration (φ) parameters being close to those used when deriving the Xuan-Li correlation (Equation 10), which was not the case with the other correlations (Equations 7 and 8).
- At 25 ^{o}C the maximum observed deviation in terms of AARE of Xuan-Li correlation (Equation 9 and 10) for laminar and turbulent flow regimes are 18%, 17%, and 16% for Al_2O_3/water, Fe_2O_3/water, and CuO/water nanofluids, respectively which are more significant than those at 65 ^{o}C with proper trend. This could be due to the effect of the thermophysical properties of nanofluids (i.e., density, specific heat capacity, thermal conductivity, and viscosity) and hence, these correlations need to be adjusted for their constants or modified.

ACKNOWLEDGMENT

The author (Zouli) would like to thank the colleagues at Multiphase Flows and Reactors Engineering and Application Laboratory (mFreal), Chemical and Biochemical Engineering Department at Missouri University of Science and Technology (Missouri S&T), Rolla, Missouri (USA), for providing help while conducting experiments. The

author (Zouli) also would like to thank the University of Jazan for giving him the financial support. The author (Zouli) also thank Dr. Abbas Sultan for his valuable comments.

NOMENCLATURE

D	tube diameter [m]	*Greek symbols*	
C_p	fluid heat capacity [J/kg K]	α	fluid thermal diffusivity [m^2/s]
h	heat transfer coefficient [W/m^2 k]	δ	thermal boundary layer thickness [m]
K	thermal conductivity [W/m K]	μ	fluid dynamic viscosity [$N.s/m^2$]
AARE	average absolute relative error	ρ	fluid density [kg/m^3]
Nu	Nusselt number [-]	∅	Volume fraction [-]
Re	Reynolds number [-]		
Pe	Peclet number [-]	*Subscript*	
Pr	Prandtl number [-]	bf	base fluid
q_i	heat flux [W/m^2]	nf	Nanofluids
n	Empirical shape factor [-]	p	Particle
T	Temperature [K]	s	surface
ν	fluid velocity [m/s]	b	bulk
L	Length [m]		

Table 1: Thermal conductivities of various solids and liquids

	Material	Thermal conductivity (W/m. K)
Metallic solids	Silver	429
	Copper	401
	Aluminum	237
Nonmetallic solids	Titanium	23
	Silicon	148
	Alumina	40
Metallic liquids	Silicon	72
Nonmetallic liquids	Water	0.61
	Ethylene glycol	0.253
	Engine oil	0.145

Table 2: Thermophysical properties of Al_2O_3, Fe_2O_3, and CuO nanoparticles

Nanoparticles	Mean Diameter (nm)	Density (kg/m^3)	Thermal conductivity (W/m.K)	Specific heat (J/gm.K)
Al_2O_3	30	3600	40	765
Fe_2O_3	30	5240	20	650
CuO	30	6350	69	550

Table 3: Enhancement of the heat transfer coefficient for Al_2O_3/water nanofluid of 30 nm for laminar flow regime at Re=1000 at fluid temperature of 25°C.

Concentration of Al_2O_3 nanoparticle (vol.%)	Thermal conductivity of Al_2O_3/water nanofluids (W/m.K)	Heat transfer coefficient ($W/m^2.K$)	Thermal boundary layer thickness (mm)	Enhancement (k) (%)	Enhancement (h) (%)	Decrease (δ) (%)
0	0.595	526	1.13	0	0	0
0.01	0.608	552	1.10	2	5	2
0.02	0.624	565	1.10	5	7	2
0.03	0.638	584	1.09	7	11	3
0.04	0.652	601	1.08	9.5	14	4
0.05	0.667	620	1.07	12	18	5

Table 4: Enhancement of the heat transfer coefficient for Al_2O_3/water nanofluid of 30 nm for turbulent flow regime at Re=2800 at fluid temperature of 25°C.

Concentration of Al_2O_3 nanoparticle (vol.%)	Thermal conductivity of Al_2O_3/water nanofluids (W/m.K)	Heat transfer coefficient ($W/m^2.K$)	Thermal boundary layer thickness (mm)	Enhancement (k) (%)	Enhancement (h) (%)	Decrease (δ) (%)
0	0.595	1410	0.42	0	0	0
0.01	0.608	1530	0.39	2	8.5	7
0.02	0.624	1625	0.38	5	15	9
0.03	0.638	1705	0.37	7	21	11
0.04	0.652	1745	0.37	9.5	24	11
0.05	0.667	1820	0.36	12	29	13

Table 5: Enhancement of the heat transfer coefficient for Al_2O_3/water nanofluid of 30 nm for turbulent flow regime at Re=10000 and fluid temperature of 55°C.

Concentration of Al_2O_3 nanoparticle (vol.%)	Thermal conductivity of Al_2O_3/water nanofluids (W/m.K)	Heat transfer coefficient ($W/m^2.K$)	Thermal boundary layer thickness (mm)	Enhancement (k) (%)	Enhancement (h) (%)	Decrease (δ) (%)
0	0.639	2270	0.28	0	0	0
0.01	0.657	2645	0.25	3	16	12
0.02	0.683	2837	0.24	7	24	15
0.03	0.707	3020	0.23	11	33	16
0.04	0.734	3148	0.23	15	38	16
0.05	0.759	3275	0.23	19	44	16

Table 6: Enhancement of the heat transfer coefficient for CuO/water nanofluid of 30 nm for laminar flow regime at Re=1000 and fluid temperature of 25°C.

Concentration of CuO nanoparticle (vol.%)	Thermal conductivity of CuO/water nanofluids (W/m.K)	Heat transfer coefficient ($W/m^2.K$)	Thermal boundary layer thickness (mm)	Enhancement (k) (%)	Enhancement (h) (%)	Decrease (δ) (%)
0	0.595	526	1.13	0	0	0
0.01	0.629	580	1.08	5	10	4
0.02	0.644	612	1.05	8	16	7
0.03	0.659	650	1.01	10	23	10
0.04	0.668	682	0.98	12	29	13
0.05	0.686	700	0.98	15	33	13

Table 7: Enhancement of the heat transfer coefficient for CuO/water nanofluid of 30 nm for turbulent flow regime at Re=2800 and fluid temperature of 25°C.

Concentration of CuO nanoparticle (vol.%)	Thermal conductivity of CuO/water nanofluids (W/m.K)	Heat transfer coefficient (W/m^2K)	Thermal boundary layer thickness (mm)	Enhancement (k) (%)	Enhancement (h) (%)	Decrease (δ) (%)
0	0.595	1410	0.42	0	0	0
0.01	0.629	1587	0.39	5	12	7
0.02	0.644	1710	0.38	8	21	9
0.03	0.659	1815	0.36	10	28	13
0.04	0.668	1874	0.35	12	32	16
0.05	0.686	1935	0.35	15	37	16

Table 8: Enhancement of the heat transfer coefficient for CuO/water nanofluid of 30 nm for turbulent flow regime at Re=10000 and fluid temperature of 55°C.

Concentration of CuO nanoparticle (vol.%)	Thermal conductivity of CuO/water nanofluids (W/m.K)	Heat transfer coefficient ($W/m^2.K$)	Thermal boundary layer thickness (mm)	Enhancement (k) (%)	Enhancement (h) (%)	Decrease (δ) (%)
0	0.639	2270	0.28	0	0	0
0.01	0.690	2815	0.25	8	24	12
0.02	0.732	3015	0.24	14	32	15
0.03	0.768	3185	0.24	20	40	15
0.04	0.782	3276	0.23	22	45	16
0.05	0.798	3480	0.22	25	53	19

Table 9: Enhancement of the heat transfer coefficient for Fe_2O_3/water nanofluid of 30 nm for laminar flow regime at Re=1000 and fluid temperature of 25°C.

Concentration of Fe_2O_3 nanoparticle (vol.%)	Thermal conductivity of Fe_2O_3/water nanofluids (W/m.K)	Heat transfer coefficient ($W/m^2.K$)	Thermal boundary layer thickness (mm)	Enhancement (k) (%)	Enhancement (h) (%)	Decrease (δ) (%)
0	0.595	526	1.13	0	0	0
0.01	0.618	561	1.10	3	6	2
0.02	0.6301	585	1.07	6	11	5
0.03	0.647	625	1.03	8	18	8
0.04	0.656	652	1.00	10	23	11
0.05	0.675	680	1.00	13	29	11

Table 10: Enhancement of the heat transfer coefficient for Fe_2O_3/water nanofluid of 30 nm for turbulent flow regime at Re=2800 and fluid temperature of 25°C.

Concentration of Fe_2O_3 nanoparticle (vol.%)	Thermal conductivity of Fe_2O_3/water nanofluids (W/m.K)	Heat transfer coefficient ($W/m^2.K$)	Thermal boundary layer thickness (mm)	Enhancement (k) (%)	Enhancement (h) (%)	Decrease (δ) (%)
0	0.595	1410	0.42	0	0	0
0.01	0.618	1561	0.39	3	10	7
0.02	0.6301	1673	0.37	6	16	11
0.03	0.647	1786	0.36	8	27	13
0.04	0.656	1838	0.35	10	37	16
0.05	0.675	1897	0.35	13	52	16

Table 11: Enhancement of the heat transfer coefficient for Fe_2O_3/water nanofluid of 30 nm for turbulent flow regime at Re=10000 and fluid temperature of 55°C.

Concentration of Fe_2O_3 nanoparticle (vol.%)	Thermal conductivity of Fe_2O_3/water nanofluids (W/m.K)	Heat transfer coefficient ($W/m^2.K$)	Thermal boundary layer thickness (mm)	Enhancement (k) (%)	Enhancement (h) (%)	Decrease (δ) (%)
0	0.639	2270	0.28	0	0	0
0.01	0.685	2785	0.25	7	22	12
0.02	0.701	2918	0.24	10	28	15
0.03	0.732	3143	0.23	14	38	16
0.04	0.762	3284	0.23	19	43	16
0.05	0.776	3401	0.23	21	50	16

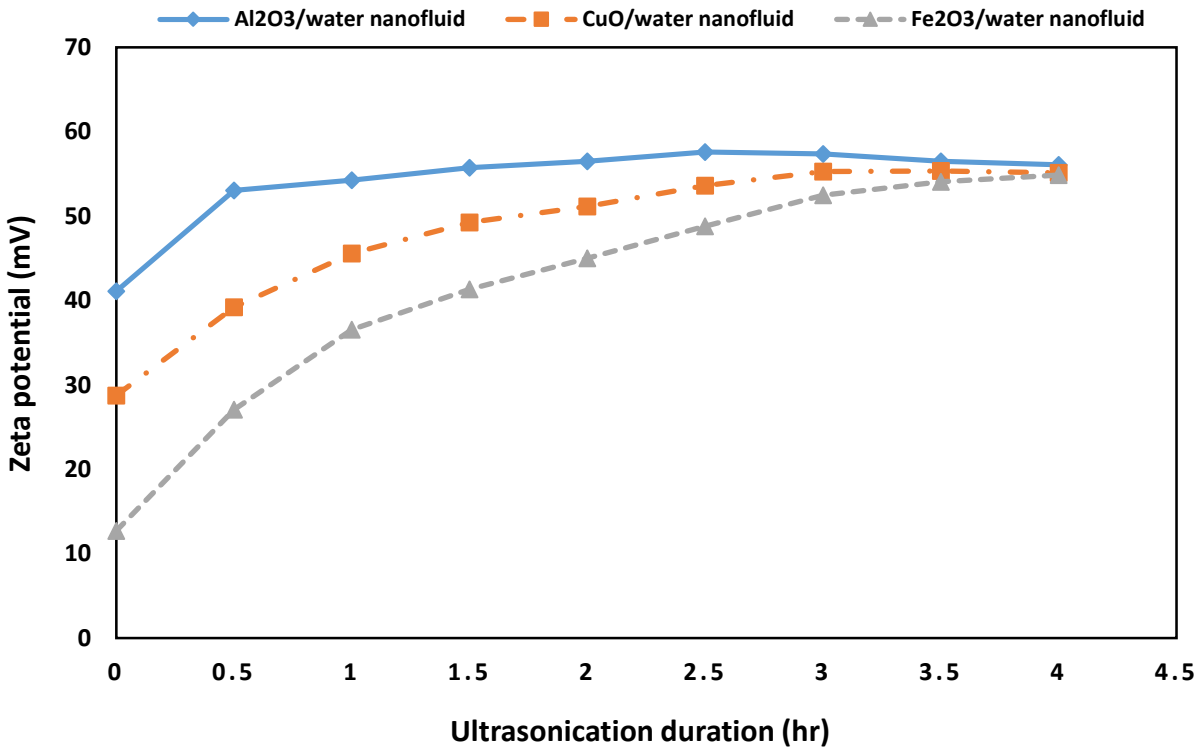

Figure 1: Zeta potentials of nanofluids after varying ultrasonication durations.

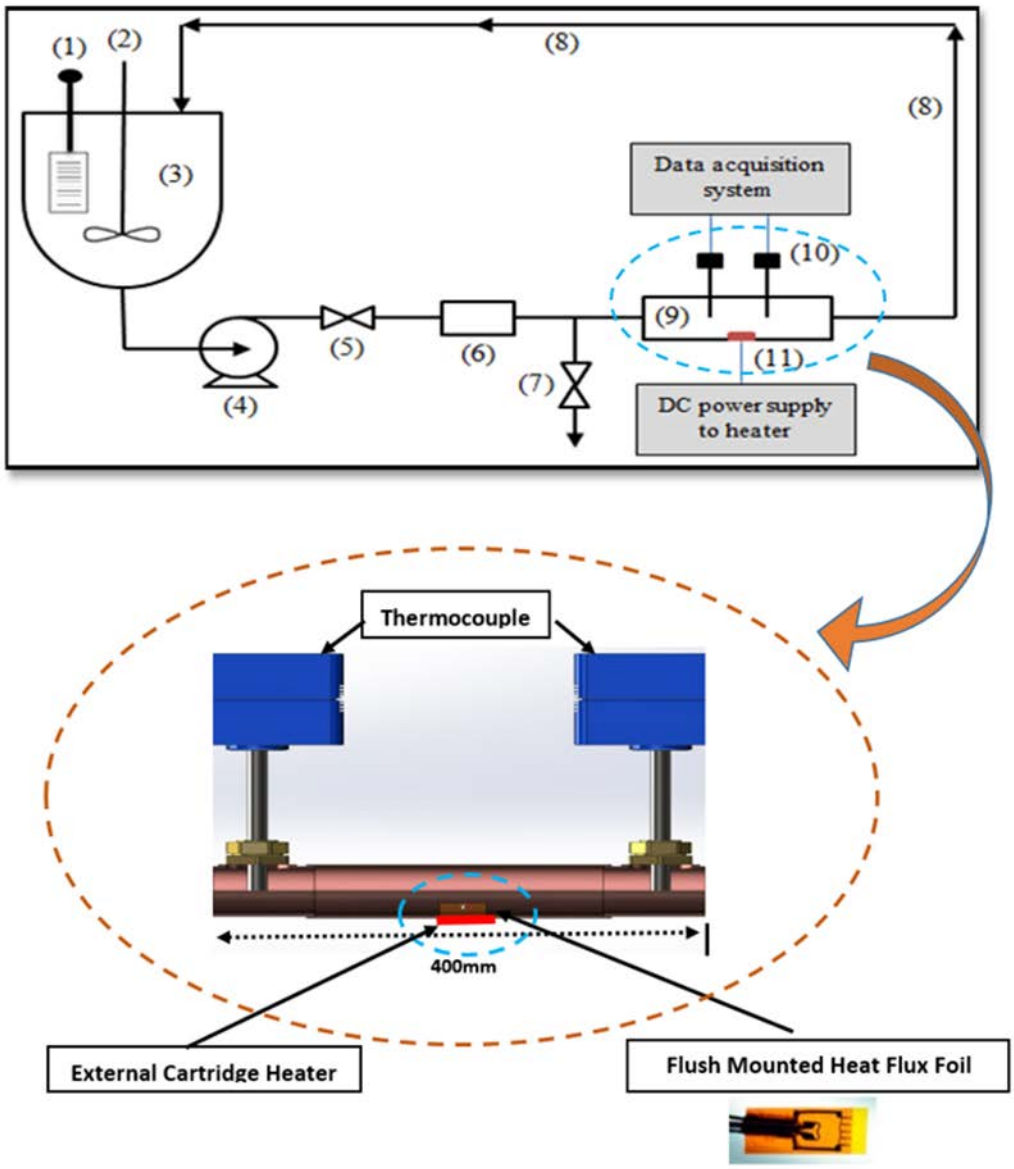

(1) Heater, (2) Agitator, (3) Reservoir tank, (4) Pump, (5) Needle valve, (6) Flow meter, (7) Drainage valve, (8) Copper tube, (9) Test section of copper tube, (10) Thermocouples, (11) Heat flux foil sensor.

Figure 2: Schematic diagram of experimental setup

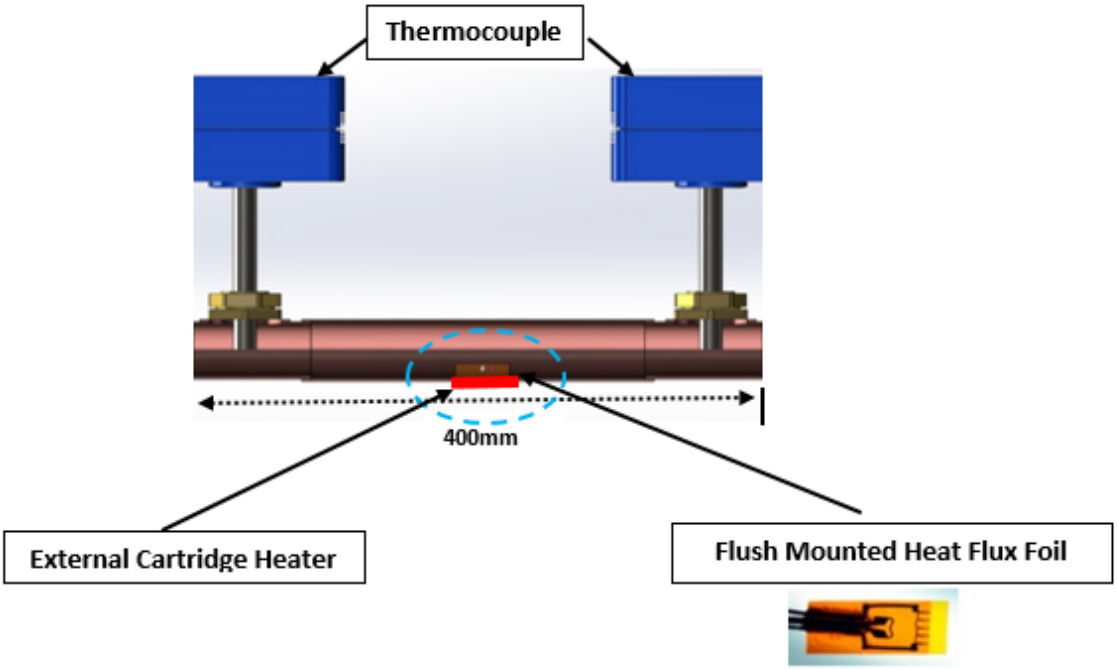

Figure 3: Schematic diagram of the non-invasive heat transfer coefficient probe (flush mounted on the inner wall surface)

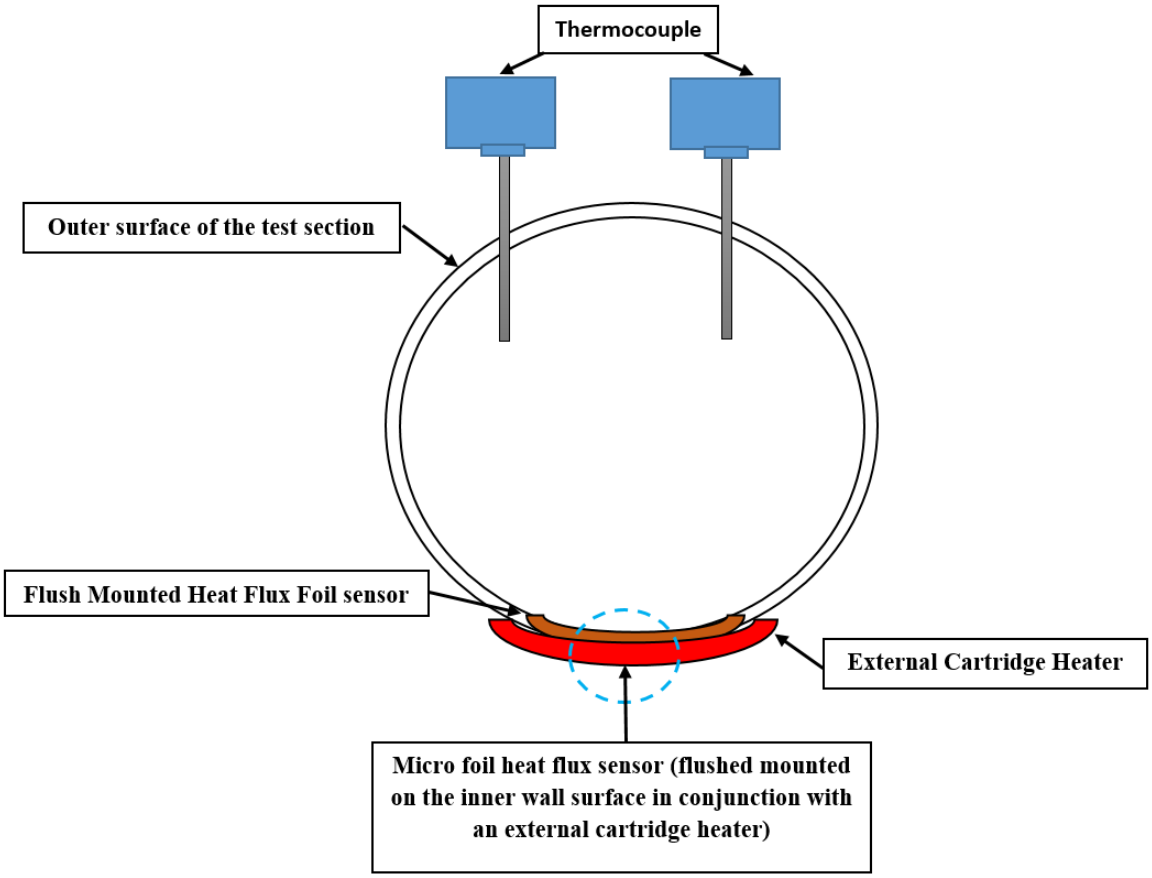

Figure 4: Schematic diagram of the non-invasive heat transfer coefficient probe (flush mounted on the inner wall surface in conjunction with an external cartridge heater)

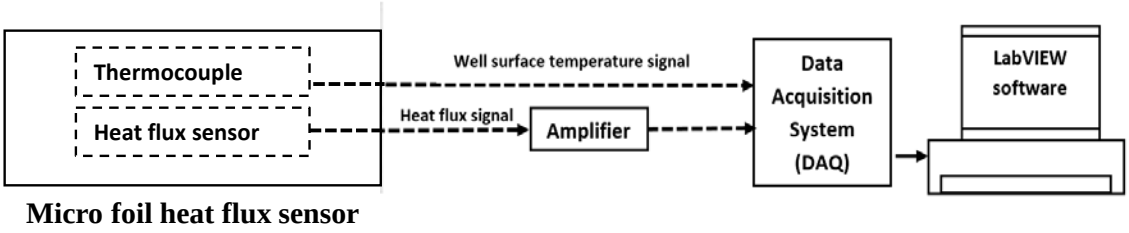

Figure 5: The sequence of the signal collection from the heat flux sensor to the data acquisition system.

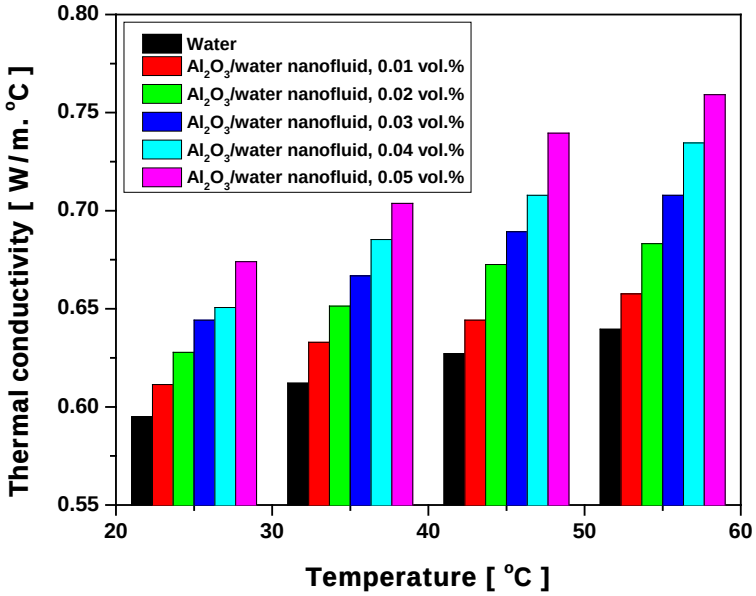

Figure 6**:** Thermal conductivity enhancement of Al_2O_3/water nanofluid as a function of volume concentration at different temperatures

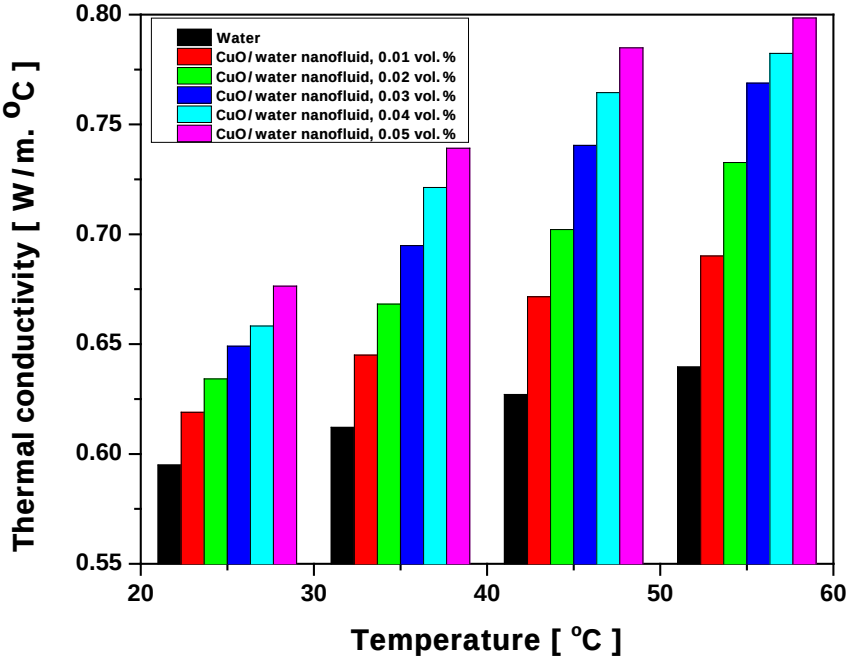

Figure 7: Thermal conductivity enhancement of CuO/water nanofluid as a function of volume concentration at different temperatures

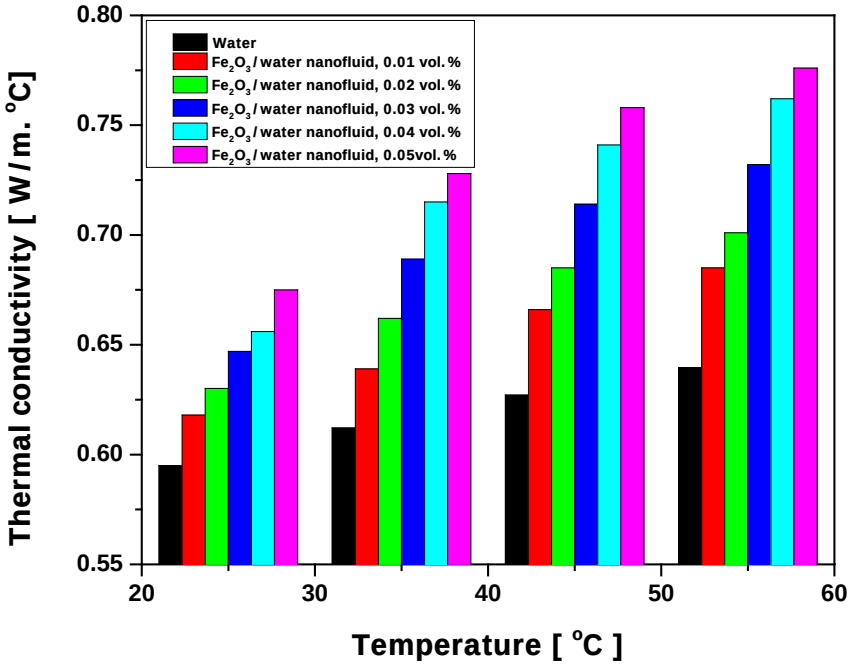

Figure 8: Thermal conductivity enhancement of Fe_2O_3/water nanofluid as a function of volume concentration at different temperatures

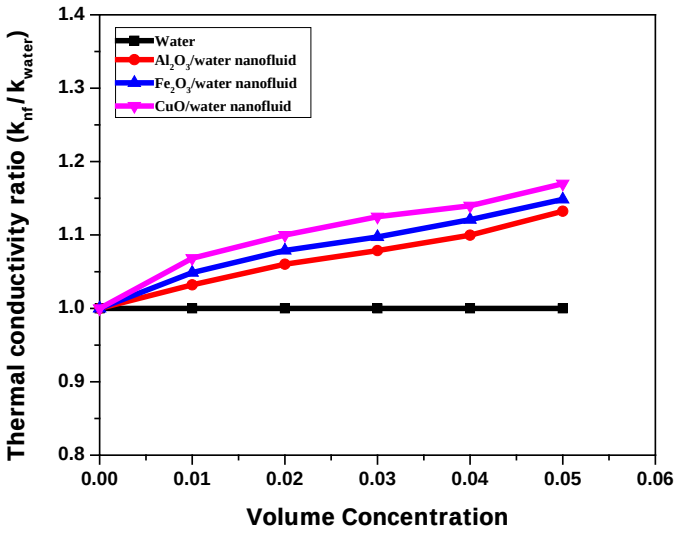

(a)

Figure 9: Variations of thermal conductivity ratio with different volume concentrations. (a) at 25 °C. (b) at 55 °C

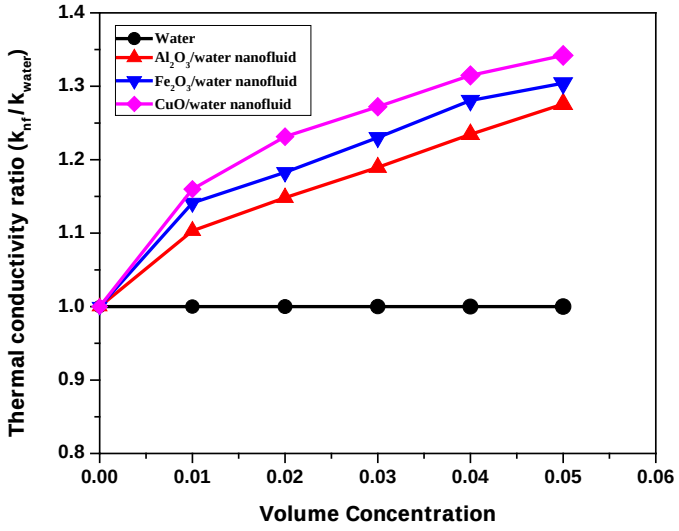

(b)

Figure 9: Variations of thermal conductivity ratio with different volume concentrations. (a) at 25 °C. (b) at 55 °C (cont.)

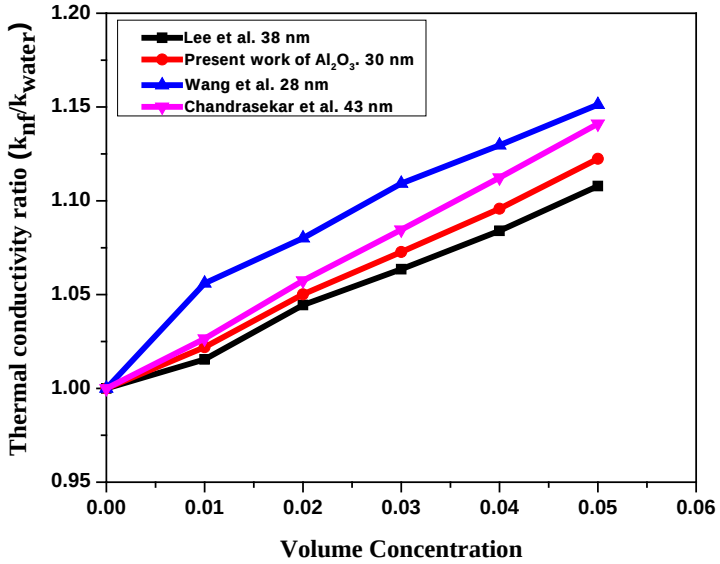

(a)

Figure 10: Comparison between results from the present work with results from other experimental work of (a) Al_2O_3/water nanofluids at room temperatures. (b) CuO/water nanofluids at room temperatures. (c) Fe_2O_3/water nanofluids at room temperatures

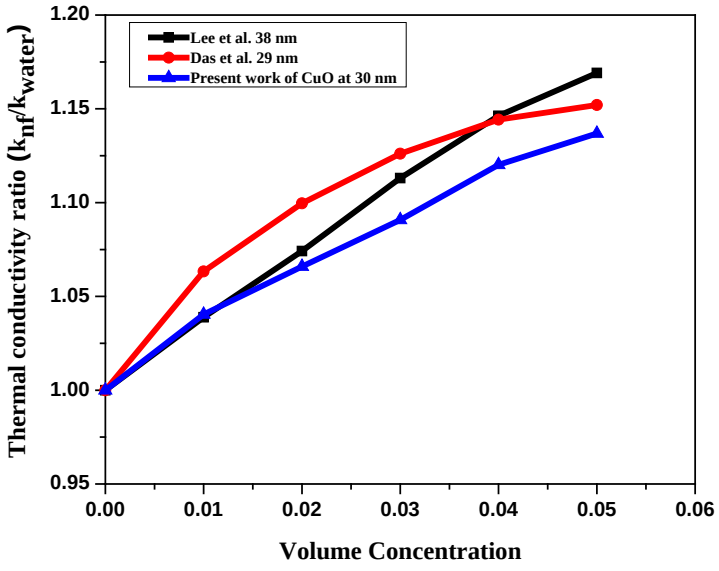

(b)

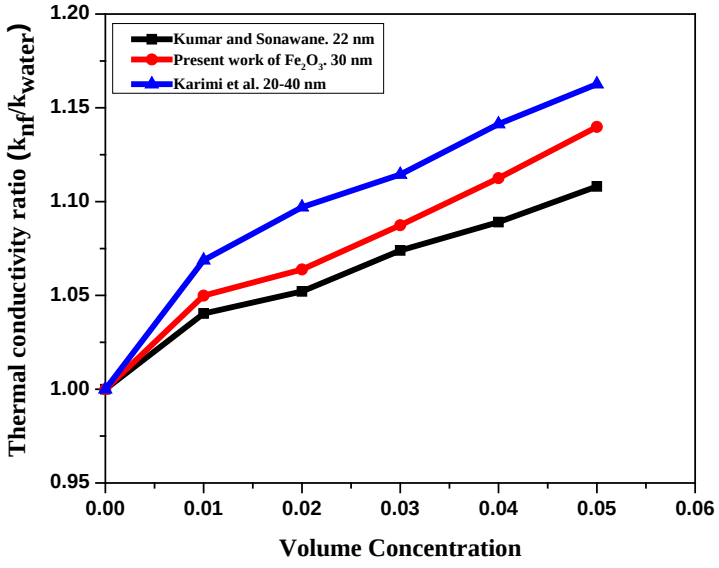

(c)

Figure 10: Comparison between results from the present work with results from other experimental work of (a) Al_2O_3/water nanofluids at room temperatures. (b) CuO/water nanofluids at room temperatures. (c) Fe_2O_3/water nanofluids at room temperatures (cont.)

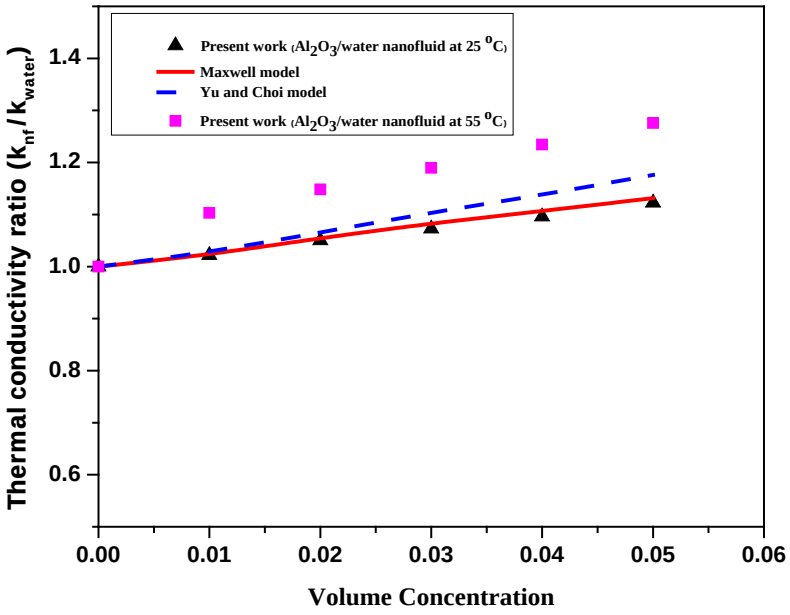

Figure 11: Comparison of the experimental results of the thermal conductivity ratio for Al_2O_3/water nanofluid with theoretical models as a function of particle volume concentration at 25 and 55°C.

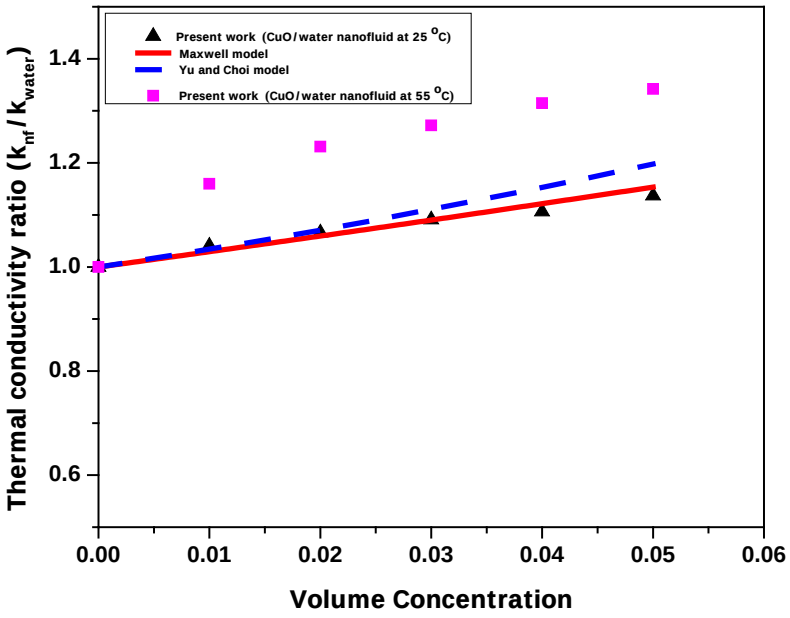

Figure 12: Comparison of the experimental results of the thermal conductivity ratio for CuO/water nanofluid with theoretical models as a function of particle volume concentration at 25 and 55°C.

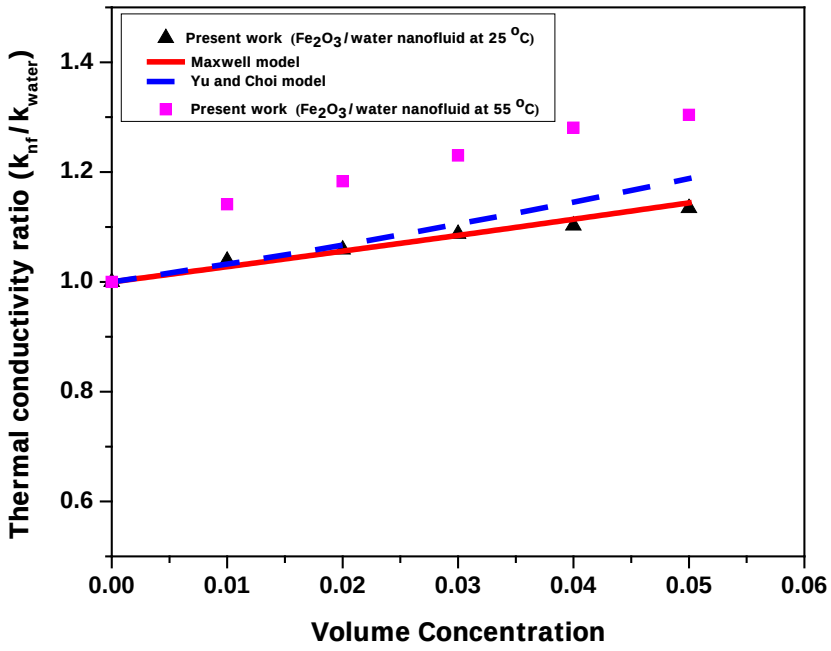

Figure 13: Comparison of the experimental results of the thermal conductivity ratio for Fe_2O_3/water nanofluid with theoretical models as a function of particle volume concentration at 25 and 55°C.

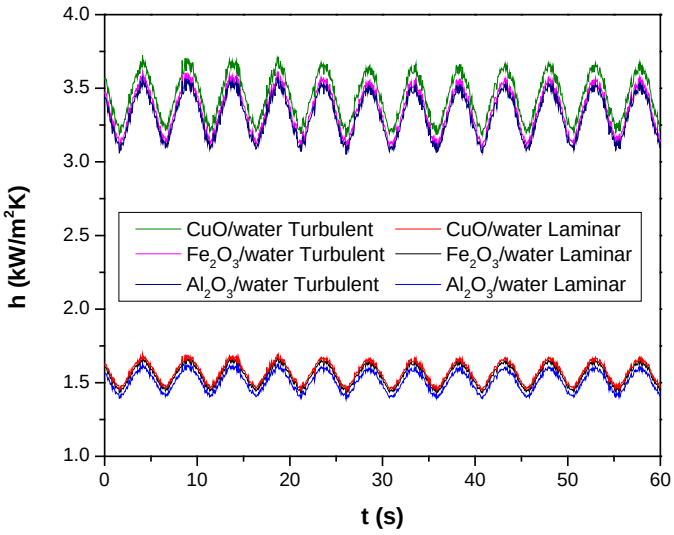

Figure 14: Instantaneous heat transfer coefficient signal for CuO/water, Fe_2O_3/water and Al_2O_3/water nanofluids at laminar and turbulent flow regimes

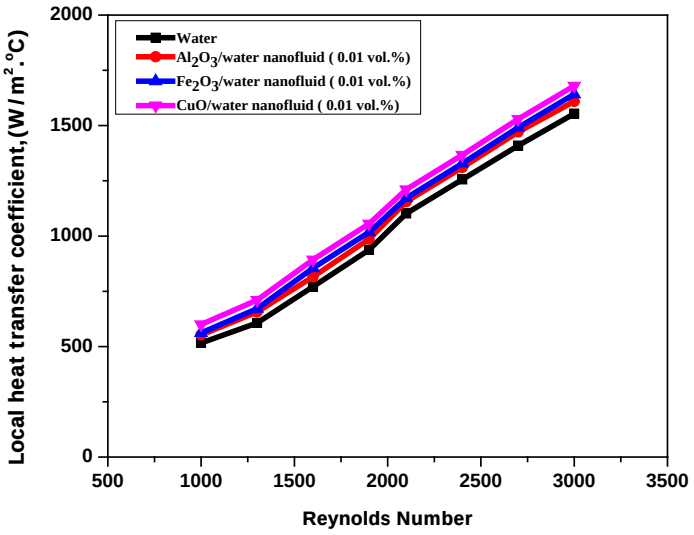

Figure 15: Local heat transfer coefficient versus Reynolds number for nanofluids of 0.01 vol.% at 25°C.

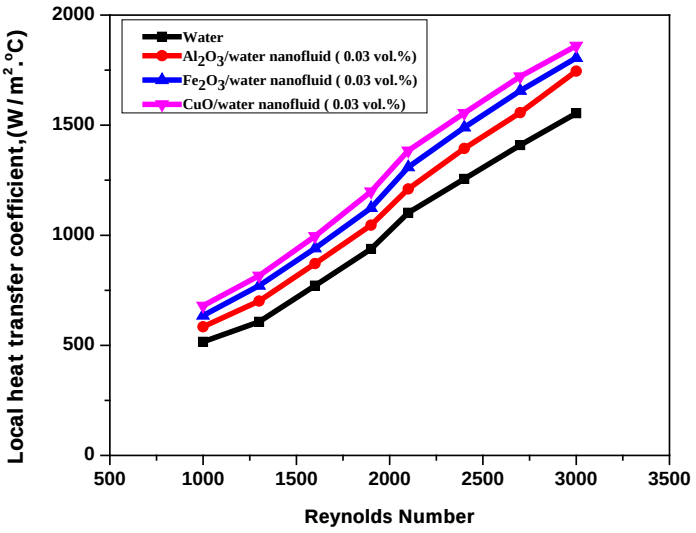

Figure 16: Local heat transfer coefficient versus Reynolds number for nanofluids of 0.03 vol.% at 25oC.

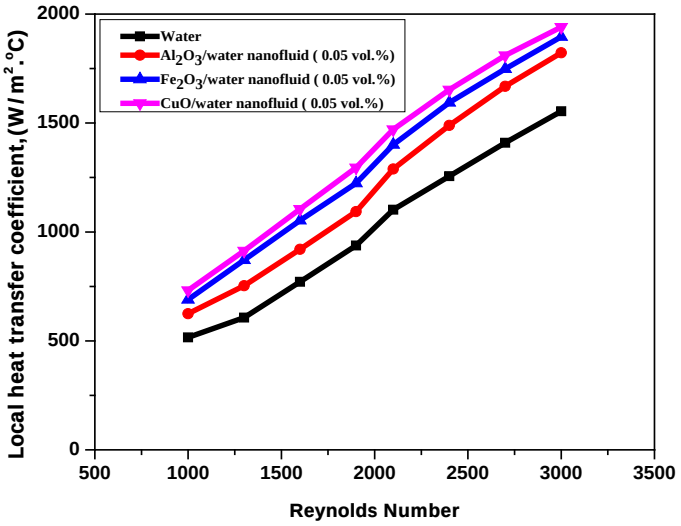

Figure 17: Local heat transfer coefficient versus Reynolds number for nanofluids of 0.05 vol.% at 25oC

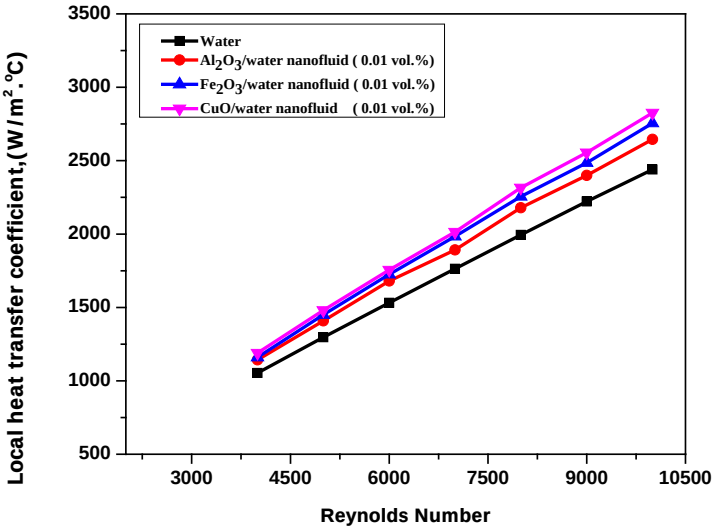

Figure 18: Local heat transfer coefficient versus Reynolds number for nanofluids of 0.01 vol.% at 55oC.

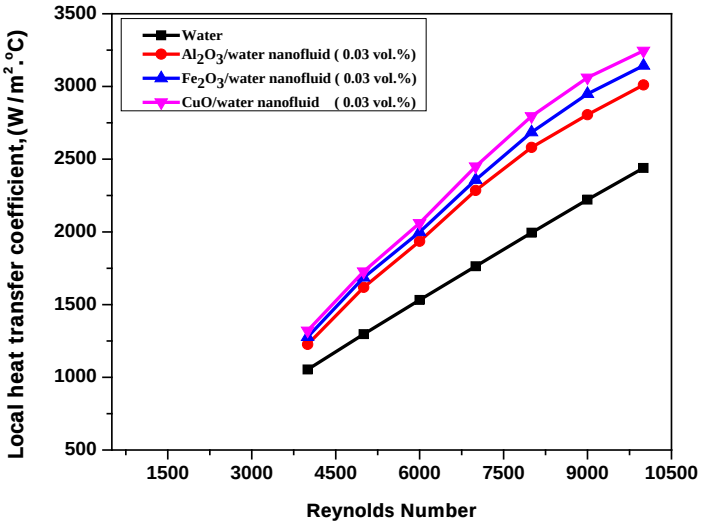

Figure 19: Local heat transfer coefficient versus Reynolds number for nanofluids of 0.03 vol.% at 55°C.

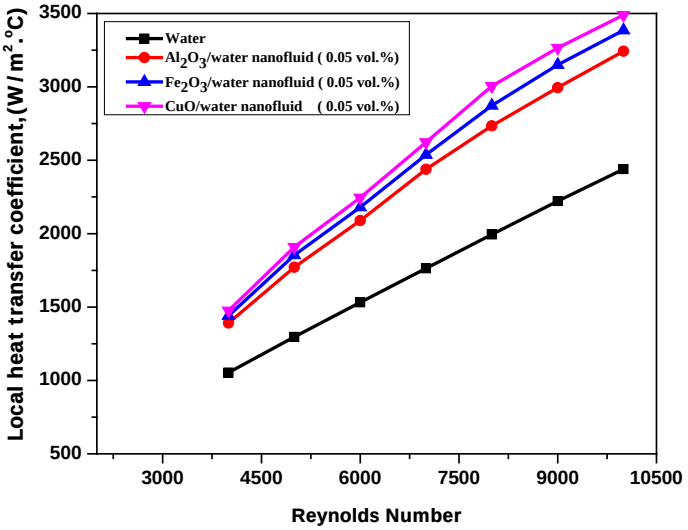

Figure 20: Local heat transfer coefficient versus Reynolds number for nanofluids of 0.05 vol.% at 55°C.

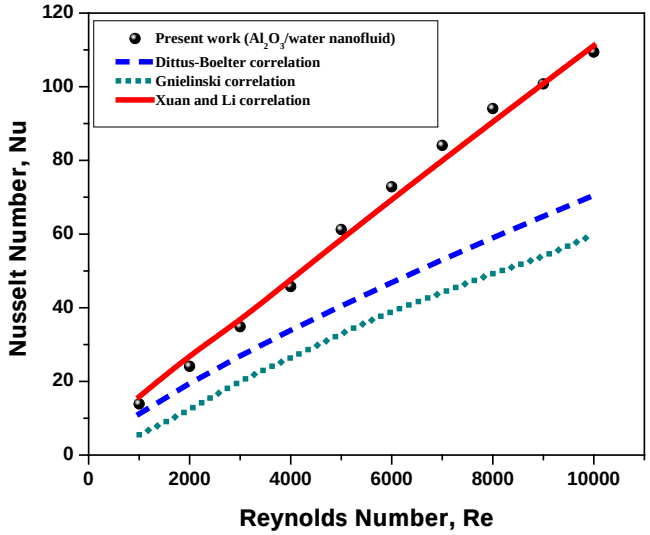

Figure 21**:** Comparison of the experimental Nusselt numbers with values predicted by existing convective heat transfer correlations for Al_2O_3/water nanofluids at 55°C

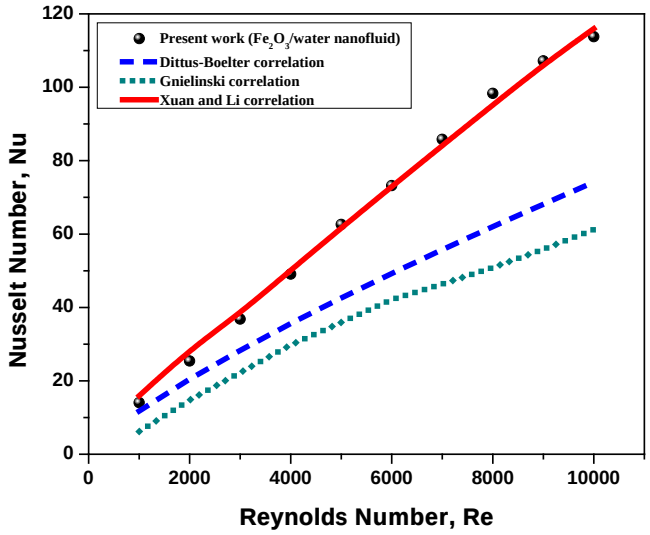

Figure 22: Comparison of the experimental Nusselt numbers with values predicted by existing convective heat transfer correlations for Fe2O3/water nanofluids at 55°C

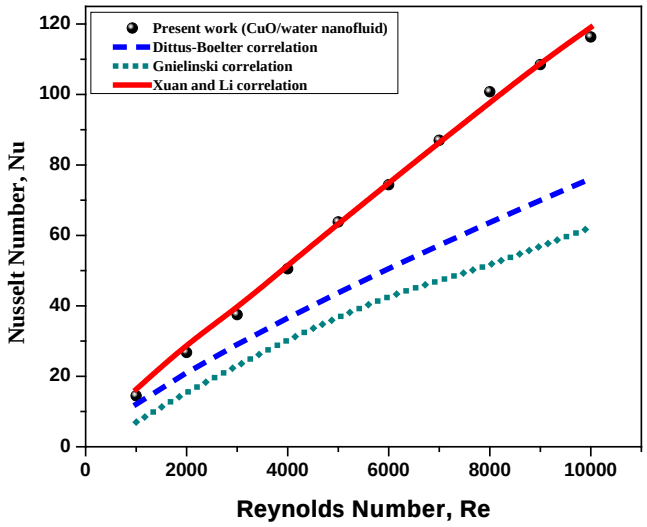

Figure 23: Comparison of the experimental Nusselt numbers with values predicted by existing convective heat transfer correlations for CuO/water nanofluids at 55°C

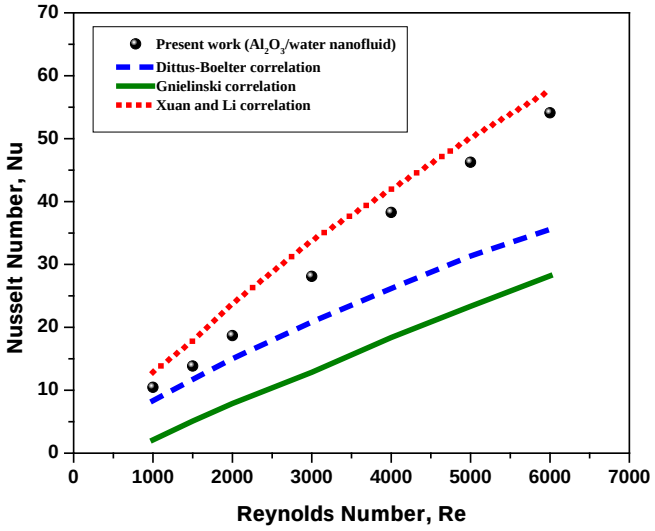

Figure 24: Comparison of the experimental Nusselt numbers with values predicted by existing convective heat transfer correlations for Al2O3/water nanofluids at 25°C

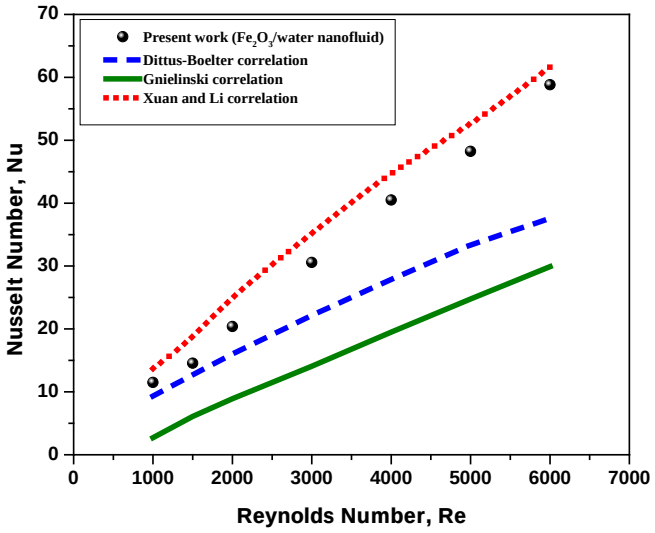

Figure 25: Comparison of the experimental Nusselt numbers with values predicted by existing convective heat transfer correlations for Fe2O3/water nanofluids at 25°C

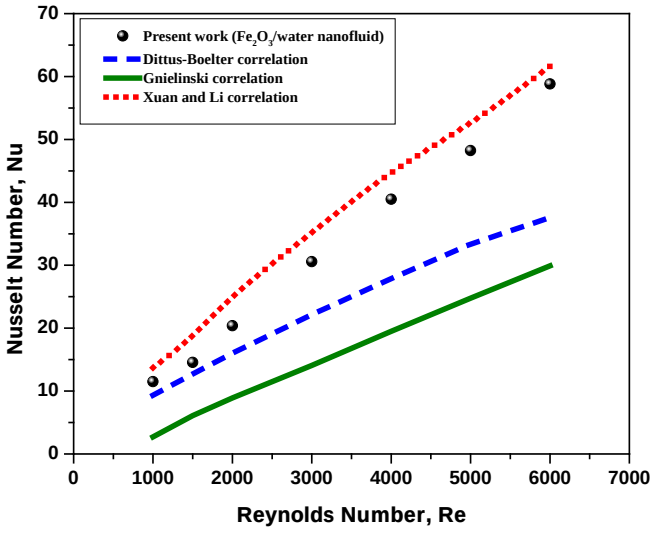

Figure 26: Comparison of the experimental Nusselt numbers with values predicted by existing convective heat transfer correlations for CuO/water nanofluids at 25°C

REFERENCES

[1] Naik, B.A.K. and A.V. Vinod, Heat transfer enhancement using non-Newtonian nanofluids in a shell and helical coil heat exchanger. Experimental Thermal and Fluid Science, 2018. 90: p. 132-142.

[2] Ahmadi, M. and G. Willing, Heat transfer measurment in water based nanofluids. International Journal of Heat and Mass Transfer, 2018. 118: p. 40-47.

[3] Kabeel, A.E. and E.M.S. El-Said, Applicability of flashing desalination technique for small scale needs using a novel integrated system coupled with nanofluid-based solar collector. Desalination, 2014. 333: p. 10-22.

[4] Wu, D., et al., Critical issues in nanofluids preparation, characterization and thermal conductivity. Current Nanoscience, 2009. 5(1): p. 103-112.

[5] Keblinski, P., et al., Mechanisms of Heat Flow in Suspensions of Nano-Sized Particles (Nano Fluids). Vol. 45. 2002. 855-863.

[6] Xuan, Y. and Q. Li, Heat transfer enhancement of nanofluids. International Journal of Heat and Fluid Flow, 2000. 21(1): p. 58-64.

[7] Zouli, N., et al., Enhancement of thermal conductivity and local heat transfer coefficients using Fe2O3/water nanofluid for improved thermal desalination processes. Journal of Nanofluids, 2018. Submitted.

[8] Özerinç, S., S. Kakaç, and A.G. Yazıcıoğlu, Enhanced thermal conductivity of nanofluids: a state-of-the-art review. Microfluidics and Nanofluidics, 2009. 8(2): p. 145-170.

[9] Das, S.K., et al., Temperature Dependence of Thermal Conductivity Enhancement for Nanofluids. Journal of Heat Transfer, 2003. 125(4): p. 567.

[10] Lee, S., S. Li, and J.A. Eastman, Measuring thermal conductivity of fluids containing oxide nanoparticles. Journal of Heat Transfer, 1999. 121(2): p. 280-289.

[11] Wen, D. and Y. Ding, Experimental investigation into convective heat transfer of nanofluids at the entrance region under laminar flow conditions. International Journal of Heat and Mass Transfer, 2004. 47(24): p. 5181-5188.

[12] Das, S.K., et al., Temperature dependence of thermal conductivity enhancement for nanofluids. Journal of Heat Transfer, 2003. 125(4): p. 567-574.

[13] Li, C.H. and G.P. Peterson, Experimental investigation of temperature and volume fraction variations on the effective thermal conductivity of nanoparticle suspensions (nanofluids). Journal of Applied Physics, 2006. 99(8).

[14] Wang, X. and X. Xu, Termal Conductivity of Nanoparticle-Fluid Mixture. Vol. 13. 1999. 474-80.

[15] Xie, H., et al., Thermal Conductivity Enhancement of Suspensions Containing Nanosized Alumina Particles. Vol. 91. 2002. 4568-4572.

[16] Xie, H., et al., Thermal Conductivity of Suspensions Containing Nanosized SiC Particles. International Journal of Thermophysics, 2002. 23(2): p. 571-580.

[17] Kumar, N. and S.S. Sonawane, Experimental study of thermal conductivity and convective heat transfer enhancement using CuO and TiO2 nanoparticles. International Communications in Heat and Mass Transfer, 2016. 76: p. 98-107.

[18] Hwang, Y.J., et al., Investigation on characteristics of thermal conductivity enhancement of nanofluids. Current Applied Physics, 2006. 6(6): p. 1068-1071.

[19] Zhang, X., H. Gu, and M. Fujii, Effective thermal conductivity and thermal diffusivity of nanofluids containing spherical and cylindrical nanoparticles. Experimental Thermal and Fluid Science, 2007. 31(6): p. 593-599.

[20] Mintsa, H.A., et al., New temperature dependent thermal conductivity data for water-based nanofluids. International Journal of Thermal Sciences, 2009. 48(2): p. 363-371.

[21] Sun, B., W. Lei, and D. Yang, Flow and convective heat transfer characteristics of Fe2O3–water nanofluids inside copper tubes. International Communications in Heat and Mass Transfer, 2015. 64: p. 21-28.

[22] Mikkola, V., et al., Influence of particle properties on convective heat transfer of nanofluids. International Journal of Thermal Sciences, 2018. 124: p. 187-195.

[23] Pak, B.C. and Y.I. Cho, HYDRODYNAMIC AND HEAT TRANSFER STUDY OF DISPERSED FLUIDS WITH SUBMICRON METALLIC OXIDE PARTICLES. Experimental Heat Transfer, 1998. 11(2): p. 151-170.

[24] Zeinali Heris, S., S.G. Etemad, and M. Nasr Esfahany, Experimental investigation of oxide nanofluids laminar flow convective heat transfer. International Communications in Heat and Mass Transfer, 2006. 33(4): p. 529-535.

[25] Zeinali Heris, S., M. Nasr Esfahany, and S.G. Etemad, Experimental investigation of convective heat transfer of Al2O3/water nanofluid in circular tube. International Journal of Heat and Fluid Flow, 2007. 28(2): p. 203-210.

[26] Kim, D., et al., Convective heat transfer characteristics of nanofluids under laminar and turbulent flow conditions. Current Applied Physics, 2009. 9(2, Supplement): p. e119-e123.

[27] Hussein, A.M., et al., Heat transfer enhancement using nanofluids in an automotive cooling system. International Communications in Heat and Mass Transfer, 2014. 53: p. 195-202.

[28] Farajollahi, B., S.G. Etemad, and M. Hojjat, Heat transfer of nanofluids in a shell and tube heat exchanger. International Journal of Heat and Mass Transfer, 2010. 53(1): p. 12-17.

[29] Aghabozorg, M.H., A. Rashidi, and S. Mohammadi, Experimental investigation of heat transfer enhancement of Fe2O3-CNT/water magnetic nanofluids under laminar, transient and turbulent flow inside a horizontal shell and tube heat exchanger. Experimental Thermal and Fluid Science, 2016. 72: p. 182-189.

[30] L.S. Sundar, M.K. Singh, and A.C.M. Sousa, Thermal conductivity of ethylene glycol and water mixture based Fe3O4 nanofluid. International Communications in Heat and Mass Transfer,, 2013. 17-24.

[31] Godson, L., et al., Convective Heat Transfer Characteristics of Silver-Water Nanofluid Under Laminar and Turbulent Flow Conditions. Journal of Thermal Science and Engineering Applications, 2012. 4(3): p. 031001.

[32] Hwang, K.S., S.P. Jang, and S.U.S. Choi, Flow and convective heat transfer characteristics of water-based Al2O3 nanofluids in fully developed laminar flow regime. International Journal of Heat and Mass Transfer, 2009. 52(1-2): p. 193-199.

[33] Abdulmohsin, R.S. and M.H. Al-Dahhan, Characteristics of convective heat transport in a packed pebble-bed reactor. Nuclear Engineering and Design, 2015. 284: p. 143-152.

[34] Said, I.A., et al., Investigation of natural convection heat transfer in a unique scaled-down dual-channel facility. AIChE Journal, 2017. 63(1): p. 387-396.

[35] Said, I.A., et al., Experimental investigation of the helium natural circulation heat transfer in two channels facility using varying riser channel heat fluxes. Experimental Thermal and Fluid Science, 2018. 93: p. 195-209.

[36] Saidur, R., K.Y. Leong, and H.A. Mohammad, A review on applications and challenges of nanofluids. Renewable and Sustainable Energy Reviews, 2011. 15(3): p. 1646-1668.

[37] Gupta, M., et al., A review on thermophysical properties of nanofluids and heat transfer applications. Vol. 74. 2017. 638-670.

[38] Sha, L., Y. Ju, and H. Zhang, The influence of the magnetic field on the convective heat transfer characteristics of Fe 3 O 4 /water nanofluids. Applied Thermal Engineering, 2017. 126: p. 108-116.

[39] Mohammed, S., N. Zouli, and M. Al-Dahhan, Removal of benzoic acid from wastewater by pickering emulsion liquid membrane stabilized by magnetic Fe2O3 nanoparticles. Vol. 68. 2017. 114-121.

[40] Sadeghi, R., et al., Investigation of alumina nanofluid stability by UV–vis spectrum. Microfluidics and Nanofluidics, 2014. 18(5-6): p. 1023-1030.

[41] Lee, J.-H., et al., Effective viscosities and thermal conductivities of aqueous nanofluids containing low volume concentrations of Al2O3 nanoparticles. International Journal of Heat and Mass Transfer, 2008. 51(11-12): p. 2651-2656.

[42] Williams, W., J. Buongiorno, and L.-W. Hu, Experimental Investigation of Turbulent Convective Heat Transfer and Pressure Loss of Alumina/Water and Zirconia/Water Nanoparticle Colloids (Nanofluids) in Horizontal Tubes. Journal of Heat Transfer, 2008. 130(4): p. 042412.

[43] Chon, C.H., et al., Empirical correlation finding the role of temperature and particle size for nanofluid (Al2O3) thermal conductivity enhancement. Applied Physics Letters, 2005. 87(15): p. 153107.

[44] Li, C.H. and G.P. Peterson, Experimental investigation of temperature and volume fraction variations on the effective thermal conductivity of nanoparticle suspensions (nanofluids). Journal of Applied Physics, 2006. 99(8): p. 084314.

[45] Syam Sundar, L., M.K. Singh, and A.C.M. Sousa, Investigation of thermal conductivity and viscosity of Fe3O4 nanofluid for heat transfer applications. International Communications in Heat and Mass Transfer, 2013. 44: p. 7-14.

[46] Holman, J.P., Experimental Methods for Engineers, ed. S.E. McGraw-Hill. 1994.

[47] Yu, W. and S.U.S. Choi, The role of interfacial layers in the enhanced thermal conductivity of nanofluids: A renovated Hamilton-Crosser model. Journal of Nanoparticle Research, 2004. 6(4): p. 355-361.

[48] Cardellini, A., et al., Thermal transport phenomena in nanoparticle suspensions. J Phys Condens Matter, 2016. 28(48): p. 483003.

[49] Jwo, C.-S., et al., Performance of overall heat transfer in multi-channel heat exchanger by alumina nanofluid. Journal of Alloys and Compounds, 2010. 504: p. S385-S388.

[50] Lee, J., et al., Nanofluid Convection in Microtubes. Journal of Heat Transfer, 2010. 132(9): p. 092401-092401-5.

[51] Peyghambarzadeh, S.M., et al., Improving the cooling performance of automobile radiator with Al2O3/water nanofluid. Applied Thermal Engineering, 2011. 31(10): p. 1833-1838.

[52] Manay, E., et al., Use of nanofluids in microchannels. Engineer and Machine, 2012. 627(53): p. 28-42.

[53] Y.M. Xuan and Q. Li, Investigation on convective heat transfer and flow features of nanofluids. ASME J. Heat Transfer 2003. 125: p. 151–155.

[54] Tijani, A.S. and A.S.b. Sudirman, Thermos-physical properties and heat transfer characteristics of water/anti-freezing and Al 2 O 3 /CuO based nanofluid as a coolant for car radiator. International Journal of Heat and Mass Transfer, 2018. 118: p. 48-57.

III. NANOFLUID EFFECT ON WATER EVAPORATION/CONDENSATION AND HEAT TRANSFER COEFFICIENT FOR DESALINATION

ABSTRACT

The present work represents the first step to improve evaporation quantity and heat transfer coefficient by the incorporation of hematite (Fe_2O_3 nanoparticles) in saline water for Multi Stage Flushing (MSF) desalination processes. A laboratory test was conducted to determine the different physical properties of saline water nanofluid including stability, thermal conductivity, evaporation quantity and rate, boiling temperature and time, and local heat transfer coefficient in stagnant conditions. The effect of salinity, nanoparticles (size and volume fraction) and pressure were considered. Stable saline water nanofluid showed lower boiling temperatures and fast boiling. This would preheat the cooling saline water quickly and at low temperatures before reaching the brine heater in real MSF process. Thus, the steam consumption reduction was estimated at 2% in the worst case. The evaporation quantity was measured through condensation content considering an ideal case, which showed an increase of 15% at atmospheric pressure and 25% at vacuum conditions. The improvement of local heat transfer coefficient of 134% was obtained at the stagnant condition for a nanoparticle size and volume fraction of 20 nm and 0.05%, respectively. This represents the first step to estimate the water production increase amount by using saline water nanofluid. The thermally conductive Fe_2O_3 nanoparticles deposition will play an important role to reduce surface thermal resistance created by the inorganic scale in MSF plants.

Keywords: Nanofluid, MSF, desalination, evaporation, heat transfer coefficient.

1. INTRODUCTION

Freshwater scarcity is a major challenge facing many countries with the high population and industrial growth. Due to the abundance of saltwater on earth which represent 98%, seawater desalination is considered as the main choice for arid countries such as Gulf Council Countries (GCC) [1]. Different technologies are adopted to desalinate seawater including thermal and Reversis Osmosis (RO) membrane based. The most mature and robust technology is the Multi Stage Flushing (MSF) desalination which is based on the evaporation of seawater under vacuum to produce high quality distillate which is post-treated to meet World Health Organization (WHO) water quality requirements. MSF desalination has been implemented worldwide, which follows the Brine Recycle (BR) configuration with practical Top Brine Temperature (TBT) reaching 110°C. This temperature is ensured through a low pressure heating steam produced from large capacity fossil fuel fired boilers. It is well accepted that heating energy added to the pumping energy represents about 68 % of the operation expenditure (OPEX) cost of MSF technology [2]. The breakdown of MSF OPEX for a plant producing 450,000 m^3/d with seawater salinity of 40,000 ppm is illustrated in Figure 1.

Therefore, the competitiveness of other desalination technologies starts from an energy perspective to reduce water production cost. That is why RO membrane desalination is gaining worldwide acceptance in addition to its low CO_2 emission [3]. Many efforts have been made to develop cost effective and reliable RO membrane based desalination technologies

However, it has been noted within the desalination community that MSF technology reached its limits with little opportunities to increase performance. We recall

that among the indicator adapted to measure the performance of MSF desalination plant, the performance ratio (PR) is the most simple indicator and its highest practical value is 9.1 as in Ras Al-Khair (Saudi Arabia) plant. Most of MSF research works were carried out by modeling/optimizing the process with the objective to reduce water production cost [4]. In terms of performance increase, Hamed *et al.* [2] suggested the increase of the flash range by either the increase of the Top Brine Temperature (TBT) or the increase of the number of stages and/or the increase of the specific heat transfer area.

In parallel, the recent development of nanofluids with super thermophysical properties [5–10] represents an exciting opportunity especially for thermal desalination improvement by using these nanofluids. Nanofluids consist of a solution containing suspended nanoparticles (typically <100 nm) with different geometries and concentrations in different heat transfer base fluids. In the present work related to the water industry, we focus on the water as the base fluid.

This mixture of nanoparticles/fluid has superior thermophysical properties such as thermal properties (thermal conductivity, heat transfer coefficient-HTC- and critical heat flux-CHF-) which improves thermal energy conversion in heating processes, such as heat exchangers, by 20-40 % [11]. Many studies obtained results indicating an increase of the CHF and no significant enhancement of nucleate boiling heat transfer coefficient [12,13].

Several reviews have been reported in the literature discussing nanoparticles effect on heat transfer characteristics over conventional heat transfer fluids along with mechanisms of forced convection heat transfer enhancement [14–17]. While the literature is divided on the nanofluids impact on HTC and CHF, in most of the studies, an enhancement of these two parameters is reported with the uses of nanofluids [16,18].

However, in some studies, a reduction of the HTC or CHF has been reported for Al_2O_3-water nanofluids. This atypical behavior is due to use of large nanoparticle size (~155nm) [19]. It is exciting to note the high interest to alumina nanoparticles and water as a base in the formulation of nanofluid as reported by Suganthy *et al.*[20]

Starting from the last decade, there has been a growing interest in nanofluids heat transfer boiling behavior either in a pool of flow conditions due to its potential applications including MSF desalination, power generation, refrigeration, chemical processing, and electronics thermal management [21].

Based on the abovementioned attributes of nanofluids, it is highly expected that the nanoparticles presence will affect the evaporation rate, saturated vapor pressure. Unfortunately, Tso *et al.*[22] reported the lack of research about the pool evaporation rate in the presence of nanofluids where authors focused only on the droplet evaporation of nanofluids and water. Previous works showed that the improvement of the droplet evaporation rate is affected by the type of the incorporated nanoparticles and the presence of stabilizers [23,24]. Such a difference in the performance between nanofluids was attributed to several factors including surface tension and nanoparticles concentration [25,26].

Zouli et al. [27–29] implemented such technique as a newly developed sophisticated noninvasive heat transfer coefficient probe to measured the local heat transfer coefficients whithin the segment of length using Fe_2O_3/water, Al_2O_3/water, and CuO/water nanofluids at the laminar and turbulent flow regimes under thermal boundary conditions of isoflux. They used a copper tube with a 950 mm length, 25.4 mm inner diameter, and 31 mm outer diameter. In their work, nanofluid temperatures were measured using two thermocouples

(T-type), which were inserted in front of the foil sensor of the test section. The micro-foil sensor was flush mounted on the inner wall surface of the test section to measure simultaneously the inner wall surface temperatures and the local instantaneous heat flux along the length of the sensor. The study demonstrated that the thermal conductivity and local heat transfer coefficient increased with the both increasing volume fractions (φ) and fluid temperature of the Al_2O_3/water, Fe_2O_3/water, and CuO/water nanofluids. Their experimental results revealed that the greatest enhancements in thermal conductivity were found to be 19%, 21%, and 25% for Al_2O_3/water, Fe_2O_3/water, and CuO/water nanofluids, respectively at φ=0.05% and 55°C. The maximum enhancements in the local heat transfer coefficients were 44%, 50%, and 53%, respectively, at the same conditions.

From desalination perspective, various studies are available in the literature where most of the authors used nanofluid as a superabsorbent of the solar energy to heat conventional MSF or humidification/dehumidification desalination or to enhance solar pond for remote area application [30–33]. In terms of performance improvement, Garg *et al.*[34] estimated through a mathematical model a Gain Output Ratio (GOR) ranging between 11 and 14 by using nanofluid based absorption solar collector to heat Brine Recycle-Multi Stage Flushing (BR-MSF) system. The study showed better performance compared to the concept of a parabolic trough collector (PTC) based BR-MSF. The model was validated by comparison with an experimental study on nanofluid-based direct absorption solar collector, but the authors did not discuss the economic estimation of water production cost.

El-said *et al.* [32] obtained a GOR equal to 7.5 when coupling nanofluid solar heater with Humidification/dehumidification and single stage flushing system producing water at

an estimated water production cost of 6.4 USD/m^3 which is very expensive. For nanofluid based solar ponds, still the number of studies is low where performance needs to be confirmed, and many issues need to be investigated such as the reliability.

In the present work, our approach is to investigate the effect of water nanofluid on the evaporation and on the heat transfer coefficient from the heating surface to the boiling water nanofluids. The question to be answered is whether the nanofluid will improve evaporation and heat transfer coefficient that will lead to enhancement of water production and BR-MSF desalination process performance by reducing the energy consumption. Fe_2O_3 nanoparticles were selected due to their magnetic properties that facilitate their removal with a magnet and be recycled with no need for separation units.

2. EXPERIMENTAL WORK

2.1 PREPARATION OF NANOFLUID

Nanofluids were prepared by dispersing different sizes (3 nm, 10 nm, and 20 nm) of Fe_2O_3 purchased nanoparticles (Alfa Aesar Company, USA) in the distilate water (DW). As mentioned earlier Fe_2O_3 have been selected since they can be collected and recycled in the desalination process using their magnetic characteristics. Nanoparticles were intimately mixed with the distilate water using digital homogenizer with a speed of 5000 rpm for 60 minutes to ensure complete dispersion of the nanoparticles. As it has been successfully demonstrated [27–29] an ultrasonic bath was used for one hour to promote uniform dispersion and minimal agglomeration of nanoparticles. Figure 2 shows SEM images for the spherical nanoparticles in the base fluid. The use of stabilizers (surfactants) was avoided due to the target application to be extended to seawater desalination to produce

fresh water. This is because the presence of surfactant will increase the level of foaming in the MSF process requiring an increase of anti-foam dozing raising the operation cost and affecting the environment. Nanoparticles volume fraction was expressed through volume fraction (φ) percentage calculated from equation (1).

$$\varphi\% = \frac{\frac{m_p}{\rho_p}}{\frac{m_p}{\rho_p} + \frac{m_{bf}}{\rho_{bf}}} \, x \, 100\ \% \qquad (1)$$

where m_P and m_{bf} are the mass of the nanoparticles and the base fluid, respectively. $\rho_P \, and \, \rho_{bf}$ are their respective densities. Different Fe_2O_3 nanoparticles volume fractions were consdiered ranging from (φ =0.01 to 0.05 %).

2.2 EVAPORATION/CONDENSATION SET-UP

Figure 3 represents a schematic diagram of the evaporation/condensation experimental setup used in the current study. It is a simple evaporation setup consisting of a round bottom flask containing the nanofluid. This flask is heated using a heating mantle and connected to a condenser, which is further connected to a conical flask where the distillate is collected. The round bottom flask was connected to a vacuum line in order to conduct the evaporation experiments under medium to high vacuum to mimic Multi Stage Flushing principle as shown in Figure 3. At the end of the experiment, the condensate volume was measured.

2.3 NANOFLUID STABILITY

The stability of the suspension of different nanofluid volume fractions represents a key property which determines the thermal conductivity of the nanofluid. The stability was

measured through the zeta potential for different nanoparticles sizes. Carried out at 25 oC using a Zetasizer instrument.

2.4 THERMAL CONDUCTIVITY MEASUREMENT

The thermal conductivity of the prepared nanofluids was measured using a portable Transient Line Source (TLS-100) thermal conductivity meter with an operating range of (0.1-5 W/m.k) and accuracy of 5%. The thermal conductivity meter was calibrated before using standard solutions of known thermal conductivity as recommended in ASTM- D5334 standard. The measurements were recorded for various volume fraction samples (0.01-0.05 vol.%) at different temperatures within the range of 25 - 100 ℃ by inserting the probe sensor vertically into the sample container. To ensure data reproducibility, each experiment was repeated five times for each sample, and each temperature and the averaged-values were taken for analysis. For all the experimental results, the standard deviations were found around 0.04 – 0.06.

2.5 HEAT TRANSFER COEFFICIENT (HTC) MEASUREMENT

Instantaneous Heat transfer coefficient (h_i) is measured by an advanced heat transfer probe that was developed and successfully implemented in this experimental. This heat transfer probe consists of a simultaneous integration of micro-foil sensor and a surface thermocouple that can be flush mounted in a non-invasive way on the inner bottom wall of the round flask. The micro-foil heat flux sensor (6.35 mm x 17.78 mm x 0.08 mm) is flush mounted using high temperature glue at the inner wall surface of the bottom of the round flask as shown in Figure 1. This sensor has a fast response that instantaneously measures

the local heat flux reliably (q_i) expressed in kW/m^2 and the surface temperature $(T_{s,i})$ in Kelvin. The adjacent fluid temperature $(T_{b,i})$ is measured by using a thermocouple directly in front of the foil sensor at the centerline of the round bottom flask. Based on these parameters, the heat transfer coefficient is calculated as follows:

$$h_i = \frac{q_i}{T_{s,i} - T_{b,i}} \; ; \; \Delta T_i = T_{s,i} - T_{b,i} \tag{2}$$

$$h_{avg} = \frac{1}{n} \sum_{i=1}^{n} \frac{q_i}{T_{s,i} - T_{b,i}} = \frac{1}{n} \sum_{i=1}^{n} h_i \tag{3}$$

where $h_i \; and \; h_{avg}$ are the instantaneous and time-averaged heat transfer coefficients respectively expressed in kW/m^2.K and n is the number of the collected data points. Previous studies [27–29] at room temperature and elevated reported that a small cartridge heater should be placed on the rear side of the micro-foil sensor to provide heating to the sensor $(i.e., T_s > T_b)$. However, this it is not used in the current study since the heating mantle where the round bottom flask is sit on it was used as a source of heating to the flask and to micro-foil sensor. The heating mantle was placed below the flushed mounted foil sensor as shown in Figure 3. The sampling time of the heat transfer probe technique is 40 seconds with a sampling frequency of 50 Hz to provide 2000 data points where the mean value of the heat transfer coefficient from the instantaneous measurements is estimated.

3. RESULTS

3.1 NANOFLUID STABILITY SUSPENSION

The results of the degree of stability of the suspension are shown in Figure 4 for different sonication periods and zeta potential for a volume fraction of 0.01% and 3, 10, and 20 nm nanoparticles sizes. Except the nanofluid with 20 nm particles size, the maximum zeta potential for the remaining sizes (3 and 10 nm) was obtained for a sonication duration of one hour with maximum values above 30 mV. It is well established that depending on the zeta potential value, the suspension stability can be considered as moderate (30 to 40 mV) or good (40 to 60 mV).

For nanofluids stability, Suganthi *et al.* [20] suggested an absolute zeta potential value greater than 30 mV corresponding to the high surface charge of particles and the stable dispersion. It is well accepted that nanoparticle size is one of the factors affecting the stability of nanofluid where most of the forces and interaction between nanoparticles is related to the particle mass and size [35]. The present results are consistent with the previous findings where there is a critical diameter for particles above which the aggregation take place, and the dispersion requires longer sonication duration [36].

Figure 5 shows the zeta potential of nanofluid prepared with two different base fluids, DW and saline water, for different volume fractions for a nanoparticles size of 20 nm and a ultrasonication duration of one hour. The results indicate that the nanofluid with the saline water as base fluid have a lower stability than the nanofluid with DW. For 20 nm nanoparticle size, we should not exceed 0.015 % to stay within moderate stability corresponding to a zeta potential above the threshold value of 30 mV.

The dependence of zeta potential on the salt concentration and the sonication time was obtained by several authors [37–41]. In agreement with zeta potential in distillate water

(DW), the increase of sonication duration does not induce a decline in the suspension stability.

It is well established that saline water has higher ionic strength and viscosity compared to the distillate water (DW). This would play major role in the synergy between the different micro forces between nanoparticles and the base fluid.

In addition, seawater would promote electrostatic forces (a function of base fluid permittivity) between particles and increase the collision probabilities between them inducing less stability (aggregation) compared to the distillate water (DW) [41]. The decrease of seawater based nanofluid stability was observed by other researchers [40] which suggest a screening effect of the electrolyte on the surface of nanoparticles which cause aggregation above certain critical salt concentration.

3.2 THERMAL CONDUCTIVITY RATIO

Figures 6-9 show the effect of temperature from 25°C to 100°C on the thermal conductivity ratio (K_{nf}/K_{bf}) between the nanofluid and base fluid (K_{nf}/K_{bf}) for different nanoparticle sizes and volume fractions. The results show clearly that the effective thermal conductivity of nanofluids increases with temperature and nanoparticles volume fraction, which is in agreement with previous studies [38]. Between 25°C and 100°C, the average an increase in thermal conductivity of approximately 13% for each nanoparticle size at volume fraction above 0.03% at higher temperature the differences among the particles sizes of (K_{nf}/K_{bf}) reduces, as shown in Figure 10. This is favorable toward the use of larger size nanoparticle for the sake of benefit in cost and handling. The linear tendency fits the

results with a slope which increase with temperature. The comparison of these results with existing models has been done in a separate publication [27].

In comparison with distillate water, the addition of nanoparticles gives a better enhancement with temperature for the high volume fraction of particles and low particle size. In the literature, different mechanisms and models are proposed to explain the enhancement of thermal conductivity of nanofluids including the increase of Brownian motion and the existence of highly conductive nanolayer between the nanoparticle and the base fluid [42–45]. However, all these mechanisms need sophisticated tools to be validated.

Figure 10 shows the thermal conductivity of nanofluid based on saline water compared to the distillate water (DW) at different temperatures from ambient to 100°C. The particle size selected for these saline water experiments was 20 nm due to its lower cost compared to the expensive low sizes for manufacturing difficulties and based on the results mentioned above. For instance, the cost of 3 nm particles is 2.8 time the cost of 20 nm. It appears clearly that saline water as base fluid enhances the thermal conductivity of the nanofluid up to 30% compared to the DW which is explained by the higher thermal conductivity attributed to its higher Total Dissolved Solids (TDS). Thus, the high TDS is favorable to the thermal conductivity improvement contrary to the nanofluid stability discussed abovementioned.

In the same figure, we can see the increase of the thermal conductivity with a temperature increase as obtained for distillate water (DW) based nanofluids in Figures 6-9 with about same slope for two volume fractions. This is in agreement with the results of many researchers where some authors proposed an empirical formula showing a proportionality between temperature and thermal conductivity of the nanofluid [42,45].

Additionally, the impact of the nanoparticles on nanofluid thermal conductivity is more significant in distillate water (DW) compared to the saline water base fluid. This would support the higher contribution of the thermal conductivity of solid nanoparticles compared to the thermal conductivity for the base fluid.

3.3 BOILING TEMPERATURES AND TIME NEED TO BOIL

Boiling temperature was also measured for the differently prepared nanofluids and compared with DW (100°C at atmospheric pressure). As shown in Figure 11, nanofluids exhibit a decrease in boiling temperatures with volume fraction increase and particle size decrease. For instance, it is interesting to note a boiling temperature of 94°C for 3 nm Fe_2O_3 particles dispersed at a volume fraction of 0.05% in distillate water. Boiling temperatures and time need to boil

Such a result could be explained by the decrease of the surface tension of the fluid by the suspended nanoparticles. Such a reduction in surface tension decreases the radius of boiling bubbles, and therefore, more active nucleation sites on the heating surface occur [25]. With improved thermal conductivity in saline water, the boiling temperature is 1°C lower than in distillate water nanofluid and increase with volume fraction increase as shown in Figure 12.

The impact of vacuum on the boiling point of saline water nanofluid with 20 nm of Fe_2O_3 nanoparticles is represented in Figure 13. For low vacuum, the boiling point decreased by 5°C, and for medium vacuum, the boiling point decreased dramatically by 20°C. Therefore, less time is needed to boil nanofluids rather than pure base fluids as shown in Figure 14 which agree with other works [46,47]. These results are very promising with

regard to the MSF process performance where less heating is required compared to the conventional process. In the following, the evaporation/condensation rate will be investigated to confirm the high performance of saline water based nanofluid.

3.4 EVAPORATION/CONDENSATION AMOUNT

During the evaporation process of the nanofluids, it should be noted that only the base fluid evaporates while the nanoparticles remain in the round flask. This leads to an increase in the volume fraction in the remaining nanofluid, and thus, and enhancement in the evaporation rate. The nanofluid evaporation rate is determined by the amount of condensate per evaporation duration. Results indicate that the evaporation quantity increase with volume fraction increases and particle size decrease.

Previous studies for different nanofluids and different nanoparticles showed two cases, i.e. a decrease of the evaporation rate with size and concentration increase (alumina based nanofluid) and an increase of the evaporation rate with size increase and concentration decrease (Titania based nanofluid) [48,49]. For the former case, the measurements demonstrated a decrease of the evaporation enthalpy with size and volume fraction increase. This was attributed to the increase of the surface tension and nanofluid viscosity.

Larger nanoparticles would hold more water molecules making it more difficult evaporation and requiring larger kinetic energy. For the second case, it was attributed to the type of interaction between nanoparticles and the water molecules which can be weak at lower nanoparticles concentration. Our results fit to the former case with minor differences in the condensation between 20 and 3 nm sizes as observed in Figures 15 a-c.

The average increase obtained in the condensate comparing with DW, at the different nanoparticle sizes were between 12%-40% for volume fraction of 0.01%, and up to 85%-128% for volume fraction of 0.05%

Taking benefit of lower temperature and faster boiling of saline water based nanofluid, the investigation of the evaporation in saline water based nanofluid was carried out for 20 nm Fe_2O_3 nanoparticles at two volume fractions and different pressure gauges representing vacuum conditions of MSF flash chambers. Figures 16 a-c shows the results where the decrease of the pressure toward medium vacuum and the increase of volume fraction induce higher evaporation. The results show an increase in the condensate for the nanofluids with 20 nm compared with DW of 23% and 53% at a pressure of 0.9 bar for volume fraction of 0.01% and 0.05%, respectively; 19% and 45.2% for 0.5 bar; and 18% and 44% for 0.07 bar.

It is noteworthy that even though the volume fraction of the nanoparticles increase as more condensate is obtained, the suspensions showed a good stability at low volume fraction. The zeta potential of the boiling saline water nanofluid was measured before the end of the evaporation and found equal to 34 mV for 0.01%, which indicate constant stability of the suspension during evaporation. However, when using the nanofluids with a volume fraction of 0.05%, the zeta potential was found to be around 20 mV, which indicate a lower stability. Despite the lower zeta potential at a higher volume fraction, no sedimentation was observed in any case.

3.5 HEAT TRANSFER COEFFICIENT

Based on the flush mounted sensor, the mean values of heat transfer coefficient were measured for different volume fractions of 20 nm nanoparticle containing base fluids. Figure 17 shows the results for the two base fluids, i.e., DW and saline water. The local heat transfer coefficient from the surface to the boiling fluid of saline water without nanoparticles was 6.015 $kW/m^2.K$. When adding a volume fraction of 0.01% in the saline water, the heat transfer coefficient increases to 6.84 $kW/m^2.K$, which is 21.4% higher than the value obtained with Fe_2O_3-DW nanofluid. This behavior is also observed at high volume fraction (0.05%), where the difference between the Fe_2O_3- saline water and Fe_2O_3-DW was found to be 28%.

The heat transfer coefficient in saline water nanofluid showed an enhancement of 134% when increasing the volume fraction from 0.01% to 0.05%. This enhancement can be explained because of the increase of the local convective heat flux (q_i), which is due to the enhancement in the heat capacity of the saline water when adding in the nanoparticles. Also, another factor that affects the obtained enhancements is the adjacent fluid temperature (T_b), which is determined by the thermophysical properties of the nanofluids, such as the density, thermal conductivity and heat capacity, all of which are modified by the inclusion of the nanoparticles.

4. DISCUSSION

The present results are very promising with regard to the increase of performance and water production either for existing or newly constructed MSF desalination plants. To predict water production in the presence of saline water nanofluid, two thermal phenomena should be considered for this first step of nanofluid implementation in MSF desalination,

i.e., evaporation and heat transfer coefficient. The former was measured in terms of quantity.

The evaporation quantity was determined through the condensation quantification, where an improvement of 15% was obtained at atmospheric pressure and continue to increase up to 23% at high vacuum corresponding to 0.9 bar, comparing the results obtained by the saline water and the Fe_2O_3- saline water nanofluid at a volume fraction of 0.01%. The boiling temperature and time were found lower for saline water nanofluid with almost 2°C (Figures 13 and 14). Hence, for the same heat input, faster evaporation and higher condensate quantity were observed, and this would increase the flushing range to generate about 30% water production more.

On the other hand, nanoparticle does not evaporate with seawater, which increases their concentration from the first stage of heat recovery to the last one when implemented in the MSF process, which causes further enhancement of the process performance. Considering the evaporation quantity increase with nanoparticles volume fraction, then two consequences are expected i.e. increase the flushed vapor quantity in low temperature stages and reduced steam consumption at the brine heater.

The first consequence will normalize vapor quantities between heat recovery stages which has never been obtained in the process of MSF desalination. The second consequence is due to the fast preheating of the cooling seawater flowing inside the condenser tube before reaching the brine heater. As a rapid estimation based on the obtained improvement of the heat transfer coefficient by 13.8% when using saline water nanofluid with 20 nm Fe_2O_3 particle at 0.01%, the performance ratio (PR) was calculated using a visual basic code showing an increase of 2.1%. This would correspond to a

reduction of the steam consumption by 2% for a desalination unit operating at TBT of 105 °C with 16 stages.

$$PR = \frac{Mass\ flow\ rate\ of\ product\ water}{mass\ flow\ rate\ of\ steam} \quad (4)$$

Although to extrapolate the findings of the present laboratory study on MSF desalination plant to predict the expected production increase, we have to mention that condensation in a real situation is a function of the heat transfer between seawater nanofluid inside condenser tubes and the vapors. This heat transfer is a combination of the convection part (flowing condition), surface thermal resistance (scale), and the wall thermal conductivity (tube material). However, our laboratory results are for an ideal heat transfer across the tubes (stagnant condition without scale and tube).

For the convection part, the authors obtained in a previous study noticeable improvements using distilled water as base fluid [27,28]. The heat transfer coefficient increase by 13% for 20 nm size nanoparticles at 0.01% volume fraction at a temperature of 65 °C and turbulent flow. It has been observed that the enhancement of the local convective heat transfer coefficient in the turbulent flow regime is larger than that of the laminar flow regime for all the experimental conditions. In a stagnant condition, the same improvement was obtained for the heat transfer coefficient with 13%. Thus, we expect higher improvement of heat transfer coefficient in the case of saline water nanofluid due to the high local convective heat flux dependent on the flow conditions.

For the surface thermal resistance, we expect its decrease for the simple reason that in a real situation, the Fe_2O_3 nanoparticles embedded in the thermally insulating inorganic scale ($CaCO_3$ and/or $Mg(OH)_2$) would reduce the total thermal resistance. Indeed, the

thermal conductivity of hematite nanoparticles measured by Ramirez *et al.* [50] was equal to 2.7 W/m.K which will shift the surface deposit toward thermally semi or conductive enough to enhance vapor condensation. Then, the frequency of chemical cleaning using acid will be reduced which contribute to the decrease of the operation and maintenance cost.

Additionally, the determination of the latent heat reduction and the conductive heat transfer coefficient across the surface deposit are essential to determine the production increase with higher accuracy. Lee [51] demonstrated experimentally that the effective latent heat of vaporization of aqueous nanofluid containing graphite and/or silver nanoparticles could be impacted by ~30% depending on size and concentration of nanoparticles.

As continuity to the present work, more systematic experimental investigation of Fe_2O_3-saline water nanofluid performance and operation challenges need to be conducted. The following aspects need to be explored at a pilot plant scale considering:

1. Heat transfer characteristics of saline water nanofluid in different flow regimes.
2. Erosion-Corrosion of condenser tubes and other parts by the nanoparticles.
3. The absence of nanoparticles in the produced distilled water.
4. The stability of the nanoparticles in concentrated brine.
5. The interaction of nanoparticles with both antifoam and antiscalant.
6. The increased viscosity of nanofluid and its impact on pumping requirement.

5. REMARKS

A laboratory test was conducted to determine different thermophysical properties of saline water nanofluid including stability, thermal conductivity, evaporation rate, boiling temperature and time, and local heat transfer in stagnant conditions, in order to study the possibility of applying nanofluids technology on seawater. The effect of salinity, nanoparticles (size and concentration) and pressure were considered. The objective of the study was to explore for the first time the potential application of nanofluid in MSF desalination process for the enhancement of both performance and water production with a minor investment. As fas as the authors concern, these results are obtained for the first time, since most of the evaporation experiments conducted in seawater nanofluid were carried out at atmospheric pressure simulating solar ponds. Based on the obtained results, the following conclusions can be drawn:

- Zeta potential measurements showed that 1 hour of ultrasonication was enough to provide stable nanofluid for both DW and seawater base fluids.
- The increase of thermal conductivity of nanofluid with nanoparticles concentration, temperature and salinity were demonstrated which agree with many researchers.
- The fast boiling of seawater nanofluid (20nm particles at 0.01% concentration) at a lower temperature will induce quick preheating of the cooling seawater before reaching the brine heater in real MSF process. This will reduce steam consumption by 2% at the worst case. Such percentage is proportional to the fuel cost and represent significant saving. In addition, this lower boiling temperature of the

sweater nanofluid will induce in the best scenarios a water production increase 30%.

- Considering an ideal case of vapors condensation, seawater nanofluid showed an increase in distilled water production by 15% and 23% at atmospheric pressure and high vacuum, respectively.
- The improvement of local heat transfer by 13% obtained in the stagnant condition for the used nanoparticle size and concentration represents the first step to estimate properly the water production increase amount by using seawater nanofluid.
- The thermally conductive Fe_2O_3 nanoparticles deposition will play an important role to reduce surface thermal resistance created by the inorganic scale in MSF plants.

ACKNOWLEDGMENT

The author (Zouli) would like to thank the colleagues at Multiphase Reactors Engineering and Application Laboratory (mReal), Chemical and Biochemical Engineering Department for providing help while conducting experiments. The author (Zouli) also would like to thank the University of Jazan for giving him the financial support.

NOMENCLATURE

DW	Dstilled Water	*Greek symbols*	
MSF	Multi Stage Flushing	δ	thermal boundary layer thickness [m]
h_i	heat transfer coefficient [W/m^2 K]	μ	fluid dynamic viscosity [N.s/m^2]
K	thermal conductivity [W/m K]	ρ	fluid density [kg/m^3]
GCC	Gulf Council Countries	φ	volume concentration [-]
RO	Reversis Osmosis	C_p	specific heat [J/kg.K]
WHO	World Health Organization	*Subscript*	
OPEX	operation expenditure	bf	base fluid
PR	performance ratio	nf	nanofluids
q_i	heat flux [W/m^2]	p	particle
HTC	heat transfer coefficient[W/m^2 K]	s	surface
CHF	critical heat flux [W/m^2]	b	bulk
T	Temperature [K]		
BR	Brine Recycling [-]		
PTC	parabolic trough collector		
GOR	Gain Output Ratio		
m	Mass [kg]		

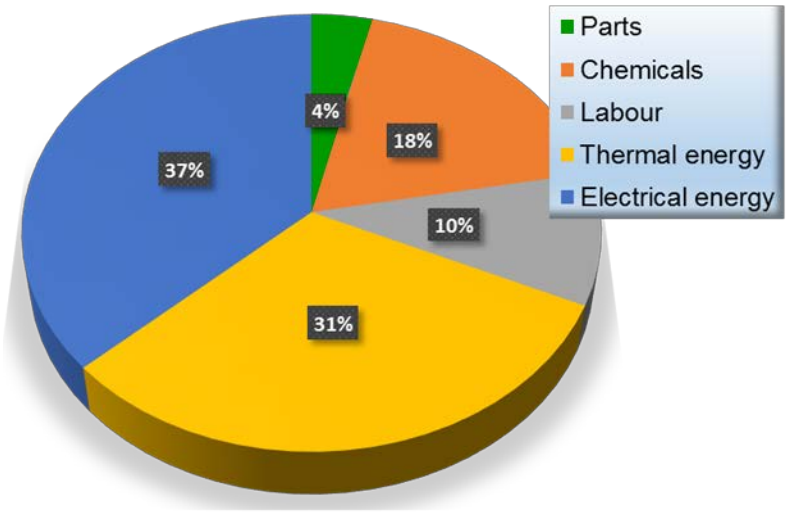

Figure 1: OPEX breakdown for an MSF plant with a production capacity of 450,000 m^3/d

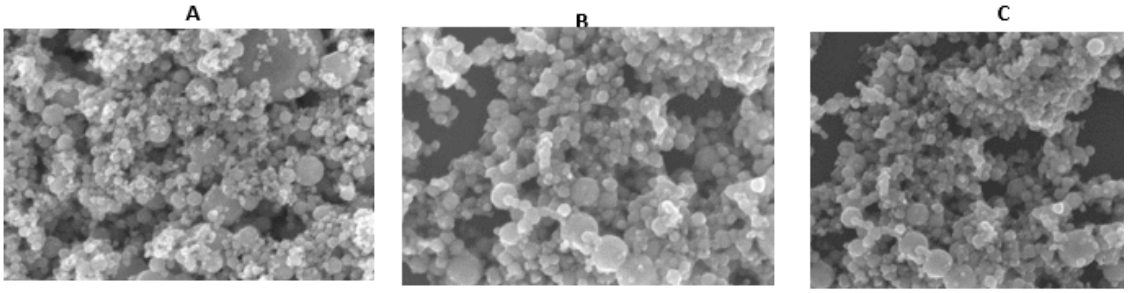

Figure 2: SEM images of Fe_2O_3 nanoparticles samples with different sizes: (a) 20 nm, (b) 10 nm, and (c) 3 nm

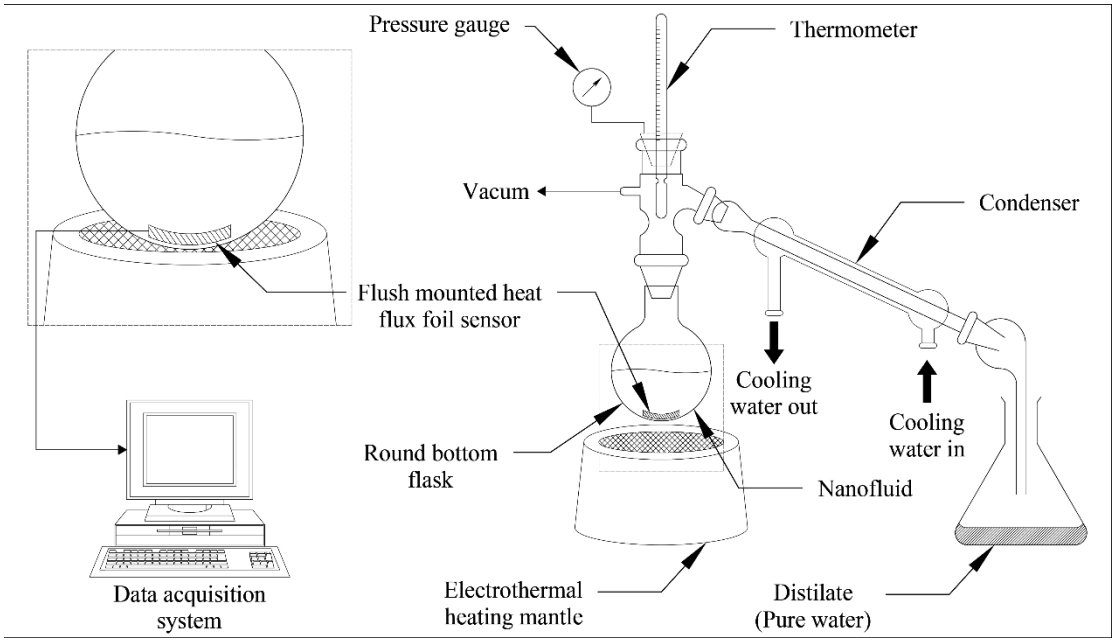

Figure 3: Schematic diagram of evaporation/condensation setup

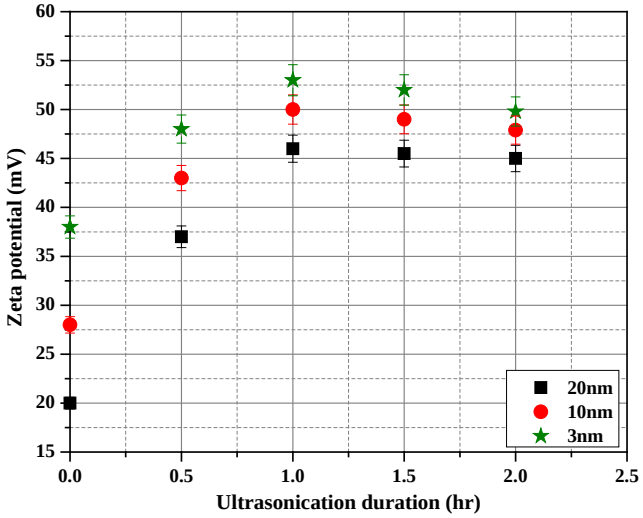

Figure 4: Zeta potentials of nanofluids after varying sonication durations

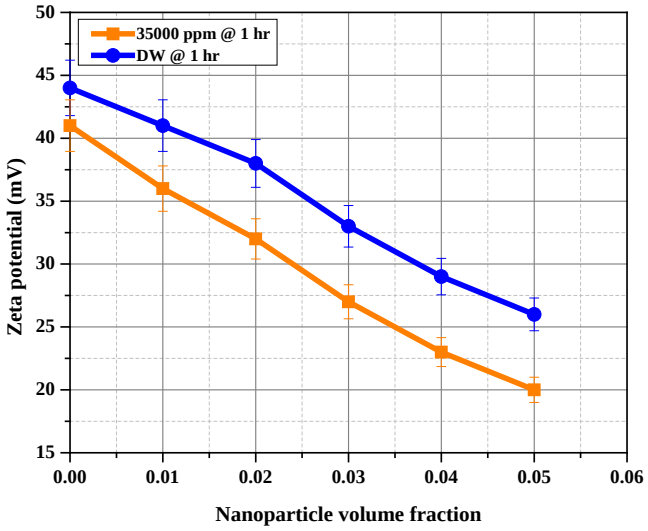

Figure 5: Zeta potentials of saline water based nanofluids with 20 nm nanoparticles for various sonication durations

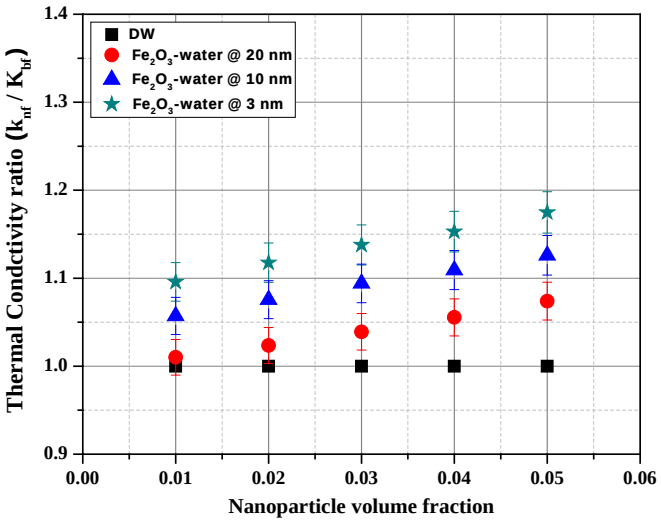

Figure 6: Effect of nanoparticle sizes on the thermal conductivity ratio (k_{nf}/k_{bf}) at 25 °C

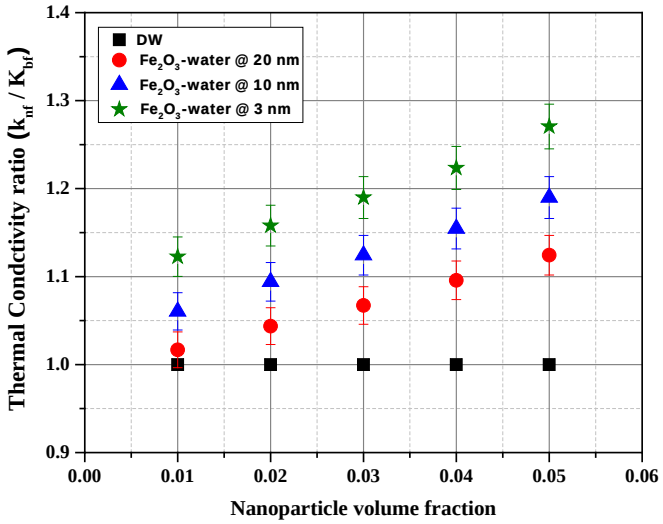

Figure 7: Effect of nanoparticle sizes on the thermal conductivity ratio (k_{nf}/k_{bf}) at 45 °C.

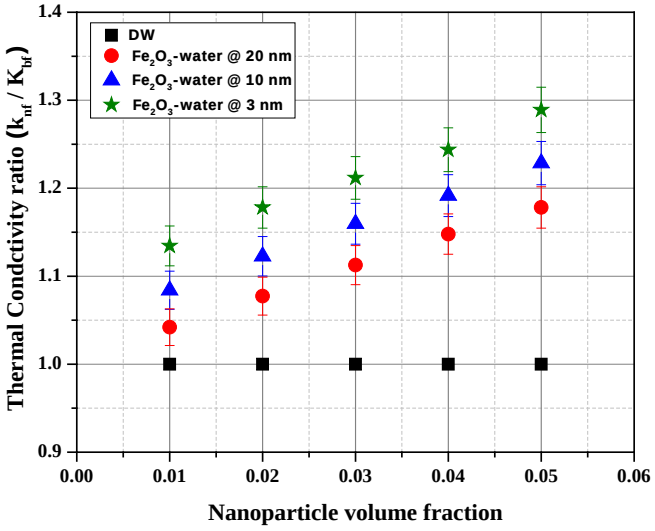

Figure 8: Effect of nanoparticle sizes on the thermal conductivity ratio (k_{nf}/k_{bf}) at 65 °C

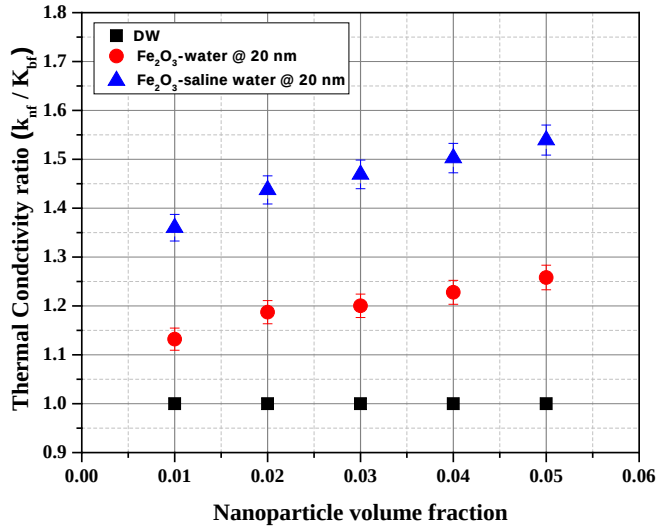

Figure 9: Comparison between the thermal conductivity ratio (k_{nf}/k_{bf}) at 100°C for Fe_2O_3-water and Fe_2O_3- saline water nanofluids

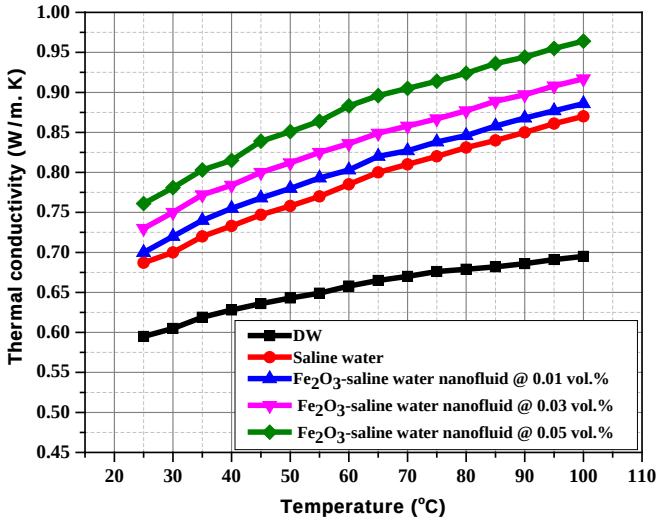

Figure 10: Effect of base fluid on thermal conductivity at different temperatures for different volume fractions of nanoparticles

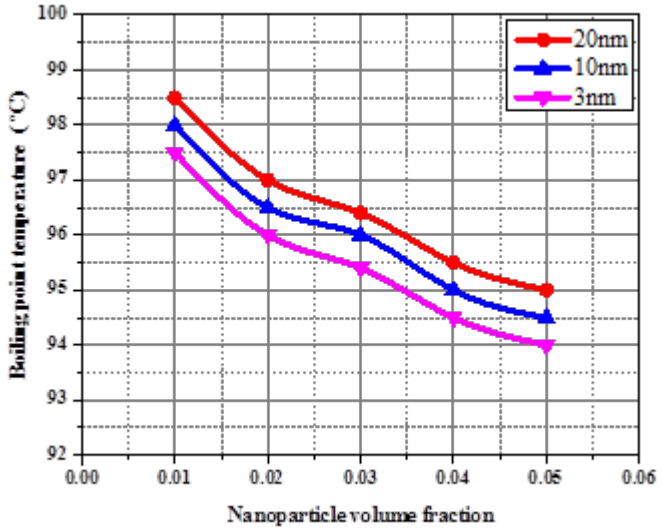

Figure 11: Boiling temperature of DW and nanofluids at different Fe_2O_3 nanoparticles sizes and volume fractions

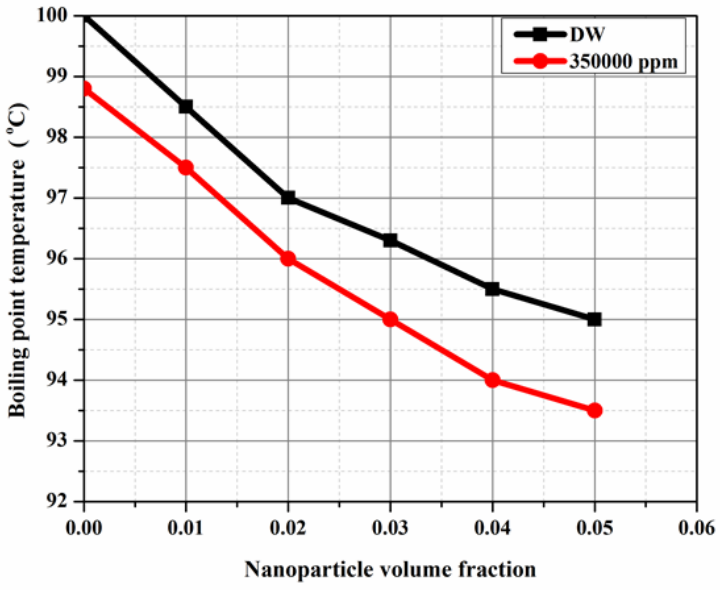

Figure 12: Boiling temperature of DW and saline water nanofluids at different 20 nm Fe_2O_3 nanoparticles concentrations

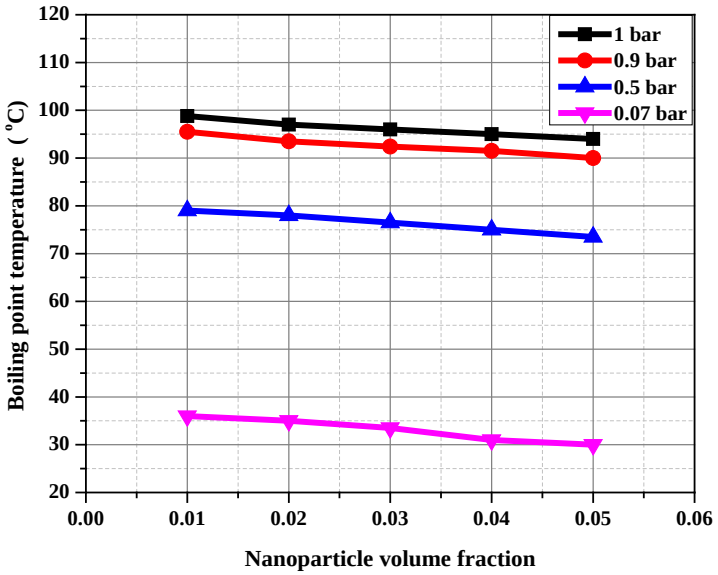

Figure 13: Boiling temperature of saline water nanofluids for different 20 nm Fe_2O_3 nanoparticles concentrations under vacuum conditions

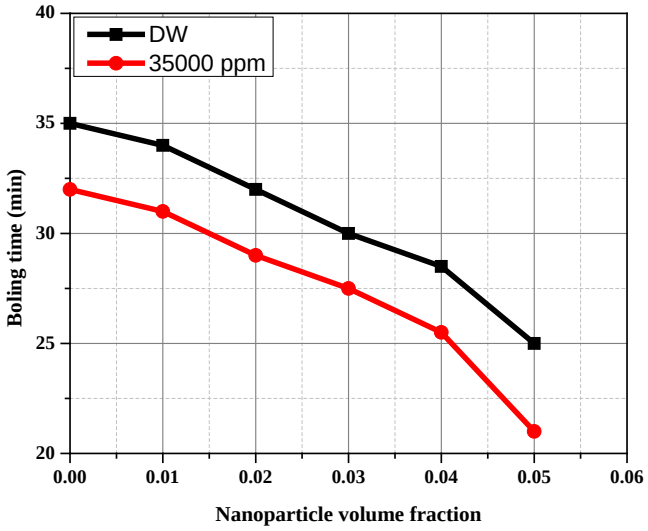

Figure 14: Boiling time of DW and saline water nanofluids at different 20 nm Fe_2O_3 nanoparticles concentrations

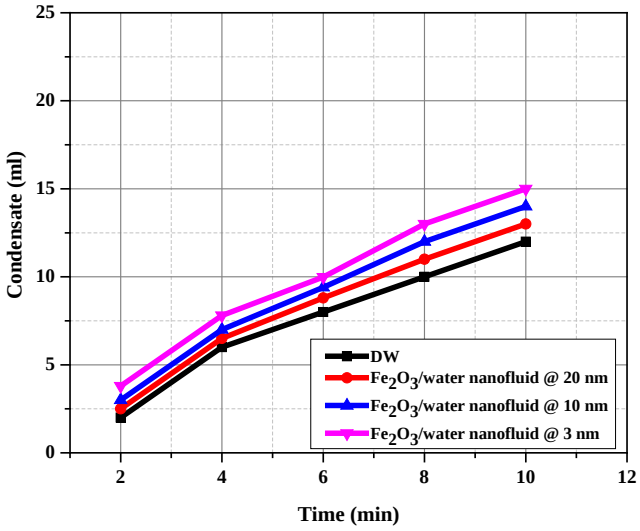

(a)

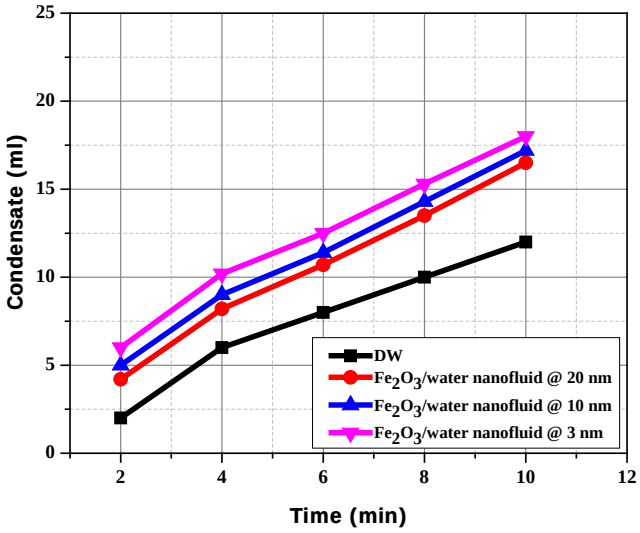

(b)

Figure 15: Condensate of DW nanofluid at (a) 0.01 %. (b) 0.03 %. (c) 0.05 %

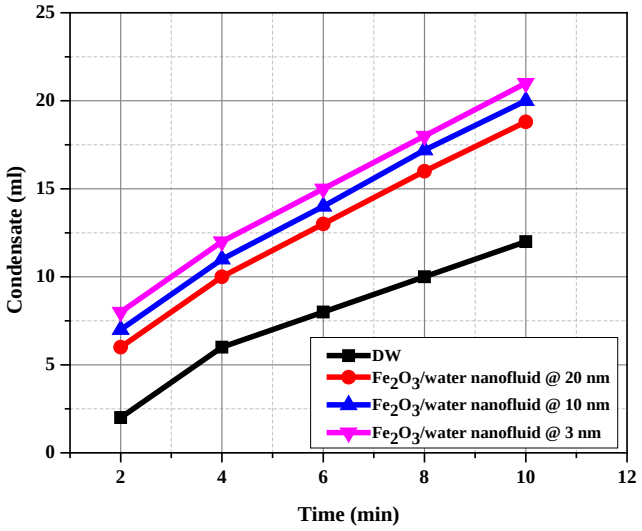

(c)

Figure 15: Condensate of DW nanofluid at (a) 0.01 %. (b) 0.03 %. (c) 0.05 % (cont.)

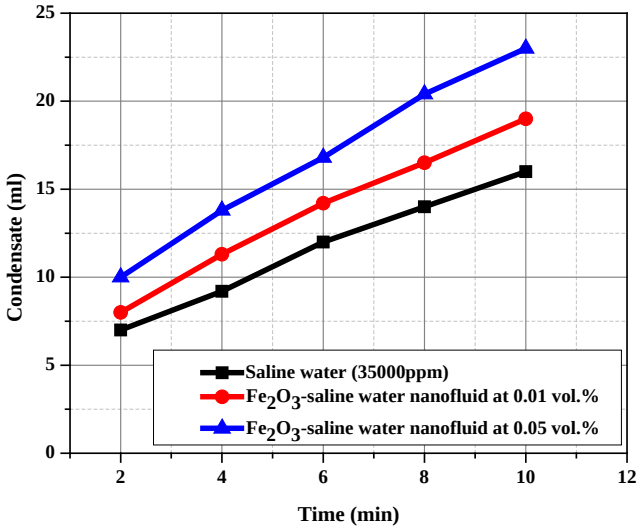

(a)

Figure 16: Condensation rate of saline water nanofluid for different volume fractions of 20 nm Fe_2O_3 nanoparticles (a) at 0.07 bar. **(**b) at 0.5 bar. **(**c) at 0.9 bar

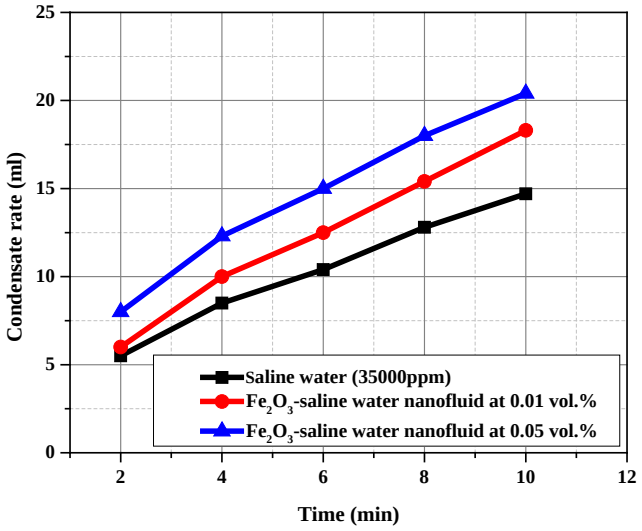

(b)

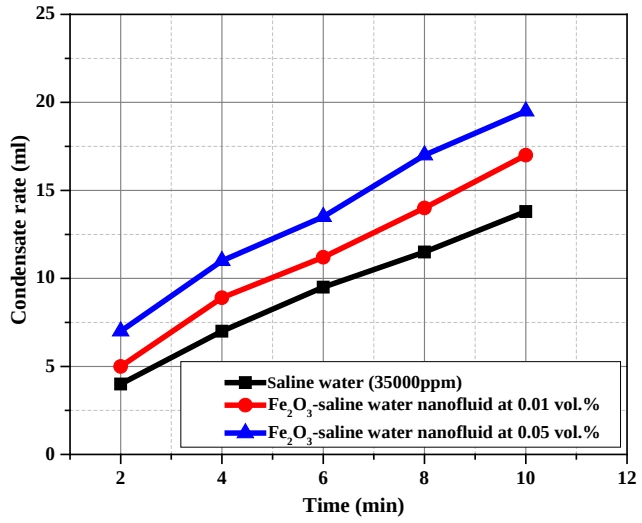

(c)

Figure 16: Condensation rate of saline water nanofluid for different volume fractions of 20 nm Fe_2O_3 nanoparticles (a) at 0.07 bar. **(**b) at 0.5 bar. **(**c) at 0.9 bar (cont.)

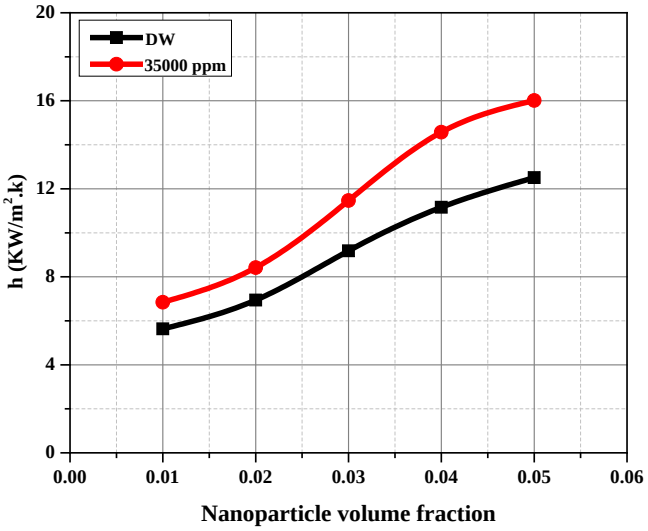

Figure 17: Local heat transfer coefficient of nanofluid for DW and saline water at different volume fractions of 20 nm nanoparticles at atmospheric pressure

REFERENCES

[1] K.R. Al-Hajri, L.A. Al-Misned, Water resources in the GCC countries: A strategic option, Renew. Energy. 5 (1994) 524–528. doi:10.1016/0960-1481(94)90428-6.

[2] O.A. Hamed, G.M. Mustafa, K. Bamardouf, H. Al-washmi, SWCC MSF DESALINATION PLANTS - CURRENT, (n.d.).

[3] R. Borsani, S. Rebagliati, Fundamentals and costing of MSF desalination plants and comparison with other technologies, Desalination. 182 (2005) 29–37. doi:10.1016/j.desal.2005.03.007.

[4] C.S. Bandi, R. Uppaluri, A. Kumar, Global optimization of MSF seawater desalination processes, Desalination. 394 (2016) 30–43. doi:10.1016/j.desal.2016.04.012.

[5] B.A.K. Naik, A.V. Vinod, Heat transfer enhancement using non-Newtonian nanofluids in a shell and helical coil heat exchanger, Exp. Therm. Fluid Sci. 90 (2018) 132–142. doi:10.1016/j.expthermflusci.2017.09.013.

[6] L. Sahota, Shyam, G.N. Tiwari, Energy matrices, enviroeconomic and exergoeconomic analysis of passive double slope solar still with water based nanofluids, Desalination. 409 (2017) 66–79. doi:10.1016/j.desal.2017.01.012.

[7] S. Manikandan, N. Karthikeyan, K.S. Rajan, Viscosity of Fe2O3 nanoparticles dispersion in water and ethylene glycol-water mixture (nanofluids), J. Nanoparticles. X (2013) 1–18. doi:10.1504/IJNP.2013.051912.

[8] Q. Li, Y. Xuan, Heat Transfer Enhancement of Nanofluids, Int. J. Heat Mass Transf. 21 (2000) 58–64.

[9] D. Sarit K., S.U.S. Choi, W. Yu, T. Pradeep, Nanofluids: Science and Technology, Wiley and Sons, Inc., 2007.

[10] I.M. Mahbubul, Preparation, characterization, properties, and application of nanofluids, 1st ed., William Andrew, 2018.

[11] P. Sivashanmugam, Application of Nanofluids in Heat Transfer, An Overv. Heat Transf. 1 (2012) 411–441. doi:10.5772/2623.

[12] S.M. You, J.H. Kim, K.H. Kim, Effect of nanoparticles on critical heat flux of water in pool boiling heat transfer, Appl. Phys. Lett. 83 (2003) 3374–3376. doi:10.1063/1.1619206.

[13] H. Sakashita, Pressure effect on CHF enhancement in pool boiling of nanofluids, J. Nucl. Sci. Technol. 53 (2016) 797–802. doi:10.1080/00223131.2015.1072482.

[14] M. Lomascolo, G. Colangelo, M. Milanese, A. De Risi, Review of heat transfer in nanofluids: Conductive, convective and radiative experimental results, Renew. Sustain. Energy Rev. 43 (2015) 1182–1198. doi:10.1016/j.rser.2014.11.086.

[15] C. Pang, J.W. Lee, Y.T. Kang, Review on combined heat and mass transfer characteristics in nanofluids, Int. J. Therm. Sci. 87 (2015) 49–67. doi:10.1016/j.ijthermalsci.2014.07.017.

[16] X. Fang, Y. Chen, H. Zhang, W. Chen, A. Dong, R. Wang, Heat transfer and critical heat flux of nanofluid boiling: A comprehensive review, Renew. Sustain. Energy Rev. 62 (2016) 924–940. doi:10.1016/j.rser.2016.05.047.

[17] Y.H. Diao, C.Z. Li, Y.H. Zhao, Y. Liu, S. Wang, Experimental investigation on the pool boiling characteristics and critical heat flux of Cu-R141b nanorefrigerant under atmospheric pressure, Int. J. Heat Mass Transf. 89 (2015) 110–115. doi:10.1016/j.ijheatmasstransfer.2015.05.043.

[18] M.R. Raveshi, A. Keshavarz, M.S. Mojarrad, S. Amiri, Experimental investigation of pool boiling heat transfer enhancement of alumina-water-ethylene glycol nanofluids, Exp. Therm. Fluid Sci. 44 (2013) 805–814. doi:10.1016/j.expthermflusci.2012.09.025.

[19] J. Gilberto Moreno, Investigation of Pool Boiling Heat Transfer with Nanofluids, THE UNIVERSITY OF TEXAS AT ARLINGTON, 2005.

[20] K.S. Suganthi, K.S. Rajan, Metal oxide nanofluids: Review of formulation, thermo-physical properties, mechanisms, and heat transfer performance, Renew. Sustain. Energy Rev. 76 (2017) 226–255. doi:10.1016/j.rser.2017.03.043.

[21] D.K. Devendiran, V.A. Amirtham, A review on preparation, characterization, properties and applications of nanofluids, Renew. Sustain. Energy Rev. 60 (2016) 21–40. doi:10.1016/j.rser.2016.01.055.

[22] C.Y. Tso, C.Y.H. Chao, Study of enthalpy of evaporation, saturated vapor pressure and evaporation rate of aqueous nanofluids, Int. J. Heat Mass Transf. 84 (2015) 931–941. doi:10.1016/j.ijheatmasstransfer.2015.01.090.

[23] K. Sefiane, R. Bennacer, Nanofluids droplets evaporation kinetics and wetting dynamics on rough heated substrates, Adv. Colloid Interface Sci. 147–148 (2009) 263–271. doi:10.1016/j.cis.2008.09.011.

[24] R.H. Chen, T.X. Phuoc, D. Martello, Effects of nanoparticles on nanofluid droplet evaporation, Int. J. Heat Mass Transf. 53 (2010) 3677–3682. doi:10.1016/j.ijheatmasstransfer.2010.04.006.

[25] M.R. Madhusoodanan, V. Sajith, C.B. Sobhan, Experimental investigation of phase change phenomena in nanofluids, Proc. Asme/Jsme Therm. Eng. Summer Heat Transf. Conf. 2007, Vol 1. (2007) 859–863. doi:10.1115/HT2007-32771.

[26] M. Moghiman, B. Aslani, Influence of nanoparticles on reducing and enhancing evaporation mass transfer and its efficiency, Int. J. Heat Mass Transf. 61 (2013) 114–118. doi:10.1016/j.ijheatmasstransfer.2013.01.057.

[27] N. Zouli, M. Al-dahhan, Impact of nanoparticles material on thermal conductivity and heat transfer coefficients of nanofluids, Submitt. Publ. (2018).

[28] N. Zouli, I.A. Said, M. Al-dahhan, enhancement of thermal conductivity and local heat transfer coefficients using Fe2O3/water nanofluid for improved thermal desalination processes, Submitt. Publ. (2018).

[29] S. Uribe, N. Zouli, M.E. Cordero, M. Al-dahhan, Development and validation of a CFD model to predict the thermal behaviour of nanofluids with three different nanoparticle materials, Submitt. Publ. (2018).

[30] A.E. Kabeel, E.M.S. El-Said, Applicability of flashing desalination technique for small scale needs using a novel integrated system coupled with nanofluid-based solar collector, Desalination. 333 (2014) 10–22. doi:10.1016/j.desal.2013.11.021.

[31] A.S. Nafey, M.A. Mohamad, S.O. El-Helaby, M.A. Sharaf, Theoretical and experimental study of a small unit for solar desalination using flashing process, Energy Convers. Manag. 48 (2007) 528–538. doi:10.1016/j.enconman.2006.06.010.

[32] E.M.S. El-Said, A.E. Kabeel, M. Abdulaziz, Theoretical study on hybrid desalination system coupled with nano-fluid solar heater for arid states, Desalination. 386 (2016) 84–98. doi:10.1016/j.desal.2016.03.001.

[33] G.M. Ayoub, L. Malaeb, Developments in solar still desalination systems: A critical review, Crit. Rev. Environ. Sci. Technol. 42 (2012) 2078–2112. doi:10.1080/10643389.2011.574104.

[34] K. Garg, V. Khullar, S.K. Das, H. Tyagi, Performance evaluation of a brine-recirculation multistage flash desalination system coupled with nanofluid-based direct absorption solar collector, Renew. Energy. 122 (2018) 140–151. doi:10.1016/j.renene.2018.01.050.

[35] N. Fuchs, The mechanics of aerosols, Oxford Pergamon, 1964.

[36] X. Song, N. Jiang, Y. Li, D. Xu, G. Qiu, Synthesis of CeO2-coated SiO2 nanoparticle and dispersion stability of its suspension, Mater. Chem. Phys. 110 (2008) 128–135. doi:10.1016/j.matchemphys.2008.01.042.

[37] W. Chen, C. Zou, X. Li, L. Li, Experimental investigation of SiC nanofluids for solar distillation system: Stability, optical properties and thermal conductivity with saline water-based fluid, Int. J. Heat Mass Transf. 107 (2017) 264–270. doi:10.1016/j.ijheatmasstransfer.2016.11.048.

[38] H.A. Mintsa, G. Roy, C.T. Nguyen, D. Doucet, New temperature dependent thermal conductivity data for water-based nanofluids, Int. J. Therm. Sci. 48 (2009) 363–371. doi:10.1016/j.ijthermalsci.2008.03.009.

[39] K. Kwak, C. Kim, Viscosity and thermal conductivity of copper oxide nanofluid dispersed in ethylene glycol, Korea Aust. Rheol. J. 17 (2005) 35–40.

[40] Y.W. Wang, J.X. Zhang, J.W. Cen, F.M. Jiang, A Feasibility Study About Using SiO2 Nanofluid Screen Mesh Wick Heat Pipe for Cooling of High-Power LEDs, Heat Transf. Eng. 37 (2016) 741–750.

[41] F. Yu, Y. Chen, X. Liang, J. Xu, C. Lee, Q. Liang, P. Tao, T. Deng, Dispersion stability of thermal nanofluids, Prog. Nat. Sci. Mater. Int. 27 (2017) 531–542. doi:10.1016/j.pnsc.2017.08.010.

[42] J. Koo, C. Kleinstreuer, A new thermal conductivity model for nanofluids, J. Nanoparticle Res. 6 (2004) 577–588. doi:10.1007/s11051-004-3170-5.

[43] K.D. Hagen, Heat Transfer with Applications, Prentice-Hall, New Jersey, 1999.

[44] P. Keblinski, S.R. Phillpot, S.U.S. Choi, J.A. Eastman, Mechanisms of heat flow in suspensions of nano-sized particles (nanofluids), Int. J. Heat Mass Transf. 45 (2001) 855–863. doi:10.1016/S0017-9310(01)00175-2.

[45] S. Pil Jang, S.U.S. Choi, Effects of Various Parameters on Nanofluid Thermal Conductivity, J. Heat Transfer. 129 (2007) 617. doi:10.1115/1.2712475.

[46] J.P. Tu, N. Dinh, T. Theofanous, An experimental study of nanofluid boiling heat transfer, in: Proc. 6th Int. Symp. Heat Transf., 2004.

[47] D.H. Shin, C.K. Choi, Y.T. Kang, S.H. Lee, Local aggregation characteristics of a nanofluid droplet during evaporation, Int. J. Heat Mass Transf. 72 (2014) 336–344. doi:10.1016/j.ijheatmasstransfer.2014.01.023.

[48] E. Salari, S.M. Peyghambarzadeh, M.M. Sarafraz, F. Hormozi, Boiling thermal performance of TiO2 aqueous nanofluids as a coolant on a disc copper block, Period. Polytech. Chem. Eng. 60 (2016) 106–122.

[49] D. Wen, Y. Ding, Experimental investigation into the pool boiling heat transfer of aqueous based γ-alumina nanofluids, J. Nanoparticle Res. 7 (2005) 265–274. doi:10.1007/s11051-005-3478-9.

[50] S. Ramirez, K. Chan, R. Hernandez, E. Recinos, E. Hernandez, R. Salgado, A.G. Khitun, J.E. Garay, A.A. Balandin, Thermal and magnetic properties of nanostructured densified ferrimagnetic composites with graphene - graphite fillers, Mater. Des. 118 (2017) 75–80. doi:10.1016/j.matdes.2017.01.018.

[51] S. Lee, A study of the latent heat of vaporization in aqueous nanofluids, Arizona State University, 2015.

SECTION

2. REMARKS

In the present work, Fe_2O_3 nanoparticles were selected after studying the thermophysical properties of different nanofluids in different conditions with different nanoparticles including CuO and Al_2O_3. In addition, the magnetic properties of hematite nanoparticles support their use highly in MSF making their recovery and recicle an easy task. The significant findings of this study can be summarized as follows:

1. The thermal conductivity and local heat transfer coefficient increased with the increase of the Fe_2O_3/water nanofluids volume fraction and temperature. Also, an enhancement on the thermal conductivity as well as the local heat transfer coefficient was observed when decreasing the nanoparticle size.
2. The local heat transfer coefficients of Fe_2O_3/water nanofluid improved with Reynolds number compared with that of a base fluid at the same Reynolds number.
3. The results indicate that when the nanoparticle sizes become very small, the effect of such small size on the heat transfer coefficients would be relatively larger than the larger size nanoparticles.
4. It is clear that the boundary layer film thickness is larger than the diameter of the nanoparticles used in this work (30 nm). This allows the nanoparticles to penetrating the film toward the wall and generate local micro eddies and local mixing within the film. This contributes to the enhancement of the local heat transfer coefficient.

5. The results indicate that the improvement we obtained in the thermal conductivity and local heat transfer coefficient will enable thermal improvement of desalination processes.
6. In terms of nanofluid stability, it appears that salinity impact is dependent on the nanoparticles concentration and size. Such property determines the performance of nanofluid critically when implemented in MSF desalination process.
7. The fast boiling in the presence of saline water nanofluid represents important benefits to the MSF process and will address for the first time a significant steam consumption and gas emission reduction.
8. The high evaporation/condensation of saline water nanofluid combined, the increase of the convective heat transfer, and the potential reduction of surface thermal resistance merit more investigation to confirm the expected improvement of distilled water production in MSF conditions.
9. It was observed that the nanofluids can also be used to in water with different salinities. The results showed that the local heat transfer coefficient and thermal conductivity were further enhanced at higher salt concentrations. Also, it was observed that the boiling temperature decreases with the increase in the salinity of water.

3. SUGGESTIONS FOR FUTURE WORK

While the present investigation results are promising, still more issues need to be addressed and studied to improve the understanding of the pro and cons of seawater nanofluid when suggested to Multi Stage Flash (MSF) desalination community. In the following, the future works are suggested in order to gain a further insight into the applications of nanofluids and their use in MSF disalination processes.

1. Regarding seawater nanofluid stability, the size and concentration of Fe_2O_3 nanoparticles should be optimized for different water salinities including concentrated brine and different temperatures. The stability of the optimized nanofluid formulation should be monitored at different nanoparticle concentrations to determine the frequency of nanofluid injection into the MSF desalination process.
2. Convective heat transfer coefficient needs to be measured in both seawater and concentrated brine at different flow regimes (laminar and turbulent) considering three temperature values covering the flash range in MSF plants.
3. In terms of surface thermal resistance, solid state experiments need to be carried out on different deposit formulations including $CaCO_3$ and $Mg(OH)_2$ mixed with different nanoparticles proportions. The wettability of this mixed deposit has to be measured to predict the evolution of both heat transfer and scale development.
4. Erosion of Fe_2O_3 nanoparticles should be studied on different MSF desalination alloys/materials considering different velocities and temperatures.

5. The stability and performance of seawater nanofluid should be investigated in the low level of dissolved oxygen, and presence of antiscalant and antifoam chemicals.
6. The increased viscosity of nanofluid due to nanoparticle concentration increase has to be checked regarding the impact on pumping requirement, which represents a potential risk of electrical energy increase.
7. To study the absence of nanoparticles in the produced distilled water, and the interaction of nanoparticles with both antifoam and antiscalant
8. Asses if Computational Fluid Dynamics modelling and simulation can capture the effect of nanofluids on the heat transfer characteristics in order to be used to asses various conditions and to optimize the industrial applications of nanofluids in MSF desalination processes and other industrial heat transfer processes.

APPENDIX

EXPERIMENTAL INVESTIGATION OF THE THERMAL PROPERTIES OF SALINE WATER NANOFLUIDS

The focus of this study is to investigate and quantify, for the first time, the effects of different concentrations of saline waters used as base fluids for Fe_2O_3 nanofluids, in order to insight into the industrial applications of nanofluids under different conditions. Therefore, it is necessary to study the differences induced by the changes in salinity of the base fluid over the nanofluid stability; to determine the heat transfer characteristics, such as the thermal conductivity and heat transfer coefficient of saline water nanofluid in different flow regimes; and to determine the effect of the salinity of the base fluid over the boiling time and boiling temperature.

Multi-Stage-Flash (MSF)

Among thermal desalination processes, Multi-Stage-Flash (MSF) is dominant in most of arid countries such as in Gulf Council Countries (GCC). Due to the cheap fossil fuel used to produce steam necessary for MSF desalination, GCC countries adopted this technology with more than 40 years of record. The success factor of this technology is based on the sustainability of the heat transfer. Indeed, due to the concentrated brine and high temperature, inorganic scale develops a thermal resistance at the heat exchanger tube surface, which requires the use of chemical and physical methods to disturb this scale. Within this context, the operation cost raises to include energy (thermal and electrical), chemicals, etc. [1].

The thermal energy increase in MSF desalination plant is dependent on the heat transfer performance, which is a function of condenser tubing material and scaling

phenomenon. Most MSF desalination plants use cupronickel alloy as tubing material due to its high thermal conductivity. In some limited cases, titanium is recommended for long life reliability depending on the market opportunity. For scale control, the use of high-temperature antiscalant chemicals dominate over the acid operation method. Antiscalant chemicals are associated with a ball cleaning system to control fouling factor as per design values. However, after a certain number of running hours, production must be stopped to conduct acid cleaning to restore the performance of the desalination MSF unit [2]. Hamed et al. [3] suggested the increase of the flash range by either the increase of the Top Brine Temperature (TBT) or the increase of the number of stages and/or the increase of the specific heat transfer area to enhancement the heat transfer performance.

Although there is lot of research efforts in the heat transfer improvement, it seems that desalination industry did not take the complete benefits. Among the very promising technologies in heat transfer topic, the nanofluids represent an interesting opportunity with their super thermophysical properties than can be beneficial to the heat transfer in MSF desalination plants.

Nanofluid Stability

Figure 1 shows the zeta potential of nanofluid for four different salinity of 0 ppm, 15000 ppm, 35000 ppm, and 55000 ppm and for different volume fractions (ranging from 0.01 to 0.05 with an increment of 0.01). As shown in Figure 5 the zeta potential values were found to decrease with increase the volume fraction, and the highest zeta potential values of nanofluids were measured as 41, 38, 36, and 32 mV for 0, 15000, 35000, and 55000 ppm , respectively after one hour of ultrasonication at low volume fraction (φ = 0.01). It appears that at high volume fraction (φ = 0.05) is detrimental to the seawater

nanofluid stability as shown in Figure 5. Several authors [4-6] obtained the dependence of zeta potential on the salt concentration and the sonication time.

It is worth mentioning that the seawater has higher viscosity and ionic strength compared to the deionized water (DW). This would play main role in the synergy between the different micro forces between Fe2O3 nanoparticles and the base fluid. In addition, seawater would promote electrostatic forces (a function of base fluid permittivity) between particles and increase the collision probabilities between them inducing less stability (aggregation) compared to the deionized water [7]. The decrease of seawater based nanofluid stability was observed by other researchers [8,9], which suggest a screening effect of the electrolyte on the surface of nanoparticles, which cause aggregation above certain critical salt concentration.

Effects of particle volume fraction and temperature on the thermal conductivity

The measured thermal conductivity of the nanofluid (k_{nf}) is normalized with respect to the thermal conductivity of the base fluid (k_{bf}). Figures 2–4 show the relationship between the thermal conductivity ratio of the nanofluid to the base fluid (k_{nf}/ K_{bf}) and the volume fraction of nanofluid at various experimental temperatures of 40°C, 70°C, and 95°C for different Total Dissolved Solids (TDS) (15000, 35000, 55000 ppm). The results indicate that, the thermal conductivity ratio (k_{nf}/ K_{bf}) increases with increasing particles volume fraction and temperatures as shown in Figures 2-4.

It appears clearly that seawater as base fluid enhances the thermal conductivity of the nanofluid by 50, 53, 56.6% for 15000, 35000, and 55000 ppm respectively, for 0.05 at 95 ^{o}C compared to the DW that is explained by the higher thermal conductivity attributed

to its higher TDS. Thus, the high TDS is favorable to the thermal conductivity improvement contrary to the nanofluid stability discussed abovementioned.

Effects of particle volume fraction and flow regime on the heat transfer coefficients

Figures 5-7 show the local heat transfer coefficient for the nanofluids with the different saline waters as bases fluids for different volume concentrations of the nanoparticles under laminar conditions. Figures 8-10 show similar results but for the case of turbulent conditions. It can be seen that, as shown in the previous studies, the local heat transfer coefficient in enhanced with the increase of the volume concentration of the nanoparticles; also, there is a further of local heat transfer coefficient under turbulent conditions than under laminar conditions. These results are in agreement with the expected behaviors based observed for the nanofluids with distilled water as a base fluid.

Regarding the effect of the salinity on the local heat transfer coefficient, it can be seen that the highest values are found for the salinity if 55000 ppm. The results for 55000 ppm show an increment in the local heat transfer coefficient of up to 27% in comparison with the nanofluid with a base fluid of distilled water. This behavior can be attributed to the higher thermal conductivity of the nanofluid observed at higher salinity of the base fluid, as shown in Figures 2-4

Effects of particle volume fraction, pressure on the boiling temperature

Figures 11-13 show the boiling temperature of the nanofluids with the different saline waters as base fluids for different concentrations of the nanoparticles, under three different vacuum pressures. It can be seen that the boiling temperature of the nanofluid decreases with the decrease of the pressure and the increase of the concentration of the nanoparticles. This result is in agreement with the observations in the previous study.

In these figures, it can also be appreciated that the increase of the salinity of the water produces a reduction in the boiling temperature of the nanofluid. The maximum reduction is found for the salinity of 55000 ppm under a vacuum pressure of 0.07 bar, with a decrease in the boiling temperature of 25%. This can be attributed to the enhanced local heat transfer coefficient and thermal conductivity of the nanofluid.

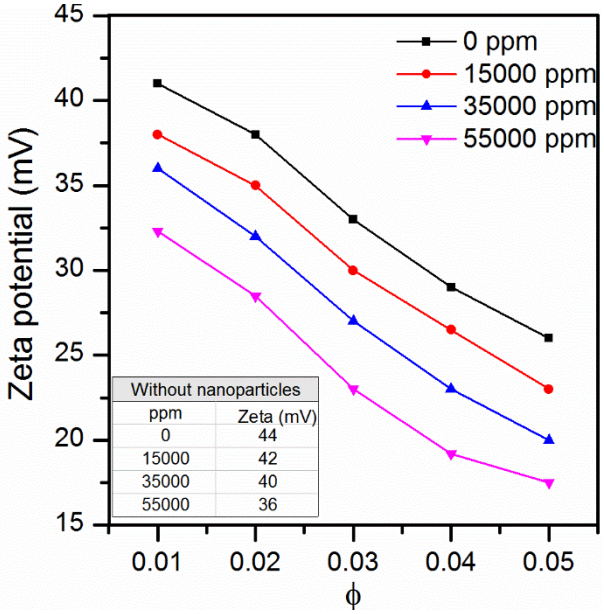

Figure 1: Zeta potential of nanofluids with different saline waters at different volume concentrations

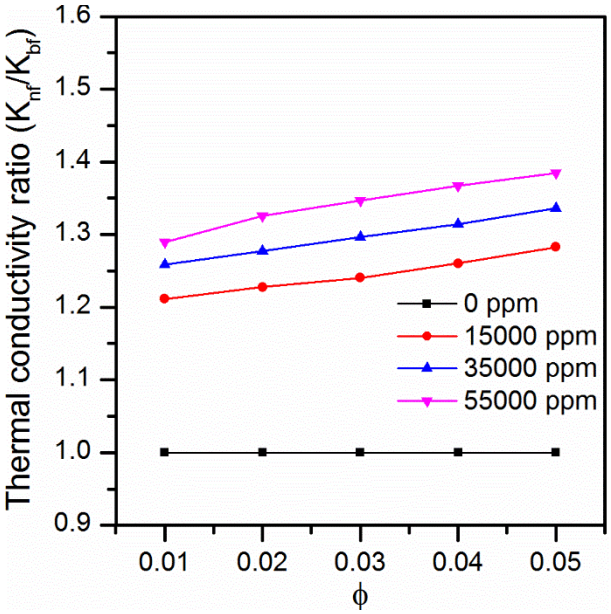

Figure 2: Thermal conductivity ratio of different saline waters nanofluids at different volume concentrations at T = 40^{o}C

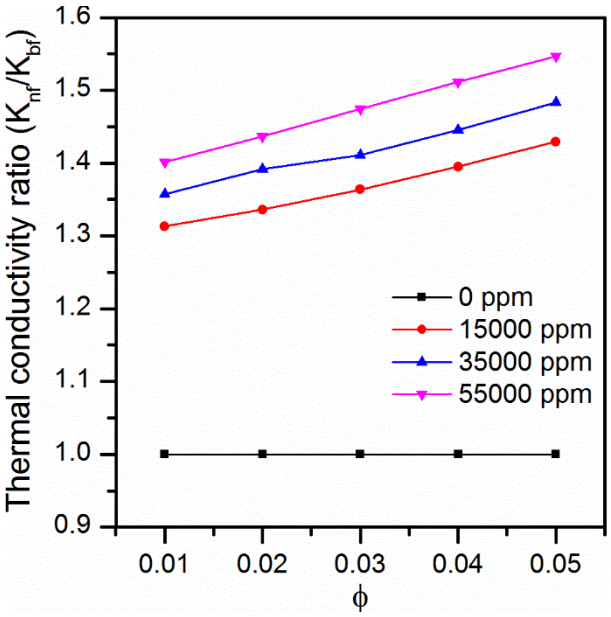

Figure 3: Thermal conductivity ratio of different saline waters nanofluids at different volume concentrations at T = 70ºC

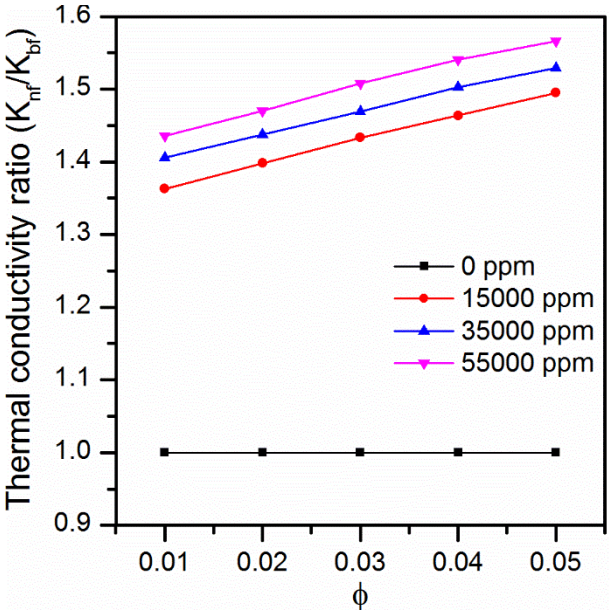

Figure 4: Thermal conductivity ratio of different saline waters nanofluids at different volume concentrations at T = 95ºC

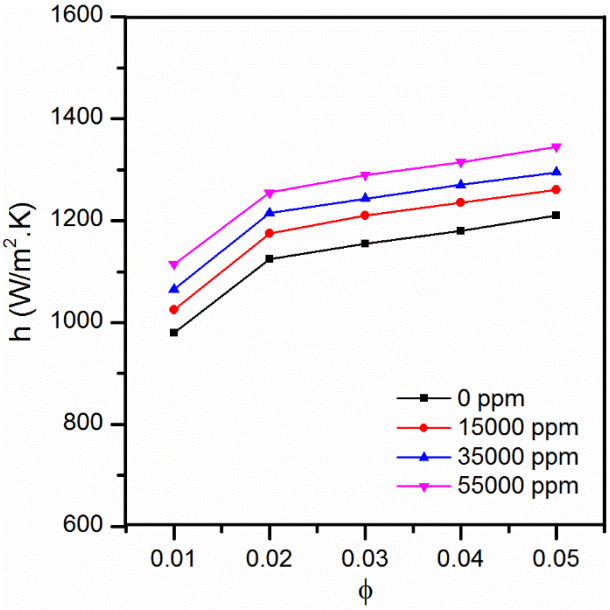

Figure 5: Heat transfer coefficient of different saline waters nanofluids at different volume concentrations under laminar conditions at T = 40°C

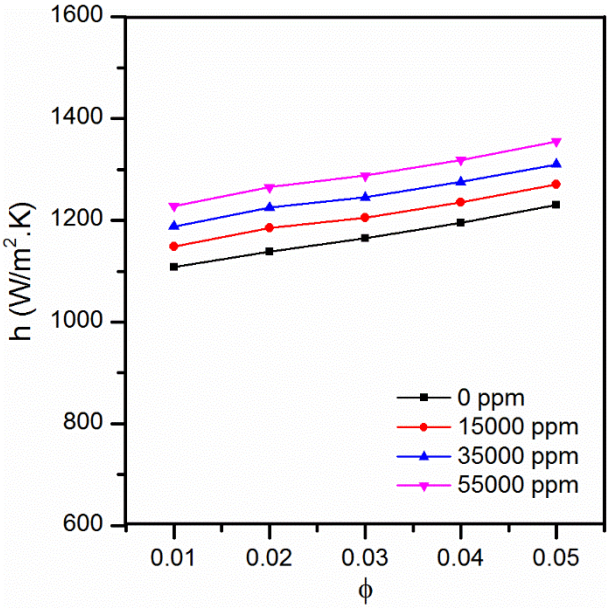

Figure 6: Heat transfer coefficient of different saline waters nanofluids at different volume concentrations under laminar conditions at T = 70°C

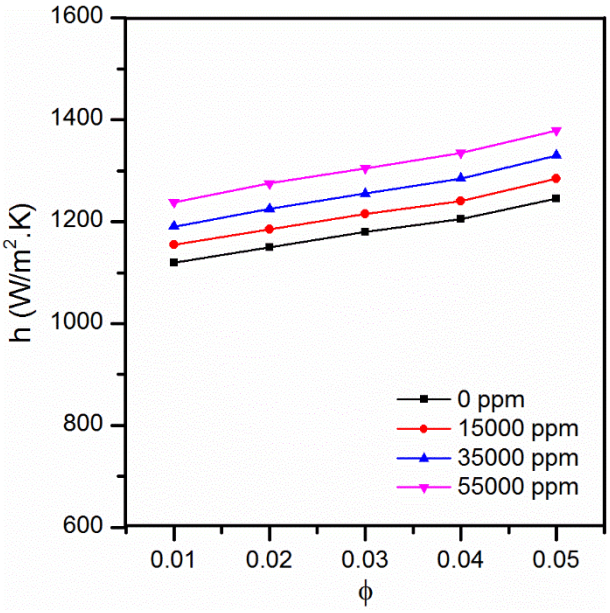

Figure 7: Heat transfer coefficient of different saline waters nanofluids at different volume concentrations under laminar conditions at T = 95ºC

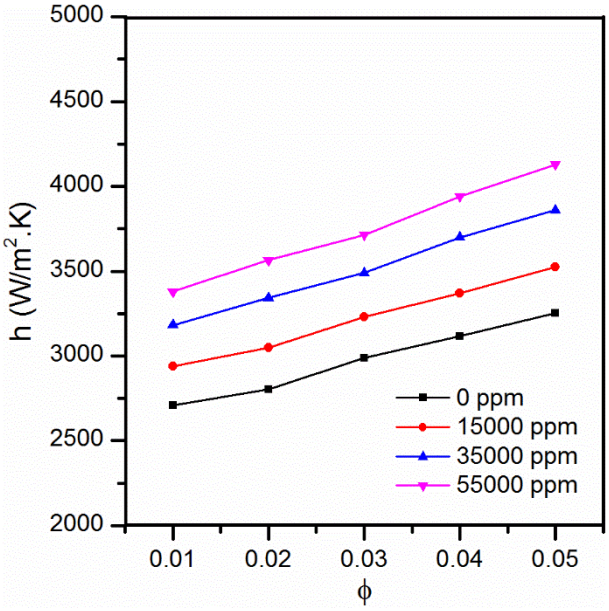

Figure 8: Heat transfer coefficient of different saline waters nanofluids at different volume concentrations under turbulent conditions at T = 40ºC

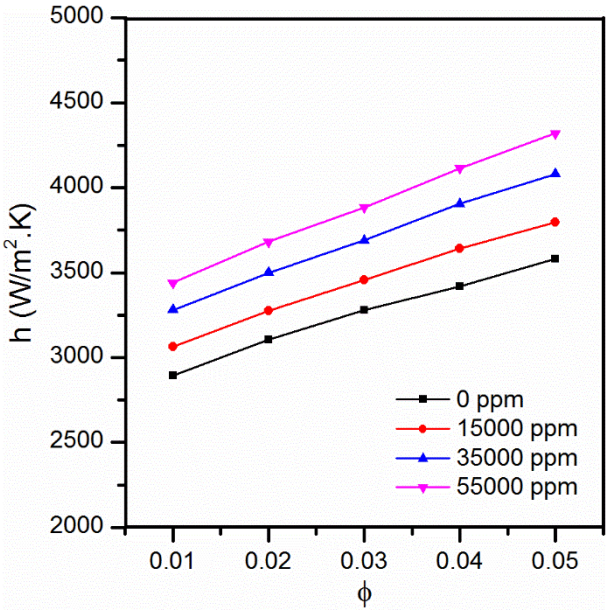

Figure 9: Heat transfer coefficient of different saline waters nanofluids at different volume concentrations under turbulent conditions at T = 70ºC

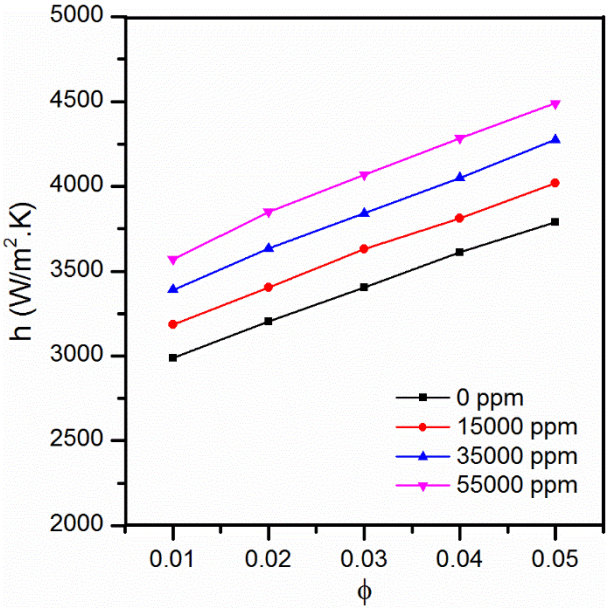

Figure 10: Heat transfer coefficient of different saline waters nanofluids at different volume concentrations under turbulent conditions at T = 95ºC

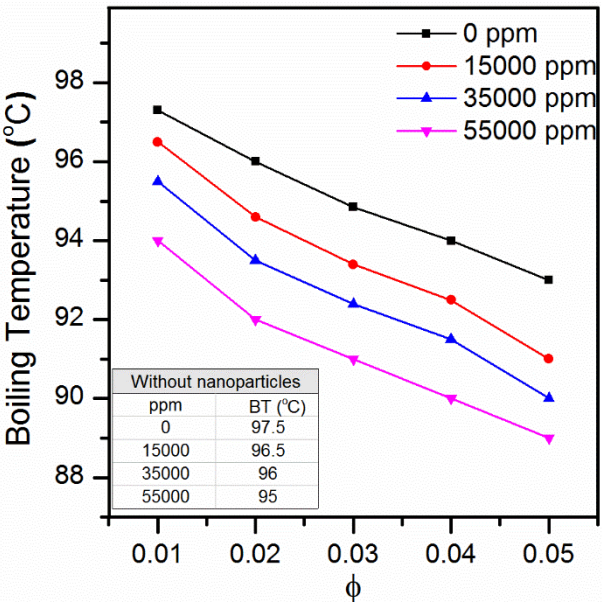

Figure 11: Boiling temperature of different saline waters nanofluids at different volume concentrations at P = 0.9 bar

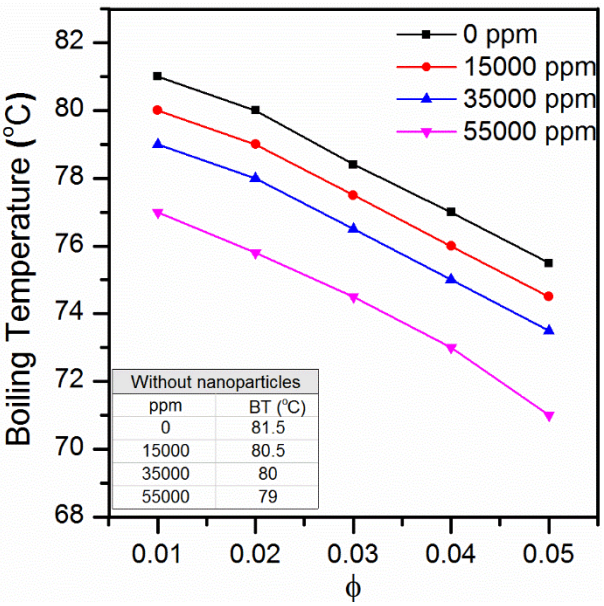

Figure 12: Boiling temperature of different saline waters nanofluids at different volume concentrations at P = 0.5 bar

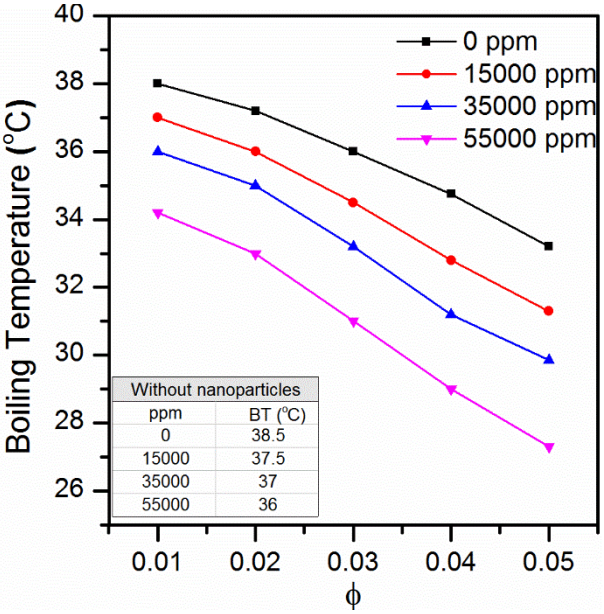

Figure 13: Boiling temperature of different saline waters nanofluids at different volume concentrations at P = 0.07 bar

REFERENCES

[1] R. Borsani, S. Rebagliati, “Fundamentals and costing of MSF desalination plants and comparison with other technologies,” Desalination 182 (2005), 29-37.

[2] W.T.Hanbury, T.Hodgkiess, K. Al-Omari, “Aspects of acid-cleaning operations in MSF plants”, Desalination 158 (2003), 1.

[3] O. Hamed, K. Bamardouf, H. Al-Washmi, K. Al-Shail, H. Abdullah, A. Al-Wadie, “Assessment of major design features of SWCC MSF desalination plants,” 4th SWCC acquired experience conference, Jeddah (2004).

[4] M. P. Beck, Y. Yuan, P. Warrier, and A. S. Teja, “The effect of particle size on the thermal conductivity of alumina nanofluids,” Journal of Nanoparticle Research, vol. 11, no. 5, pp. 1129–1136, 2009.

[5] Abdulmohsin, R.S. and M.H. Al-Dahhan, Characteristics of convective heat transport in a packed pebble-bed reactor. Nuclear Engineering and Design, 2015. 284: p. 143-152.

[6] G.M. Ayoub, L. Malaeb, Developments in solar still desalination systems: a critical review, Crit. Rev. Environ. Sci. Technol. 42 (2012) 2078–2112.

[7] E.M.S. El-said, A.E. Kabeel, M. Abdulaziz, Theoretical study on hybrid desalination system coupled with nano-fluid solar heater for arid states”, Desalination 386 (2016) 84-98.

[8] M. J. Pastoriza-Gallego, L. Lugo, J. L. Legido, and M. M. Pi˜neiro,“Thermal conductivity and viscosity measurements of ethyleneglycol-based Al2O3 nanofluids,” Nanoscale Research Letters, vol. 6, no. 1, p. 111, 2011.

[9] M. P. Beck, Y. Yuan, P. Warrier, and A. S. Teja, “The effect of particle size on the thermal conductivity of alumina nanofluids,” Journal of Nanoparticle Research, vol. 11, no. 5, pp. 1129–1136, 2009.

REFERENCES

[1] C. Schlosser, K. Strzepek, X. Gao, The Future of Global Water Stress: An Integrated Assessment, Earth's Future. 2 (2014) 341–361.

[2] A. Maddocks, R.S. Young, P. Reig, Ranking the World's Most Water-Stressed Countries in 2040, 2015.

[3] O.A. Hamed, G.M. Mustafa, K. Bamardouf, H. Al-washmi, SWCC MSF DESALINATION PLANTS - CURRENT, (n.d.).

[4] R. Borsani, S. Rebagliati, Fundamentals and costing of MSF desalination plants and comparison with other technologies, Desalination. 182 (2005) 29–37.

[5] W.T. Hanbury, T. Hodgkiess, K. Al-Omari, Aspects of acid-cleaning operations in MSF plants, Desalination. 158 (2003) 1.

[6] A.Y. Kalendar, A.J. Griffiths, Performance study of enhanced and smooth surface tubes in a system condenser of a multistage flash desalination unit, Desalination. 134 (2001) 269–283.

[7] A.E. Al-Rawajfeh, S. Ihm, H. Varshney, A.N. Mabrouk, Scale formation model for high top brine temperature multi-stage flash (MSF) desalination plants, Desalination. 350 (2014) 53–60.

[8] B.A.K. Naik, A.V. Vinod, Heat transfer enhancement using non-Newtonian nanofluids in a shell and helical coil heat exchanger, Exp. Therm. Fluid Sci. 90 (2018) 132–142.

[9] M. Ahmadi, G. Willing, Heat transfer measurment in water based nanofluids, Int. J. Heat Mass Transf. 118 (2018) 40–47.

[10] P. Sivashanmugam, Application of Nanofluids in Heat Transfer, An Overv. Heat Transf. 1 (2012) 411–441.

[11] B. Sun, W. Lei, D. Yang, Flow and convective heat transfer characteristics of Fe2O3-water nanofluids inside copper tubes, Int. Commun. Heat Mass Transf. 64 (2015) 21–28.

[12] S.M. You, J.H. Kim, K.H. Kim, Effect of nanoparticles on critical heat flux of water in pool boiling heat transfer, Appl. Phys. Lett. 83 (2003) 3374–3376.

[13] H. Sakashita, Pressure effect on CHF enhancement in pool boiling of nanofluids, J. Nucl. Sci. Technol. 53 (2016) 797–802.

[14] M. Lomascolo, G. Colangelo, M. Milanese, A. De Risi, Review of heat transfer in nanofluids: Conductive, convective and radiative experimental results, Renew. Sustain. Energy Rev. 43 (2015) 1182–1198.

[15] C. Pang, J.W. Lee, Y.T. Kang, Review on combined heat and mass transfer characteristics in nanofluids, Int. J. Therm. Sci. 87 (2015) 49–67.

[16] X. Fang, Y. Chen, H. Zhang, W. Chen, A. Dong, R. Wang, Heat transfer and critical heat flux of nanofluid boiling: A comprehensive review, Renew. Sustain. Energy Rev. 62 (2016) 924–940.

[17] Y.H. Diao, C.Z. Li, Y.H. Zhao, Y. Liu, S. Wang, Experimental investigation on the pool boiling characteristics and critical heat flux of Cu-R141b nanorefrigerant under atmospheric pressure, Int. J. Heat Mass Transf. 89 (2015) 110–115.

[18] M.R. Raveshi, A. Keshavarz, M.S. Mojarrad, S. Amiri, Experimental investigation of pool boiling heat transfer enhancement of alumina-water-ethylene glycol nanofluids, Exp. Therm. Fluid Sci. 44 (2013) 805–814.

[19] J. Gilberto Moreno, Investigation of Pool Boiling Heat Transfer with Nanofluids, THE UNIVERSITY OF TEXAS AT ARLINGTON, 2005.

[20] K.S. Suganthi, K.S. Rajan, Metal oxide nanofluids: Review of formulation, thermo-physical properties, mechanisms, and heat transfer performance, Renew. Sustain. Energy Rev. 76 (2017) 226–255.

[21] D.K. Devendiran, V.A. Amirtham, A review on preparation, characterization, properties and applications of nanofluids, Renew. Sustain. Energy Rev. 60 (2016) 21–40.

[22] C.Y. Tso, C.Y.H. Chao, Study of enthalpy of evaporation, saturated vapor pressure and evaporation rate of aqueous nanofluids, Int. J. Heat Mass Transf. 84 (2015) 931–941. doi:10.1016/j.ijheatmasstransfer.2015.01.090.

[23] K. Sefiane, R. Bennacer, Nanofluids droplets evaporation kinetics and wetting dynamics on rough heated substrates, Adv. Colloid Interface Sci. 147–148 (2009) 263–271.

[24] R.H. Chen, T.X. Phuoc, D. Martello, Effects of nanoparticles on nanofluid droplet evaporation, Int. J. Heat Mass Transf. 53 (2010) 3677–3682.

[25] M.R. Madhusoodanan, V. Sajith, C.B. Sobhan, Experimental investigation of phase change phenomena in nanofluids, Proc. Asme/Jsme Therm. Eng. Summer Heat Transf. Conf. 2007, Vol 1. (2007) 859–863.

[26] M. Moghiman, B. Aslani, Influence of nanoparticles on reducing and enhancing evaporation mass transfer and its efficiency, Int. J. Heat Mass Transf. 61 (2013) 114–118.

[27] A.S. Nafey, M.A. Mohamad, S.O. El-Helaby, M.A. Sharaf, Theoretical and experimental study of a small unit for solar desalination using flashing process, Energy Convers. Manag. 48 (2007) 528–538.

[28] A.E. Kabeel, E.M.S. El-Said, Applicability of flashing desalination technique for small scale needs using a novel integrated system coupled with nanofluid-based solar collector, Desalination. 333 (2014) 10–22.

[29] E.M.S. El-Said, A.E. Kabeel, M. Abdulaziz, Theoretical study on hybrid desalination system coupled with nano-fluid solar heater for arid states, Desalination. 386 (2016) 84–98.

VITA

Nasser Zouli was born in Jazan, Saudi Arabia. He received his B.S. in chemical engineering from the King Saud University, Riyadh, Saudi Arabia in 2002. He was ranked out the first of the students in the class and received honors with distinction. From 2002 to 2003, he worked as a supervisor on Metito company in Jeddah, Saudi Arabia. Afterwards, he worked in the Saudi Government corporation Saline Water Conversion Corporation (SWCC) from 2003 to 2009, working as shift charge engineer. He obtained his M.S. in Chemical Engineering from the Newcastle upon Tyne University, UK, in 2010. On 2012 he joined the Jazan University in Saudi Arabia as a lecturer. He started at Missouri University of science and technology during the spring semester of 2013 to work under the supervision of Dr. Muthanna Al-Dahhan. He obtained his second M.S. in Chemical Engineering from Missouri S&T in December 2015. During his stay in the Missouri S&T, Nasser worked on project related to the uses of nanofluids to improve the thermal desalination processes. He also outreached to the Missouri S&T community serving as the president of the Saudi Student Association (SSA), and he is a member of AIChE and Society of Chemical Industry (SCI). His research activities included two publications in peer-reviewed journals and eight national and international conference presentations. Nasser received his Ph.D. in Chemical Engineering from Missouri S&T in December 2018.